# The Long-term Dynamics of the Glacially-fed River Systems in Patagonia

Thesis submitted in accordance with the requirements of the University of Liverpool for the degree of Doctor of Philosophy by

Grace Katherine Skirrow.

July 2022

**Abstract**

The acceleration of global glacier retreat in the 21st century will likely see glacially-fed rivers decouple from their glacial sources across all latitudes, incurring substantial changes to fluvial drivers and sensitivity to change. In Patagonia, water supply to the major eastward draining river systems is heavily reliant on drainage from the Andes Mountains which have undergone extensive changes in drainage dynamics during glacial periods caused by fluctuations in the extent of the Patagonian Ice Sheet. Key Climate systems (e.g. the southern westerlies) are important drivers of precipitation to Patagonia. They have responded to past shifts in temperature and are predicted to play a crucial role in future changes to weather patterns across Patagonia and the globe. Existing research on the glacial, lacustrine, vegetation and fire history has reconstructed the paleoenvironmental conditions in Patagonia, but the response of the major eastward draining rivers is largely unknown. This study combines geomorphological mapping, sedimentological and stratigraphic analysis, and luminescence dating techniques to investigate the preservation, timescales and drivers of past fluvial behaviour of the Río Chubut catchment (~42°S, ~70°W), Argentina.

This thesis concludes that the Río Chubut catchment preserves a host of palaeofluvial features that formed on timescales as old as the last interglacial (MIS 5) and as recent as the last millennium (Late Holocene). The catchment preserves evidence of: (1) deep valley incision; (2) the aggradation and incision of glacially-derived sediments; (3) the shift from a braided to a meandering planform; and (4) the evolution of the contemporary meandering system. Under glacial conditions, the Río Chubut was braided and dominated by glaciofluvial outwash. Injections of sediment, from repeated glaciation of the headwaters, continued to be mobilised as a paraglacial braided river after decoupling from the ice sheet at the end of the last deglaciation. Whilst the sediment supplied by glaciation was vital to braiding in the Río Chubut, the water supply was not; this study shows that the last paraglacial braided planform was abandoned because of a reduction in precipitation via a weakening and southward shift in the southern westerlies, which caused a planform shift to the contemporary meandering regime. The contemporary regime has evolved to a mature meandering system, operating in a flood basin. Millennial-scale floodplain residence time preserves morphological evidence of substantial channel avulsions and meander migration. Still dependent on drainage from the Andes, the Río Chubut has persisted through the variable climatic conditions of the Holocene. This research suggests that modern paraglacial braided rivers may be vulnerable to future climate change as shown by the sensitivity of the Río Chubut to precipitation change in the Andes.

**Acknowledgements**

This thesis would not have been possible without the invaluable guidance from my supervisory team Dr Rachel Smedley, Prof Richard Chiverrell and Prof Janet Hooke. Thank you for your wisdom, your time, and your patience. Special thanks are owed to Rachel, for her teachings and unwavering support; without you this thesis would be plagued with rogue capital letters. A great deal of thanks is also owed to lab technicians Jenny, Luke and Mariann for their practical help and their friendship all the way through this project. Gratitude is also extended to all of the landowners Señor Don Manuel and Señor Pascini who generously granted us access to their land, and to Laura and Daniel, for their hospitality at Mirador Huancache and for their local knowledge whilst on fieldwork.

My academic progress would never have reached this far without my lecturers from Liverpool John Moores and Royal Holloway universities. Particular thanks are owed to Prof Chris Hunt, who showed me that post graduate research was within my reach.

I am so grateful to all of my friends for riding the ups and downs of this journey with me, thank you all for your support. It has been a pleasure to work alongside the PhD students of the EAO DTP and the Roxby building. Thank you to my PhD elders, Dr. Maddy, Dr. Thea, Dr. Hannah, Dr. Simon, Hazel and Dr. Fiona, for taking me under your wing and pulling me through with Ristorante pizza and prosecco. To Liverpool Victoria Rowing Club, especially Kate, Beth, Bev, Kath and Rhianna, rowing with you has helped keep me sane; thank you for bringing me joy every week, keeping me grounded and making sure I ate (Kate and Beth). Thank you, Connor, for making a joke out of everything, even when you shouldn't. Thank you, Kaja, for your pep talks in the later stages of writing. Thank you, Molly, for being the best office neighbour. Thank you to, Mik and Ana for your wisdom and support. Thank you, Ethan, for stopping at every tiny bit of flowing water to look for fluvial processes. Thank you to the Ball family, Kells, John, Hope, Jesse and Daisy for taking me into your family when I had to spend long away from my own. Especially, thank you Hope, the best flatmate I could ask for, my lockdown gal. Thank you for going insane with me, thank you for doing more than your fair share of washing up, and thank you for being such an amazing support.

Laura, I wish everyone could have a best friend like you. Even from 200 miles away your encouragement, energy, care, and advise gives me so much strength. Thank you for proof reading, listening to my river ramblings, giving me somewhere to escape to and sending the next best thing when I needed comfort, Casa Italia carbonara. I

am also grateful to you for bringing me Sophie, your daytime distractions have inadvertently led to so many solutions to the challenges I encountered, and your unwavering cheerleader energy has kept me writing.

Thank you to my family for your lifelong support and encouragement. To Mum and Dad for showing me the beauty and value of the natural world from childhood from which my curiosity was sparked; and to my sisters, Emily and Alice, thank you for your patience when this thesis consumed our conversations, and thank you for being here for me every step of the way. And to Mandy and Shmoo, this thesis would have been insurmountable without you.

I am so grateful for all of these people who have supported me through this journey. I am so immensely proud; this thesis represents, strength, perseverance, and my shameless love for rivers.

**Table of contents**

**List of Tables**

Table 5.1. Environmental dose-rate results for the sedimentary samples taken from the Río Chubut, Argentina. Environmental dose-rates were determined using ICP-MS to determine K, U and Th concentrations. The dose-rates were calculated using the conversion factors of Guerin et al., (2011) and alpha (Bell, 1980) and beta (Guerin et al., 2012) dose-rate attenuation factors. Water contents were estimated following measurement in the laboratory; these values are expressed as a percentage of the mass of dry sediment. An internal K-content of 10 ± 2% (Smedley et al., 2012) were used to determine the internal dose-rates. An a-value of 0.10 ± 0.02 (Balescu and Lamothe, 1993) was used to calculate the alpha dose-rates. Cosmic dose-rates were determined after Prescott and Hutton (1994). Dose-rates were calculated using the Dose Rate and Age Calculator (DRAC; Durcan et al., 2015).

Table 5.2. Luminescence dating results for the sedimentary samples taken from the Río Chubut Argentina. The g-values (%/decade) were measured using the pIRIR225 signal for three aliquots of K-feldspar for each sample, normalised to 2 days and are presented as weighted means and standard errors. The number of grains that were used to determine a De value (n) are shown as a proportion of the total grains measured (N). The CAM or MAM were used to determine the De for age calculations for samples deemed to have been well bleached and partially bleached, respectively. The u-MAM was used for samples where the De was approaching zero Gy. The $\sigma$b value (0.3) was estimated by combining overdispersion from internal (see Fig. S10 for dose-recovery experiment results) and extrinsic sources in quadrature.

**Chapter 6: Timescales for channel activity in the contemporary meandering planform of the Río Chubut (~42 °S, 70°W) Argentina.**

Table 6.1. Environmental dose-rate results for the sedimentary samples taken from the Río Chubut, Argentina. Environmental dose-rates were determined using K, U and Th concentrations measured with ICP-MS. The dose-rates were calculated using the conversion factors of Guerin et al., (2011) and alpha (Bell, 1980) and beta (Guerin et al., 2012) dose-rate attenuation factors. Water contents were estimated following measurement in the laboratory; these values are expressed as a percentage of the mass of dry sediment, and were representative of the water contents over the burial period. An internal K-content of 10 ± 2% (Smedley et al., 2012) were used to determine the internal dose-rates. An a-value of 0.10 ± 0.02 (Balescu and Lamothe, 1993) was used to calculate the alpha dose-rates. Cosmic

**List of figures**

**Chapter 1: Introduction**



**Chapter 2: Study Site**

valley (Leger et al., 2021a) Chilean Lake District (Moreno et al., 2015), and Lago Belgrano (Medelova et al., 2020a (age errors quoted in Mendelova et al., 2020b)) and the Luminescence chronology for Ice margins at Lago Buenos Aires (Smedley et al., 2016). Palaeoenvironmental records including the dust record (Dust abundance correlates with colder conditions) (Lambert et al., 2008) and temperature anomaly reconstruction (Jouzel et al., 2007) from the EPICA Dome C Ice Core, Antarctica show climatic variability on millennial timescales over the last two glacial cycles. Global ice volume and Sea surface temperature reconstructions were sourced from the Benthic δ18O marine stack (Lisiecki and Raymo, 2005) and marine core PS75/034-2 from the Pacific sector of the Southern Ocean (Ho et al., 2012), respectively. Grey, vertical bars indicate glacial periods, peach dashed lines indicate the OSL ages presented in this study and the peach vertical bars mark their error range.

**Chapter 5: Planform change of the Río Chubut (~42°S, ~70°W, Argentina) in response to climate drivers in the southern Andes.**

Figure. 5.1. Location of Río Chubut catchment in context of the major southern South American rivers overlain by PATICE ice sheet and glacial lake reconstructions (Davies et al., 2020). Locations of places of interest and monitoring stations mentioned in this article (left). P.d. Sapo and P.d. Indigo refer to the small settlements Paso del Sapo and Paso del Indios, respectively. F.A Dam complex refers to the Florentino Ameghino Dam Complex (left). The study reach is shown (right) in context of the wider Río Chubut catchment and the study area (red box) corresponds to the area shown in Fig. 2. The major tributaries of the Río Chubut are labelled (right). Moraine ridges (Davies et al., 2020 [northwest of Palena]; Leger et al., 2020 [southwest of Palena]) and Atlantic-Pacific drainage divide (southwest of Palena mapped by Leger et al., 2020) presented in context of the modern and glacial drainage regimes. The satellite imagery basemaps are from the ESRI Global Basemap (ESRI, 2009).

Figure. 5.2. Geomorphological map of the study reach along the Río Chubut demonstrating the elevation of the lower level terraces and position of alluvial fans in relation to the modern-day channel. Remote mapping scale 1:20,000 supplemented with field observations.

Figure 5.3. High resolution geomorphological mapping (1:8000) identifying landforms sampled for luminescence dating, including braided samples CHUB1918 (site CHUB6), CHUB1914 (site CHUB5), CHUB1917 (site CHUB4), CHUB1920 (site

Fig S3. Sample CHUB1918, collected by the borehole sampling procedure. Sample taken from the boundary between the braided gravels and overlying floodplain sediments. Age represents the timing of the end of the braiding activity on site CHUB6.

Fig S4. Sample CHUB1920, collected by the borehole sampling procedure. Sample taken from the boundary between the braided gravels and overlying floodplain sediments. Age represents the timing of the end of the braiding activity on site CHUB1.

Fig S5. Sample CHUB1915, collected by standard horizontal tube procedure. Sample taken from the fine grained homogenous unit at the base of the alluvial fan exposure. Age represents the oldest activity of the alluvial fan.

Fig S6. Sample CHUB1916, collected by standard horizontal tube procedure. Sample taken from the fine grained homogenous unit at the top of the alluvial fan exposure. Age represents the youngest activity of the alluvial fan.

Figure S7. Schematic explaining the borehole sampling technique of braided sediments.

Figure S8. Results from dose recovery (DR) and residual dose experiments. The given dose used in DR was 52.5 Gy. The DR ratio is the residual subtracted from the DR, divided by the given dose. Grey line shows CAM De Value.

# Chapter 1

# Introduction

Patagonia is a globally important land mass as it intersects with the key climate and oceanic systems of the Southern Hemisphere. Terrestrial records from this region preserve the land system response to climate change through time. Glacial, lacustrine and vegetational records are well documented but the response to long-term climate change in the major river systems that drain the eastern Andes Mountains are largely unstudied. This thesis focuses on the Río Chubut (~42°S), Argentina and discerns the drivers of geomorphological and behavioural change on long (i.e. multi-millennial) to short (i.e. sub-millennial) timescales.

## 1.1 Rationale

Patagonia is a climatically important region of the world, uniquely situated across a large latitudinal transect in the ocean-dominated Southern Hemisphere. The land mass hosts a vast array of terrestrial environments, which makes for an ideal place to observe the terrestrial impacts of climate change. Fjords, mountains, valleys, dense forests, glaciers, lakes, and rivers can be found across Patagonia. Coastal, temperate and steppe climates occur across the east-west transect caused by the rain shadow created by the Andes Mountains, and all these systems are sensitive to climate change (Pasquini et al., 2008; Quattrocchio et al., 2008; Marengo et al., 2011; Jara and Morneo, 2012; Mundo et al., 2012; Recasens et al., 2012; Sagredo and Lowell, 2012; Marín et al., 2013; Aguayo et al 2019; Moreno, 2020).


Figure 1.1. Current position of the Southern Westerlies Winds (SWW), Polar Front (PF) and Sub Tropical Front (STP) in the Southern Hemisphere. Adapted from Bendle et al., 2017 and Fraser et al., 2012. Base map sourced from Baker, 2009 (commons.wikimedia.org/wiki/File:Southern_Hemi_Antarctica.png).

The southern westerlies and the El Niño southern oscillation (ENSO) are key climate systems in this region. The southern westerlies are the prevailing winds of the Ferrel Cell (30 – 60˚S), a global wind circulation pattern driven by the Coriolis force impacting upon global air circulation and bounded by the subtropical front and the polar front (Fig. 1.1). The westerlies in the Southern Hemisphere are stronger than in the Northern Hemisphere because of the greater area of ocean in their path, and they bring heavy rainfall to the western coasts of the Southern Hemisphere land masses. The core of the contemporary southern westerlies is focused between 50 and 55˚S, where the winds are strongest but palaeoenvironmental reconstructions from sites across the Southern Hemisphere show that the latitudinal extent of the southern westerlies has changed over time (Van Daele et al., 2016). The position of the westerlies is dictated by the latitudinal temperature gradient between the equator and the poles (Chavaillaz et al., 2013); longer-time scales see the core of the southern westerlies expand and contract in response to glacial-interglacial cycles. During the last glaciation, it has been suggested that the core reached further north to ~45˚S (Markfraf et al., 1992), ~44°S (Herman and Brandon, 2016) or ~45-50°S (Hulton et al. 1994; Denton et al. 1999). During cooler periods, the change in temperature gradient causes the southern westerlies to expand in latitudinal extent and weaken

within the core, whereas during warmer periods, the southern westerlies contract and strengthen within the core (Lamy et al. 2010). The southern westerlies are also sensitive to centennial (Moreno et al., 2009) to seasonal (Betrand et al., 2014) fluctuations in temperature. With anthropogenic climate warming over the last few decades, increases in latitudinal temperature gradients have been observed that have forced the mid-latitude storm tracks and westerlies to intensify and contract in a more southerly position, and spatially redistribute precipitation (Lamy et al. 2010; Lopez et al. 2010; IPCC AR6, 2021). For example, Chile experienced widespread drought in 2016 when precipitation decreased by 50 % (Garreaud, 2018).

ENSO is driven by the heating of equatorial surface waters and easterly trade winds over the tropical Pacific Ocean in the Southern Hemisphere. Under neutral conditions warmer surface waters are blown to the west, allowing an upwelling of cooler water in the east. The warmer surface waters of the eastern Pacific bring rainfall to this region including eastern Australia and Indonesia. El Niño conditions are characterised by a weaking of the trade winds, and the warmer surface waters shift east bringing drought to parts of the western pacific and severe rainfall and flooding to the eastern Pacific (tropical South America). La Niña conditions sees the reverse, a strengthening in the trade winds pushes the warmer surface waters further west, and the upwelling of cooler water in the east expands west. Driving intense rainfall in the west pacific regions and intense drought in the eastern pacific regions. The impacts of the ENSO are global but concentrated over the tropical Pacific Ocean. The impact of ENSO on Patagonia is an increased precipitation over the eastern coast (Agosta et al., 2020), but palaeoenvironmental evidence suggests that ENSO did not strengthen until ~7 ka in Patagonia (Moreno, 2004)

There is extensive research that reconstructs the glacial and lacustrine history of Patagonia through multiple glacial and interglacial cycles of the Quaternary period. Extensive mapping of the glacial features of Patagonia shows the extents of former glaciations and the subsequent processes and landforms associated with their retreat (Caldenius, 1932; Glasser and Jansson, 2008). Moraine and glaciofluvial outwash complexes preserve evidence of glacial advances as old as the Great Patagonian Glaciation (GPG), ~1 Ma. (Singer et al., 2004; Hein et al., 2011). Pollen records from lakes sediments shed light on past climatic conditions based on the vegetation composition (Markraf et al., 2002) and span variable timescales, mostly limited by the last occupation of the Patagonian Ice Sheet in respective valleys (Iglesias et al., 2014; Moreno, 2004, 1997). However, the eastward draining rivers that ultimately drain melt water from the ice sheet into the southern Atlantic Ocean have been overlooked.

These extensive records of past climate and environmental change provides important environmental context for novel research on the major river systems that drain the Patagonian Andes mountains.

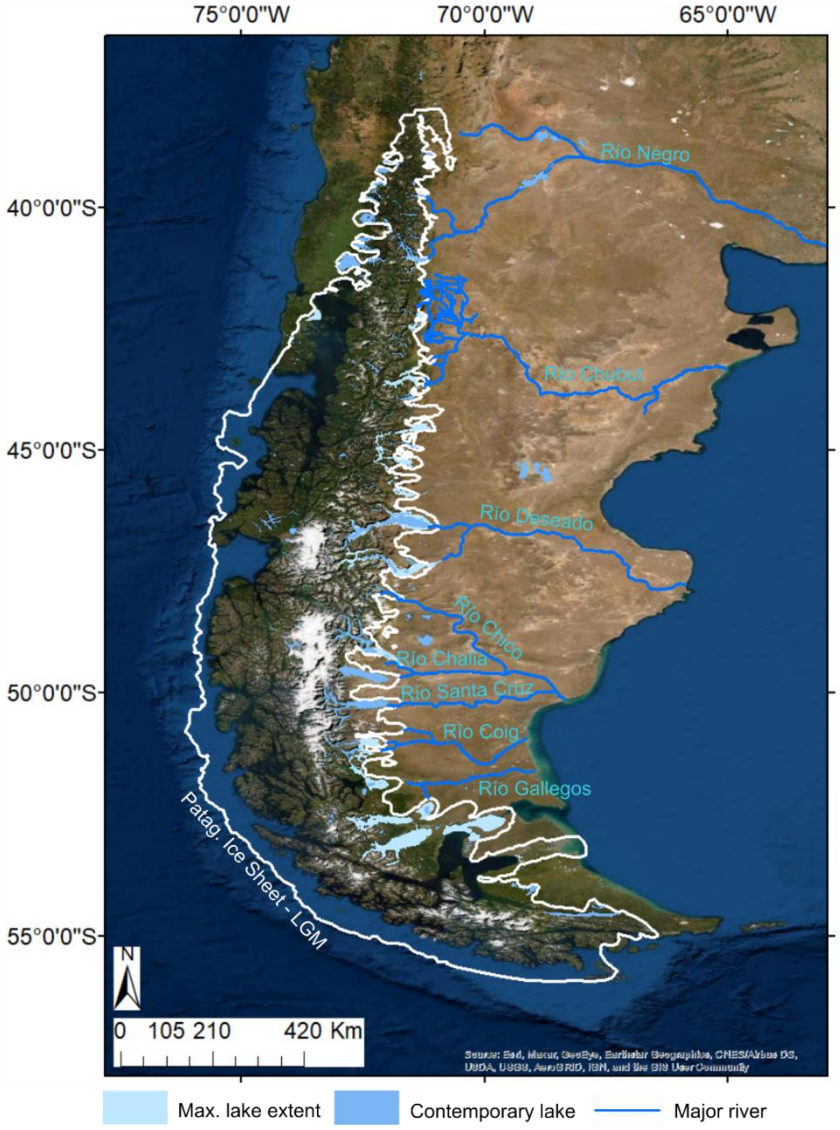


Figure 1.2. Major eastward draining river systems in Patagonia and their past interaction with the Patagonian Ice Sheet and proglacial lakes. Modelled Patagonian Ice Sheet extent at 35 ka (Davies et al., 2020). Modelled maximum proglacial lake extents (Davies et al., 2020; Leger et al., 2021a).

There are eight major river systems that drain the Andes Mountains and flow east, through the Patagonian steppe, to meet the southern Atlantic Ocean (Fig. 1.2). Most of them drain one or two large lakes except for the Río Chubut that drains a complex catchment fed by precipitation, snow melt and groundwater. All of the major river systems show evidence of past interactions with the Patagonian Ice Sheet, which occupies the Andes during glacial periods (Caldenius, 1932; Glasser et al., 2008;

Davies et al., 2020). In its contemporary state, the Andes are still occupied by glaciers but to a much lesser extent and are confined predominantly to the Northern and Southern Patagonian Icefields between 46˚S and 51˚S (Fig 1.2.), the Cordillera Darwin Icefield (~55°S, 70-72°W) and the Gran Campo Nevado (53-54°S, 73°W). Long-term climate change is known to impact the feeders of these river systems whether it was glacial, lacustrine or precipitation drainage. However, the impacts that this climate change has had on the dynamics and regimes of these rivers has not been investigated.

This thesis focuses on the Río Chubut, which was glacially-fed when it was connected to the Patagonian Ice Sheet during glacial periods, and fed by precipitation, snowmelt and groundwater during interglacial periods, such as today. This shift in feeders of the Río Chubut during glacial and interglacial periods is valuable in studying the impact climate and environmental change has had on rivers that interact with glaciers on millennial timescales. It also allows observations to be made of the same river under different regimes to understand how spatially variable and dynamic the changes are through time alone. Investigation of the same river under different regimes shapes the scope for identifying drivers of river behaviour. For example, bedrock, broad valley geometry and autogenic climate/environmental controls (such as elevation and latitude) remain broadly consistent over the time periods studied here and reducing sources of uncertainty in interpretations.

This thesis identifies, describes, and constrains the timing of large-scale shifts in river regime for the first time in the Río Chubut, Argentina. Key findings include glacially-fed sandur activity that predates the last glacial cycle, deep valley incision forming a multi-valley terrace framework, and a major planform shift from a braided to a meandering regime that occurred around the onset of the Holocene in response to climate change. As well as in-depth knowledge of river landscapes and processes, a good understanding of proglacial processes and landforms and the key climate drivers to the region was crucial to critically evaluate the impact of these system on the Río Chubut. Interpreting the drivers of these large-scale shifts in behaviour required understanding of a range of secondary data principally paleoenvironmental records including vegetation (pollen), fire (charcoal), aridity and temperature (dust), global ice volume ($\delta^{18}O$), ice sheet surface temperature ($\delta D$ and $\delta^{15}N$), and sea surface temperature ($U^{K}_{37}$) records to appropriately apply reconstructions that were representative of the study region.

This research is important to understanding the long-term drivers of change in glacially-fed river systems and their sensitivity to climate change when decoupled from glacial feeders. These eastward draining river corridors are a crucial water supply to the population of Argentina; particularly those who rely on their water supply to the semi-arid Patagonian steppe (Torres and Campodonico, 2022), and to the hydroelectric power plants that account for 41% of national electricity production (Secretaría de Energía Presidencia de la Nación, 2020). Global climate models predict a decrease in water yield by up to 40% to the headwater regions in northern Patagonia under the 1.5˚C warming scenario which highlights the need to better understand the sensitivity of these of river systems (Natalia et al., 2020).

### 1.2 Research questions

The aim with this research is ***to understand the long-term dynamics of the glacially-fed river systems in Patagonia.*** Field, Laboratory and remote sensing techniques were used to address this aim by combining geomorphology, geochronology, sedimentology and stratigraphy techniques to investigate the following research questions:

**Research Question 1: Are different fluvial regimes recorded in the geomorphology of the Río Chubut?**

To understand the long-term dynamics of the Río Chubut, firstly, the contemporary river regime is described and historic changes in fluvial regime are identified by interpreting the geomorphology in the valley. Abandoned channel forms and fluvial surfaces preserve evidence of past fluvial behaviour which shed light on the processes and dynamics driving former regimes. Research Question 1 is addressed by the following objectives:

> **Objective 1.1:** To generate a high-resolution map of the geomorphological features along a 75 km study reach.
>
> **Objective 1.2**: To assess the changes in the fluvial processes that drove changes in fluvial regime.
>
> **Objective 1.3:** To map the higher-level terraces along the study reach and associated tributaries.
>
> **Objective 1.4:** To assess the elevation relationship between the higher-level terraces along the study reach and the associated tributaries.

**Research Question 2: What were the environmental conditions that conditioned or forced the aggradation of the higher-level terraces in the Río Chubut?**

Discerning the environmental drivers of the aggradation of the higher-level terraces in the Río Chubut sheds light on the long-term dynamics that impact the river. Understanding the formation, timescales, and drivers of these large-scale shifts in river regime provides insight into systems and processes that govern the long-term dynamics in the Río Chubut. Research Question 2 is addressed by the following objectives:

> **Objective 2.1:** To characterise the depositional environments of the two higher-level terraces.
>
> **Objective 2.2:** To constrain the age of aggradation in two of the higher-level terraces along the study reach.
>
> **Objective 2.3:** To investigate the drivers of aggradation and incision in the context of published palaeoenvironmental records.

**Research Question 3: What were the driving environmental conditions that forced the Río Chubut to change its planform?**

The shift in river planform indicates a substantial change in dynamics of the Río Chubut. Understanding the timescale and drivers of the braided planform and its eventual abandonment, identifies the environmental systems that the Río Chubut braided planform was sensitive to. This also contributes conceptual insight in the potential impacts of contemporary climate change on modern braided rivers. Research Question 3 is addressed by the following objectives:

> **Objective 3.1**: To produce a chronology for the abandonment of the braided planform regime.
>
> **Objective 3.2**: To characterise the processes involved in the abandonment of the braided planform regime.
>
> **Objective 3.3**: To explore the drivers of planform change in the context of published palaeoenvironmental records.

**Research Question 4: How rapidly is the modern meandering Río Chubut evolving?**

The excellent preservation of fluvial features on the modern floodplain enables analysis of the long- and short-term dynamics of the contemporary meandering regime. Understanding the timescales and processes in the meandering Río Chubut sheds light on the contemporary dynamics of the river, and the resilience of that meandering planform to environmental change. Furthermore, this research question contributes to the discussion on the potential impacts of future climate change on the eastward draining rivers in Patagonia. Research Question 4 is addressed by the following objectives:

> **Objective 4.1**: To constrain the timescales of key floodplain and flood basin processes.
>
> **Objective 4.2**: To explore the autochthonous and allochthonous drivers of meander belt and flood basin evolution.

### 1.3 Structure of thesis

This thesis is presented as a series of academic papers. Therefore, each 'results' chapter (Chapters 3-6) presents methods, findings, contextual literature, and discussion pertaining to one or more of the research questions set out above. The papers are organised from the largest (catchment) to the smallest (channel) spatial scale. This thesis includes four manuscripts; Chapter 5 was published in November 2021, Chapter 3 has been submitted to the Journal of Maps and is awaiting review, Chapter 4 is ready for submission, and Chapter 5 is in preparation for future submission.

**Chapter 1** provides the rationale for this thesis, illustrating the wider context of land system response to environmental change and the significance of Patagonia in the study of climate-driven change to terrestrial environments. The gap in the knowledge – where this thesis contributes – is explained and the research questions are outlined.

**Chapter 2** introduces the selected study area where this research was situated. The modern context for the whole river is also described including the contemporary climate and river conditions, human occupation and land/river management.

**Chapter 3** presents and addresses **Research Question 1.** This paper describes the geomorphology of the lower-level valley along the study reach and the higher-level

terraces in the wider catchment. Key changes in fluvial regimes are identified, which are investigated further in Chapters 4, 5 and 6.

The paper presented in **Chapter 4** addresses **Research Question 2**. Luminescence dating is applied to two terrace levels from the terrace and lithostratigraphical framework outlined in Chapter 3. Environmental drivers are discussed in the context of published palaeoenvironmental records (including Chapter 5) and existing literature interpreting similar lithostratigraphical formations in the wider region.

**Chapter 5** is a paper that addresses **Research Question 3** by applying luminescence dating, and sedimentology and stratigraphy analysis to the abandoned braided surfaces identified in the lower-level valley in Chapter 3. Environmental drivers are discussed in the context of published palaeoenvironmental records from the wider region.

**Chapter 6** presents a paper that addresses **Research Question 4**. Geomorphological evidence is drawn from Chapter 3 and luminescence dating is applied to constrain the timescales of evolution in the contemporary meandering regime.

**Chapter 7** concludes the thesis by summarising the key findings and purpose of the work undertaken. This chapter provides an extended discussion and synthesis on the wider implications of this research, which comments on the current literature and wider utility of the findings.

### 1.4 Status of manuscripts and author contributions

**Chapter 3 – The fluvial geomorphology of the Río Chubut valley and tributaries (~42°S, ~70°W, Argentina).**

*Status: Submitted to Journal of Maps*

**Skirrow. G.K -** main author, organised and led fieldwork; collected, analysed and interpreted all of the data included and wrote the manuscript.

Chiverrell. R.C - in-depth discussions and detailed manuscript review.

Smedley. R.K - in-depth discussions and detailed manuscript review.

Hooke. J.M - in-depth discussions and detailed manuscript review.

**Chapter 4 – A chronology for the La Pampas Formations: Late MIS 5 and MIS 2 sandur deposits in the Río Chubut Valley (~42˚S) Argentina.**

*Status: In preparation for submission to the Journal of South American Earth Sciences*

**Skirrow. G.K –** main author, organised and led fieldwork; collected samples and conducted laboratory work; collected, analysed, and interpreted all of the data; and wrote the manuscript.

Smedley. R.K – conducted fieldwork; assisted in the collection of samples and laboratory work; in-depth discussions and detailed manuscript review.

Chiverrell. R.C – conducted fieldwork; in-depth discussions and detailed manuscript review.

**Chapter 5 – Planform change of the Río Chubut (~42°S, ~70°W, Argentina) in response to climate drivers in the southern Andes.**

*Status: Published in Geomorphology (November 2021)*

**Skirrow. G.K –** main author, organised and led fieldwork; collected samples and conducted laboratory work; collected, analysed, and interpreted all of the data; and wrote the manuscript.

Smedley. R.K – conducted fieldwork; assisted in the collection of samples and laboratory work; in-depth discussions and detailed manuscript review.

Chiverrell. R.C – conducted fieldwork; collected raw UAV imagery and assisted in the computer processing; in-depth discussions and detailed manuscript review.

Hooke. J.M - in-depth discussions and detailed manuscript review.

**Chapter 6 – Timescales for channel activity in the contemporary meandering planform of the Río Chubut (~42 °S, 70°W) Argentina.**

*Status: In preparation submission to Earth Surface Processes and Landforms*

**Skirrow. G.K –** main author, organised and led fieldwork; collected samples and conducted laboratory work; collected, analysed, and interpreted all of the data; and wrote the manuscript.

Smedley. R.K – conducted fieldwork; assisted in the collection of samples and laboratory work; in-depth discussions and detailed manuscript review.

Chiverrell. R.C – conducted fieldwork; collected raw UAV imagery and assisted in the computer processing; in-depth discussions and detailed manuscript review.

# Chapter 2

# Study site

The Río Chubut's glacial history, natural drainage, complex catchment and extensive preservation of large terraces and more subtle lower-level features makes this river appropriate for the research questions of this thesis (detailed in chapter 1). The availability of high-resolution satellite imagery of the Río Chubut valley and medium to low resolution elevation data facilitates geomorphological mapping and topographical analysis, supplemented by field observations.

The complex drainage basin is unique from the other major river systems draining the eastern flanks of the Andes Mountains, this means that the response to environmental change is a regional signal. Former interaction of the Río Chubut with the former Patagonian Ice Sheet gives further insight into the land system response to environmental change in addition to the well documented glacial and lacustrine settings.

The Río Chubut river system was selected for this research project because it drained the former Patagonian Ice Sheet during glacial periods (e.g. Davies et al. 2020) and preserves extensive terraces and relict fluvial surfaces that give new insights into its past behaviours. The eastward drainage route through Argentina to the Atlantic Ocean means the river extended past the maximum ice limits of the former Patagonian Ice Sheet allowing for preservation of palaeofluvial features that were undisturbed by glacial advance. The Río Chubut is unique from the other major eastward draining river systems that drained the glacial lakes of the eastern Andes. The Río Chubut has a complex catchment which drains a network of headwater valleys across an area of ~20,000 $km^2$, which means river regimes - past and present - reflect environmental conditions on a regional scale. The modern regime of the Río Chubut has not been heavily impacted by large-scale human modification (e.g. dam building for hydroelectric power), however, future projections suggest that temperature-induced migration of the Southern Westerlies could alter precipitation patterns across the region (Lamy et al., 2010). Between 2010 and 2018, Chile was subject to widespread drought conditions when precipitation decreased by between 20% - 40% (Garreaud et al., 2020).

## 2.1 Chubut Region

### 2.1.1 Headwaters

The modern-day headwaters of the Río Chubut drain the eastern flanks of the Andes Mountains, extending north from Epuyen toward San Carlos de Bariloche in the Río Negro province (Fig. 2.1). Through a complex pattern of tributaries, the catchment branches south to the Palena region giving coverage between 41.4˚S and 43.7˚S. The catchment is fed predominantly by snowmelt and precipitation runoff, lake drainage contributions are negligible in its contemporary state. Mean monthly temperature ranges from 12.8°C (summer) and 4.8°C (winter) at Esquel (42.54°S, 71.18°W 655 m a.s.l.) (Lawrimore et al., 2011). There is a mean annual precipitation in in the Andean foothill headwaters of 458 mm $a^{-1}$ at Esquel (Peterson and Vose, 1997). These climatic conditions support the dominant vegetation; Nothofagus and Austrocedrus forests (Iglesias et al., 2012). Cretaceous-Tertiary volcanic, Palaeozoic intrusive and Precambrian undifferentiated bedrock dominates the northern headwaters of the river (Fig. 2.2; Schenk et al., 1999).

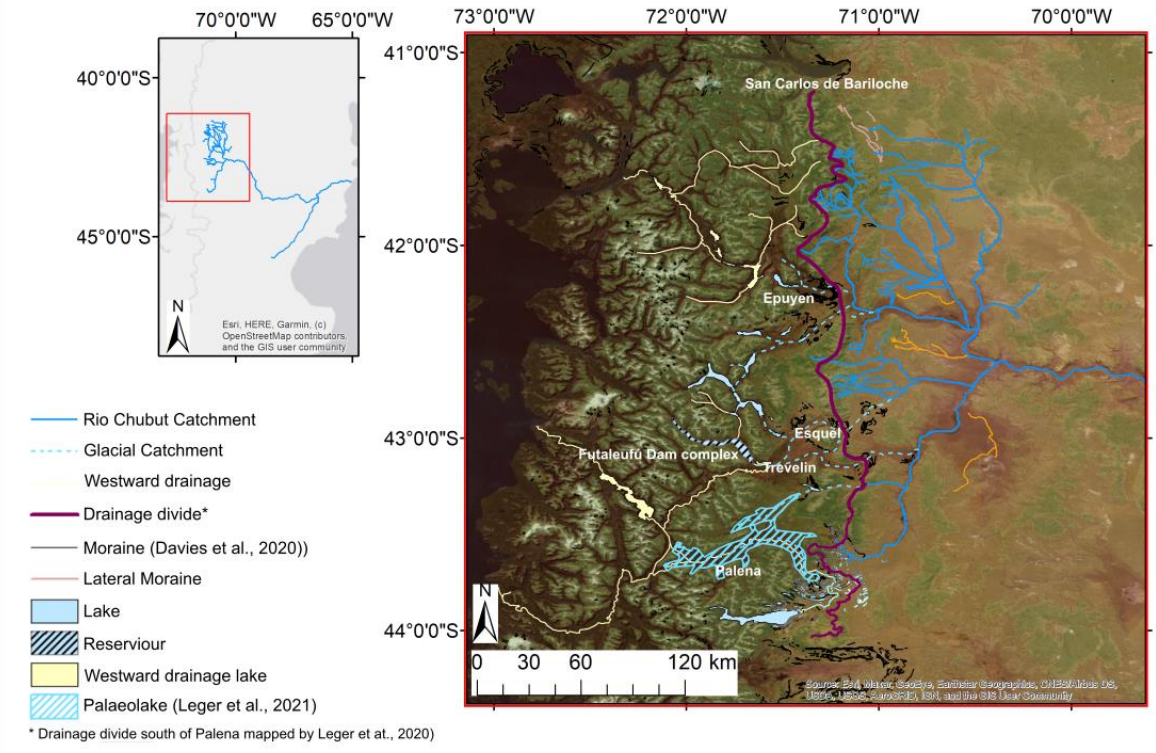


Figure 2.1. Modern and glacial drainage regimes of the Río Chubut. Locations of places of interest and monitoring stations mentioned in this Chapter are labelled in white.

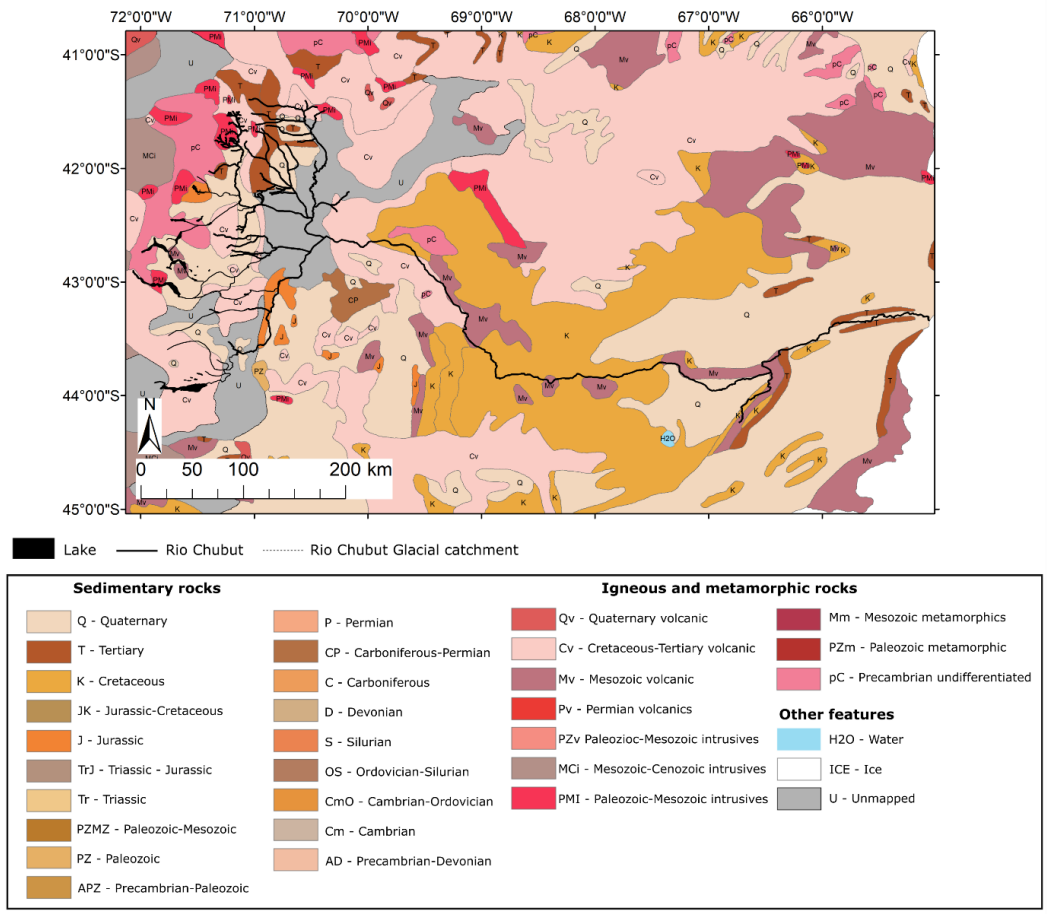


Figure 2.2. Geological map of study region, after Schenk et al. (1997).

The population residing in the headwaters of the Río Chubut is concentrated in large towns such as Esquel (population: 32,758), Epuyen (population: 1,749) and Trevelin (population: 7,908) (DB City, 2022). The primary industry in Esquel is tourism, with tourist infrastructure offering Skiing, trekking and fishing activities. Hydroelectric power is also an economic activity located in this region. Although the Futaleufú Dam Complex is located close to the headwaters of the Río Chubut, the drainage of this valley is not coupled to the Río Chubut under its contemporary regime. Therefore, the Río Chubut headwaters has maintained natural drainage throughout postglacial times.

### 2.1.2 Middle course

The middle course river is predominantly a single thread sand and gravel-bedded wandering to meandering channel (Fig. 2.3). The valley is wide and flat with extensive accommodation space for the underfit contemporary river. A 75 km study reach was selected as the focus of this research as this reach incorporates the confluences of all the major headwater tributaries (Río Ñorquincó, Río Chico (upper) and Río Gualjaina) and has good preservation of relict fluvial surfaces (Fig. 2.3). The Río

Chubut from 4/2018 to 2/2020 varied around an average annual daily maximum discharge of 29.9 $m^3 s^{-1}$, 10% exceedance of 52.2 $m^3 s^{-1}$ and maximum discharge of 75.7 $m^3 s^{-1}$.(Secretería de Infraestructura y Política Hídricia, 2018). The Río Chubut flows in the study reach at Gualjaina (42.612648°S, 70.384877°W; station 2211) vary around an average daily discharge (average over a 31 year record (1990-2021)) of 31.9 $m^3 s^{-1}$, 10% exceedance of 66.4 $m^3 s^{-1}$. A maximum discharge of 801.8 $m^3 s^{-1}$ was recorded in July 2004 and 12 others exceeding 200 $m^3 s^{-1}$ throughout the record (Secretería de Infrastructura y Política Hídricia, 2018). Environmental conditions along the middle course of the river are drier than the headwaters due to the strong orographic rainfall gradient. Average precipitation is expectedly lower in the steppe conditions of the study reach with 196 mm $a^{-1}$ at Paso de Indios (-43.82°S, -68.88°W, 460 m above sea level (a.s.l.), Fig. 2.1) (Peterson and Vose, 1997). Mean monthly temperature ranges increase moving downstream from the headwaters, averaging 16.7°C (summer) and 6.7°C (winter) at Paso de Indios (Lawrimore et al., 2011). Vegetation is sparse, where small, drought-tolerant shrubs occupy the floodplains and terraces, and riparian Poplar trees (Populus) line the riverbanks where moisture is more readily available. Extensive gullying in the semi-arid badland hillslopes feeds sediments to numerous alluvial fans along the length of the study reach. Flow in these gullies is ephemeral, and they primarily contribute water supply during seasonal snowmelt and in heavy local precipitation events usually associated with easterly atmospheric systems (Agosta et al., 2015; Garreaud et al., 2013). The sediments deposited in the alluvial fans have locally been eroded by the modern channel. The bedrock differs from the headwaters and is characterised by Quaternary/Tertiary sedimentary bedrock in the study reach area (Fig. 2.2; Schenk et al., 1999).

The middle course is sparsely populated, and settlements are considerably smaller than the large towns located in the headwaters (Gualjaina population: 1,183; Paso del Sapo population: 472; Cushamen: 740) (DB City, 2022). Small holdings inhabit the banks and floodplain, some small-scale irrigation is evident on the floodplains along the study reach where river water is diverted onto the floodplain for vegetation growth to support the grazing of livestock (Fig. 2.4). Large portions of land are owned

and managed as part of Estancias in the region who farm the land on a larger, more commercial scale.

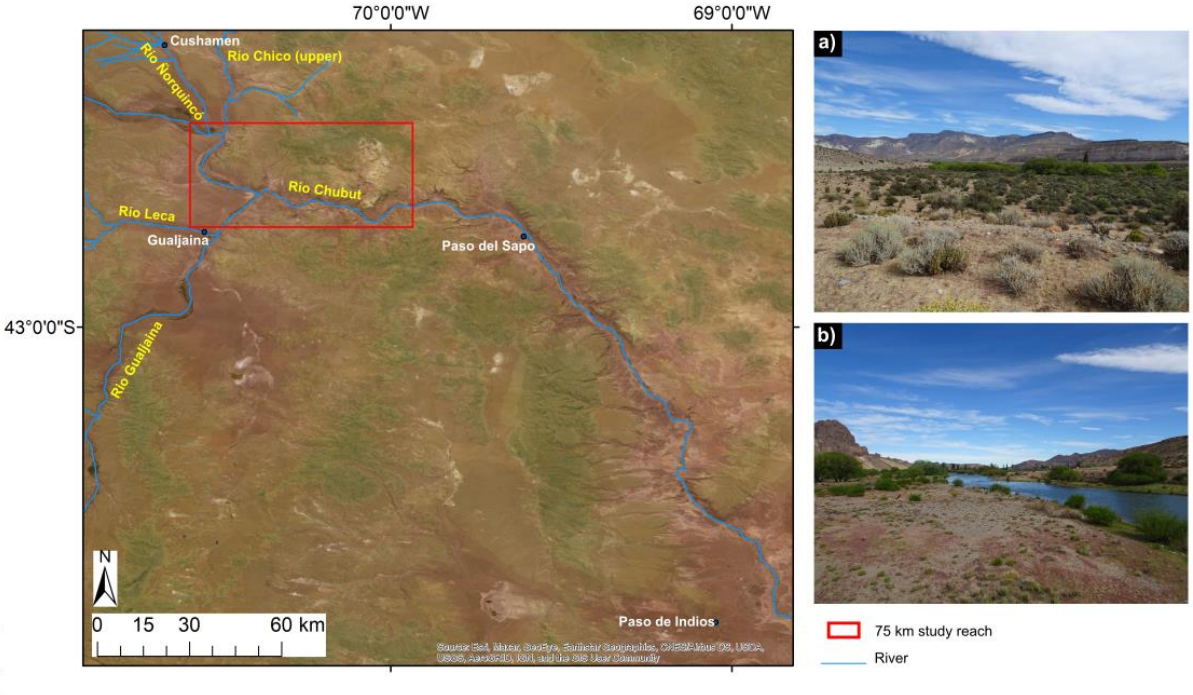


Figure 2.3. Middle course of the Río Chubut. Key tributaries labelled in yellow, locations of places of interest and monitoring stations mentioned in this chapter are labelled in white. Photographs a) and b) were taken along the 75 km study reach from the Río Chubut floodplain.

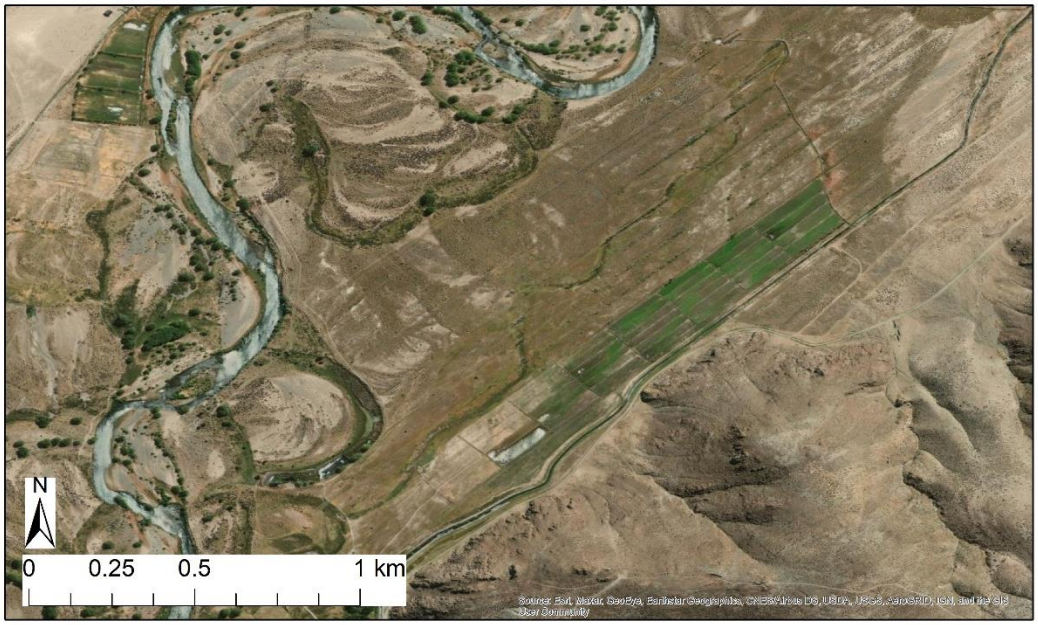


Figure 2.4. Small scale irrigation on the Rio Chubut floodplain.

### 2.1.3 Lower course

The lower course climate is the warmest and driest section of the Río Chubut; average precipitation is 169 mm $a^{-1}$ at Trelew (43.20°S, 65.27°W 43 m a.s.l.) (Peterson and Vose, 1997), and mean monthly temperatures range from 18.1˚C (summer) and 8.8˚C (winter) ( Lawrimore et al., 2011).The Florentino Ameghino Dam is located in the lower reaches of the Río Chubut, downstream of the confluence with the Río Chico (lower) tributary (Fig. 2.5). The reservoir floods ~50 km of the valley upstream of the Dam and also inundates ~30 km of the Río Chico (lower). Downstream of the Florentino Ameghino Dam, satellite imagery shows evidence of large-scale irrigation of the floodplains between Dolavan and Trelew to support farming practices that utilise water from the Río Chubut (Fig. 2.5). Population increases dramatically towards the coast in the densely-populated cities of Trelew (population: 99,430) and Rawson (population: 31,787) (DB city, 2022).

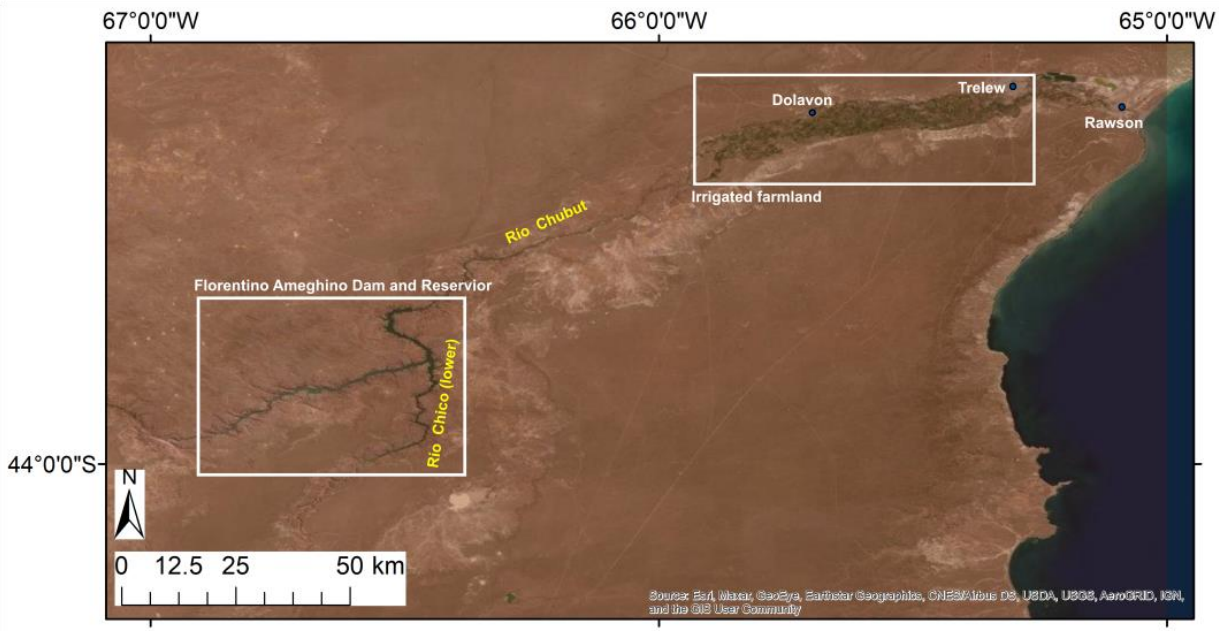


Figure 2.5. Lower course of the Río Chubut. Locations of places of interest and monitoring stationed mentioned in this chapter are labelled in white.

## 2.2 Quaternary history

There were eight major eastward draining river systems in Patagonia which drained the former Patagonian Ice Sheet during the last glaciation (Davies et al. 2020). Today, these rivers drain discrete catchments fed by large proglacial lakes, except for the Río Chubut which drains a complex catchment totalling ~32,000 $km^2$ between 41°S

and 44°S. During glacial periods, the extent of the Río Chubut catchment expanded west and received drainage in the form of glacial meltwater from a larger glacially connected area (Fig. 2.1). During periods of glacial retreat proglacial lakes formed in the Río Corcovado and Río Huemul valleys, which supplied the Río Chubut with lake drainage after ~20.7 ka (Leger et al., 2021), in addition to the existing Lago Epuyen and Lago Palena (Fig. 2.1). Further glacial retreat caused a drainage reversal from east to west, where lower elevation drainage routes were exposed to the west allowed the lakes to drain into the Pacific Ocean. This drainage reversal decoupled the proglacial lakes and other valleys from the contemporary Río Chubut catchment draining east towards the Atlantic Ocean during postglacial and interglacial stages (i.e. Caldenius, 1932; Thorndycraft et al., 2019). Modern satellite imagery shows clear drainage channels from the lakes, former lakes and previously glaciated valleys, which demonstrates the diversity of feeders and extent of the catchment as a result of climate change on millennial timescales (Glacial catchment, Fig. 2.1). The drainage reversal would have been a highly impactful event with a dramatic shift in drainage area and mode of water supply, but the timing or rapidity in which it took place is not yet precisely constrained for Río Chubut catchment. Records throughout Patagonia suggest that these events occurred during a period of deglaciation before the region experienced interglacial conditions of the Holocene (e.g., Bendle et al., 2017; Garcia et al 2019; Thorndycraft et al., 2019; Hein et al., 2010). This concurs with a recent study by Leger et al (2021) who reported that the drainage reversal of the Corcovado and Huelmul valley lakes occurred prior to ~16.3 ka. There has been debate over the drivers of Patagonia's paleoclimate, the last glacial and its termination is of particular focus. Initial theories suggested that global glacial-interglacial cycles are initiated in the high-latitude ice masses of the northern hemisphere, triggered by changes in orbitally forced summer insolation (Murphy, 1869; Milankovitch, 1941; Mercer, 1976; Mercer 1984). However, the greater availability and detail of chronological data for glaciation/termination, shows that southern hemisphere ice masses fluctuated in phase with and independently of northern hemisphere influences in (Mercer, 1976; Mercer, 1984; Kelley et al., 2014). Explanations for this argue that changes in the southern hemisphere ocean-atmosphere system impacted greenhouse gas concentrations and atmospheric albedo which in turn influenced glacier expansion/retreat (Broecker and Denton, 1989; Doughty et al., 2015). Denton et al. (2021) present the theory of the 'Zealandia switch' whereby the position of the southern westerlies in relation to the Australia/Zealandia landmasses restricts (under glacial conditions) or allows (under interglacial conditions) the oceanic exchange

between the southern ocean and those connected. Thus, enforcing climatic controls on global glacial fluctuations.

### 2.3 Definition of terms

As definitions of the catchment area vary greatly between glacial and interglacial conditions, the catchment is termed the ‘glacial catchment’ when referring to the catchment under glacial conditions and termed the ‘contemporary catchment’ when referring to the catchment under post-glacial and interglacial conditions. Note that the change from a ‘glacial catchment’ to ‘contemporary catchment’ was potentially time-transgressive because of the complex pattern of tributaries for the Río Chubut and multiple proglacial lakes that may have drained asynchronously.

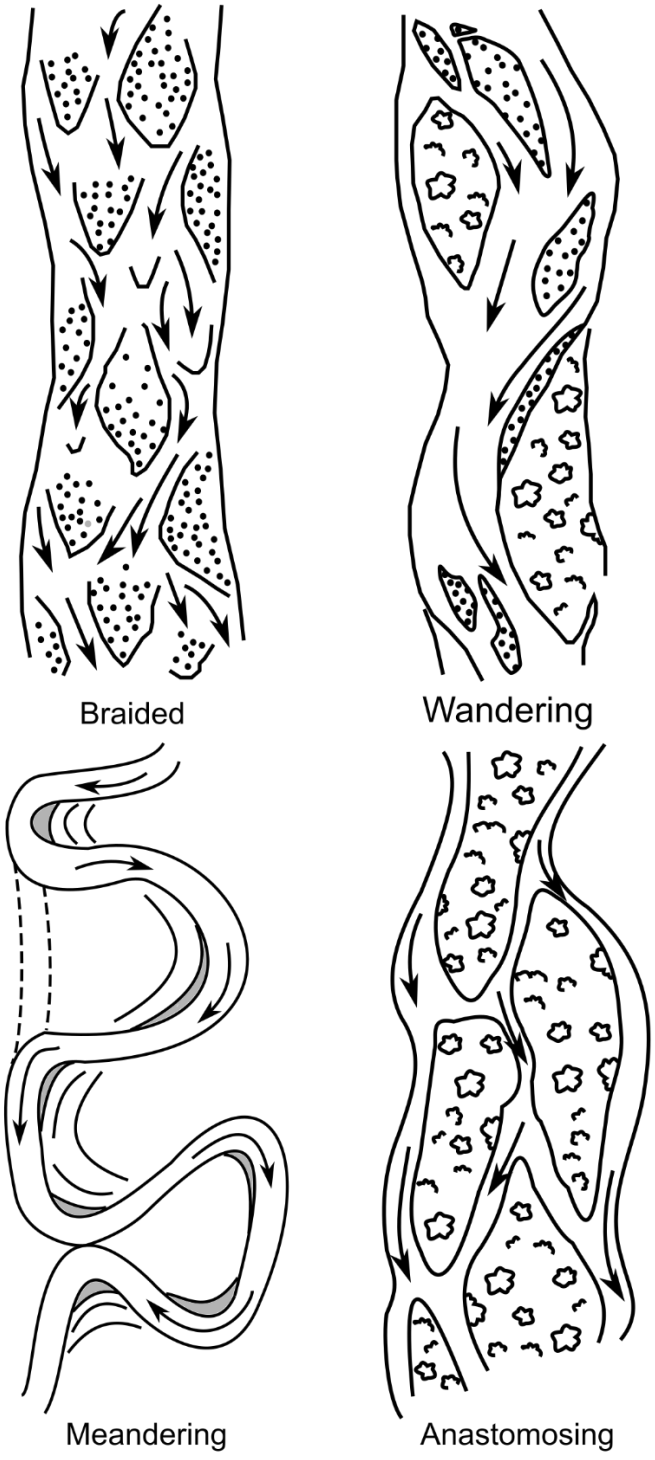


Figure 2.6. Visual characteristics of the channel patterns discussed in this thesis. Adapted from Buffington and Montgomery, 2013.

Changes in planform are reported in this thesis and are described as braided, anastomosing, meandering, and wandering. These terms are defined as follows (also see fig 2.6):

- A **braided planform** is a shallow, multiple-channel river, separated by unvegetated channel bars. This planform occurs in sediment rich, steep valleys with high energy flow. Braided rivers experience high mobility of sediment which is evident in unstable channel bars (Leopold and Wolman, 1957, Schumm 1985).
- A **wandering planform** is a single channel, moderately sinuous river with frequent channel bars and islands. This planform is considered a transitional planform between braided and meandering regimes. The thalweg follows an irregular sinuous course as it splits around bars. Discontinuous zones of aggradation produce intermittent formation of channel bars and islands of variable stability (Church 1983; Ferguson and Werritty, 1983).
- A **meandering planform** is a single channel, highly sinuous, laterally mobile river characterised by meander bends alternating in direction. This planform occurs in valleys with wide alluvial floodplains with sufficient accommodation space to facilitate lateral erosion, which is integral to the formation of the characteristic meander loop – a concave meander apex coupled with a convex point bar. Mature meandering rivers abandon excessively sinuous, and thus inefficient, channels through neck cut-off (the convergence of the channel at the neck of a meander) or chute cut off (the formation of a straight channel that bypasses the meander) processes (Leopold and Wolman, 1957; Hooke, 1984; Schumm, 1985).
- An **anastomosing planform** is a stable, low-energy, low-gradient, multiple-channel river, separated by vegetated islands which are cut from the floodplain. Formed as a result of crevasse splay, anastomosing rivers require high energy flow to erode new, or reactivate old channels on the floodplain which continue to flow contemporaneously with the 'parent' channel under normal flow conditions. Anastomosing rivers are typically stable systems as the division of channels disperses the flow strength and resistant bank material reduces bank erodibility. The anastomosing planform is distinct from the umbrella term 'anabranching' because of its' low energy, resistant banks and slightly depositional sediment balance; this typically results in a fine grain and/or organic channel substrate and narrow, uniform channels that show little to no evidence of lateral migration (Smith and Smith, 1980; Rust, 1981; Knighton and Nanson 1993; Nanson and Knighton,1998).

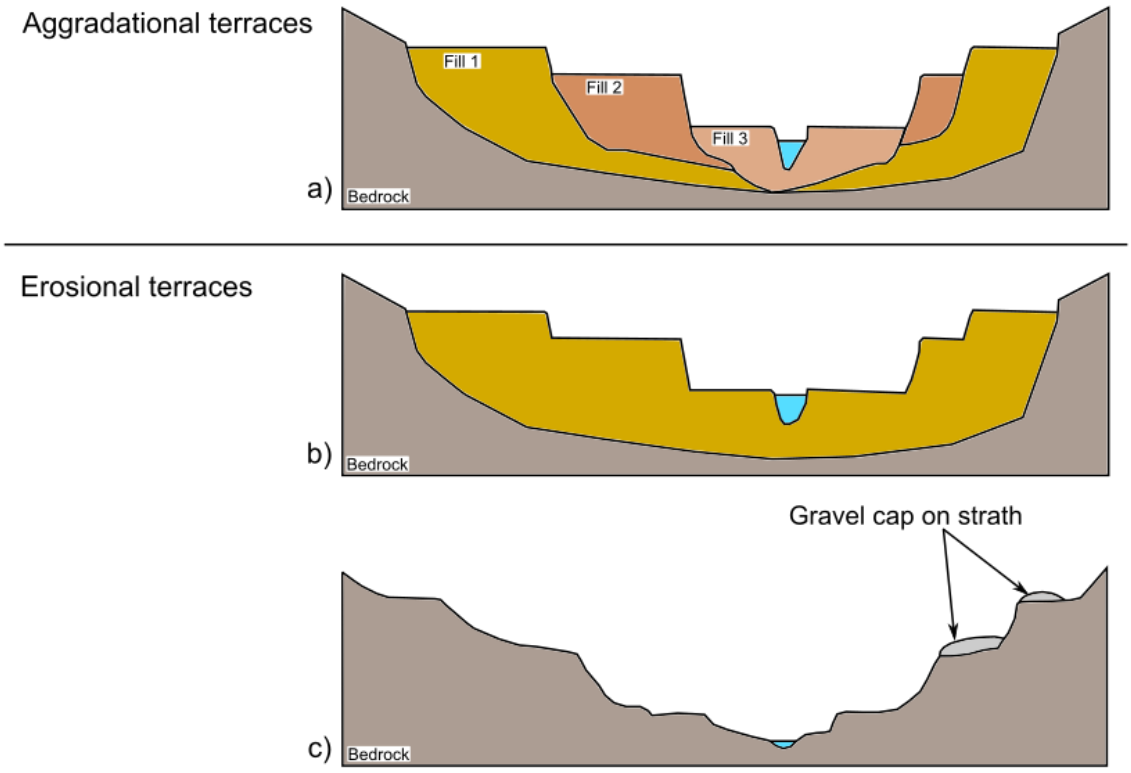


Figure 2.7. Formation of aggradational an erosional fluvial terrace. Adapted from Kamp and Owen, 2013.

Terrace formation is discussed in this thesis and is described as aggradational or erosional (Fig 2.7). A river terrace is an abandoned fluvial surface, situated higher than the active floodplain; a staircase of paired or unpaired terraces can form in a valley as the river preferentially incises over time. **Aggradational terraces** are formed through cut and fill cycles where a river switches between a depositional and erosional sediment balance, depositional (fill) phases see the aggradation of sediment in the valley which gets abandoned as terrace formations when an erosional phase causes the river to incise (cut) (Fig 2.7a) (Leopold and Miller, 1954, Schumm, 1965). **Erosional terraces** are formed through progressive incision without interruption of aggradational phases. Erosional terraces can form as multiple phases of incision through a single unit of sediment (Fig 2.7a) (i.e. one phase of aggradation followed by multiple stages of incision) or through bedrock, known as strath terraces, which commonly occur with gravel caps on the strath surface (Fig 2.7c) (Kamp and Owen, 2013).

# Chapter 3

## The fluvial geomorphology of the Río Chubut valley and tributaries (~42°S, ~70°W, Argentina).

This chapter characterises the contemporary Río Chubut and identifies different fluvial regimes of the past from geomorphological evidence that is preserved in the valley (Research Question 1). High-resolution geomorphological mapping of the fluvial features along the 75 km study reach (Objective 1.1) sheds light on the processes that drove the different river regimes (Objective 1.2). Mapping and assessing the elevation relationship between the higher-level terraces along the study reach and associated tributaries (Objective 1.3 and 1.4) characterises the generally lowering of the valley over time in stages of aggradation and incision. Also, the linking of terrace levels across multiple valleys indicates regional drivers of river regime from the headwater catchment.

Grace. K. Skirrow, Richard. C. Chiverrell, Rachel. K. Smedley, Janet. M. Hooke

Chapter based on paper Submitted to Journal of Maps

**Abstract**

Mapping by a combination of field survey and remote sensing of a 75 km study reach in the Rio Chubut and associated tributary valleys presents a catchment wide framework of extensive remnant fluvial surfaces flanking the contemporary river system. At a large scale, the landform record divides into a series of higher altitude surfaces (n=59) situated ~70 to 10 m above the present river, and a lower elevation fluvial terrain swathed with well-preserved channel forms located topographically within 3 m of the contemporary river. This terrace sequence is displayed across the catchment and resembles the product of an incision and aggradation regime that has gradually lowered the valley thalweg over time, leaving multiple remnant alluvial surfaces.

Where these higher-level terrace remnants persist and correspond in elevation across multiple valleys, they divide into three major stages. Floodplain has aggraded to ~60-70 m above the modern river profile after which the river level was then lowered by ~20 m to aggrade fluvial surfaces at ~40-50 m, before further incision of ~30 m to the lowest and youngest of these higher-level terraces at ~10-20 m.

Particularly well-preserved terrace staircases occur at the Chubut-Ñorquincó confluence and through the Río Gualjaina.

In the lower elevation terrain, the Rio Chubut shifted from a braided regime to the mature meandering channel system that persists today. At these lower elevations, the study reach preserves channel features that are synonymous with flood basin style dynamics. These include the broad (ca. >2 km) floodplain accommodation space, subdued fluvial surfaces and features, channel planforms evidencing avulsion and migration across an extensive floodplain that also sustained a local, shallow, evaporitic lake.

**Key Highlights**

- Higher-level terrace fragments correlate across multiple tributaries in three major stages (~60-70 m, ~40-50 m and 10-20 m) indicating regional change to sediment balance.
- DEM and satellite imagery inform a re-evaluation of the lower La Pampas formations in the Río Gualjaina.
- A paleolake supplied water to the Rio Gualjaina via an inactive tributary which grades to a higher-level terrace suggesting past environmental conditions of sustained increased precipitation.
- Mapping of the well preserved lower-level valley characterises past planform change from a braided to meandering regime and contemporary flood basin features including avulsion channels and an ephemeral lake.

**Keywords**

fluvial, geomorphology, glacially-fed river, terrace framework, flood basin, planform change, Patagonia

## 3.1 Introduction

Environmental change across Patagonia has been related to key climate systems such as the ENSO (e.g. Moreno, 2004; Moy et al., 2002) and the mid-latitude storm tracks and westerlies (e.g. Lamy et al., 2010). Palaeoenvironmental (e.g. Moreno, 2004; Markraf & Huber, 2010; Iglesias et al., 2014, 2016; Bendle et al., 2017; Moreno et al., 2018) and glacial records (e.g. Glasser et al., 2008; Hein et al., 2010; Sagredo and Lowell, 2012; Smedley et al., 2016) document how the landscape of the Andes has responded to large-scale shifts in climate throughout the last glaciation (Fig. 3.1). However, little is known about the evidence preserved of past environmental change in the major river systems that drain this region. The sediments and landforms of fluvial environments can present important terrestrial records of Quaternary

environmental change, often manifesting as sequences of aggradational river-terrace deposits that evidence responses to drivers of environmental changes (e.g. climate, tectonics) (Vandenberghe, 1995; Maddy, 1997; Bridgland and Westaway, 2014). Situated beyond Pleistocene ice sheet limits, these sequences can extend back to the pre-Quaternary (Mercer, 1976, Martinez and Coronato, 2008).

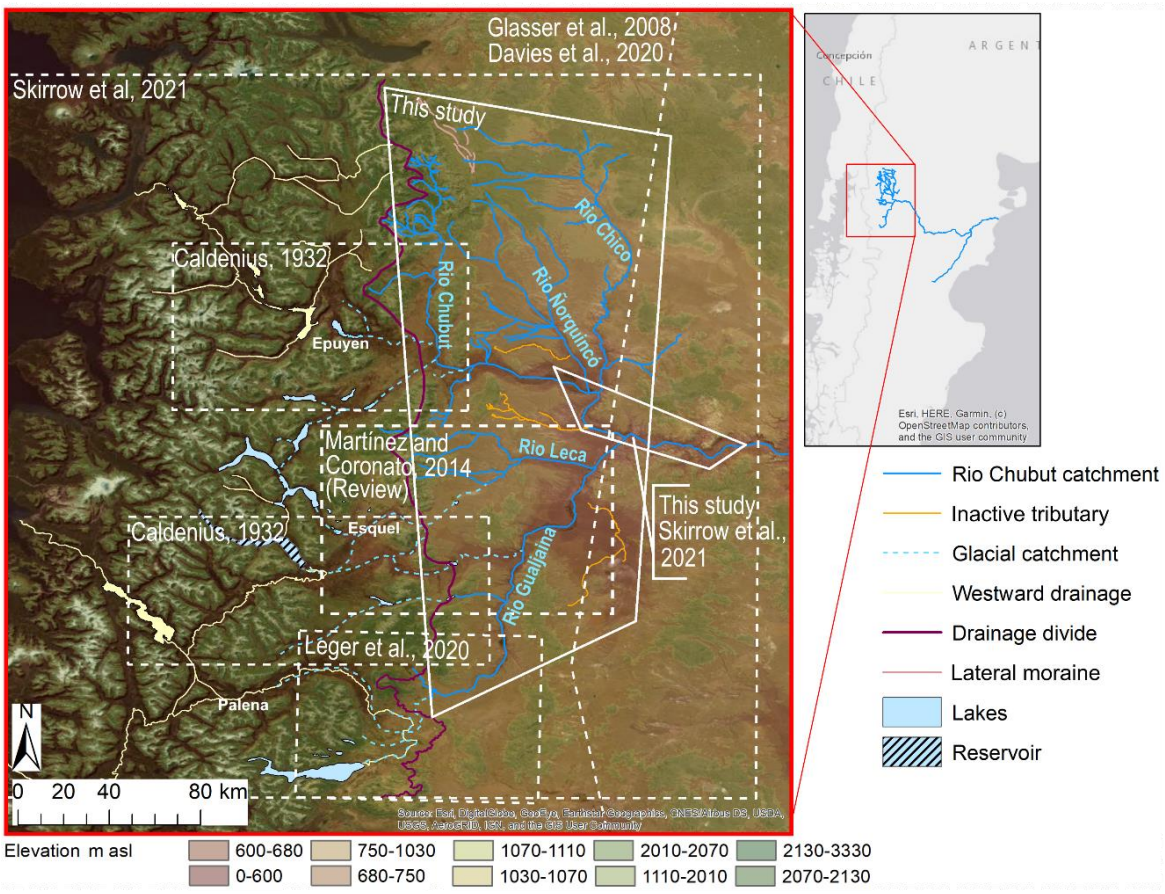


Figure 3.1. The Río Chubut catchment highlighting key differences between the contemporary catchment and former drainage pathways (Skirrow et al., 2021). White dashed boxes demarcate the extents of previous mapping in this region. “Drainage divide” refers to the Atlantic-Pacific drainage divide (southwest of Palena mapped by Leger et al., 2020) (see Table 1). The satellite imagery base map is from ESRI World Imagery sourced from Maxar (Vivid, 21/03/2015) and the elevation data is sourced from the SRTM 30 m DEM (see Section 2.1).

This study documents the contemporary and past fluvial geomorphology of a 75 km reach of the Río Chubut and the sequence of fluvial terraces present in the associated tributaries (Fig. 3.1). Previous geomorphological mapping in the headwater region of the Río Chubut catchment has been carried out at a variety of scales (Fig. 3.1) and has shed light on the interactions of regional glaciers with the Río Chubut catchment during recent glacial cycles through documenting and dating glacial maxima and

retreat (Caldenius, 1932; Glasser et al., 2008; Davies et al., 2020; Leger et al., 2020), and lake formation and drainage (Glasser et al., 2008; Davies et al., 2020; Leger et al., 2020, 2021) associated with the Río Chubut catchment. Geomorphological mapping by Skirrow et al. (2021) details the change in drainage area and headwater characteristics from a glacial to a deglacial catchment following ice retreat. For example, during glacial conditions the Río Chubut headwaters were occupied by outlet glaciers of the Patagonian Ice Sheet and so the river was fed by glacier melt and/or proglacial lake drainage. When the region experienced deglaciation, the retreating ice exposed lower elevation drainage pathways to the west, forming a lattitudinal drainage divide (Fig. 3.1), through which the lakes emptied. The smaller, deglaciated (contempoary) catchment is fed explicitly by precipitation run off and snowmelt, where its westward extent is confined by the drainage divide.

Initially mapped by Caldenius (1932), Volkheimer (1963) classified five levels of gravel mantles that are topographically stepped eastward from the piedmont of the Andes ~60-80 km across the Chubut province (Fig. 3.1). These gravel mantles are locally known as “pampas”, in order of elevation (highest to lowest; west to east) they are named: the Martín, Blancura, Fita Michi, Cabaña and Confluencia Formations. Most recently, they have been attributed to glaciofluvial outwash, except for the highest Martín Formation, which was identified as a Piedmont deposit (González Díaz, 1993a, b; González Díaz and Andrada de Palomera, 1996). The Martín, Blancura and Fita Michi Formations are located west of, and higher than, the terrace sequences mapped in this study. The Cabaña and Confluencia gravel sheets overlap with the mapping of the highest terrace levels in this study.

The Río Chubut is at present a single thread sand/gravel-bedded meandering river and is one of the eight major rivers that drain the eastern Andes. Situated ~42°S, 71-65°W, the river flows ~800 km through the Patagonian steppe of Argentina to the southern Atlantic Ocean. The Río Chubut flows in the study reach at Gualjaina (42.612648°S, 70.384877°W; station 2211) vary around an average daily discharge (average over a 31 year record (1990-2021)) of 31.9 $m^3 s^{-1}$, 10% exceedance of 66.4 $m^3 s^{-1}$. A maximum discharge of 801.8 $m^3 s^{-1}$ was recorded in July 2004 and 12 others exceeding 200 $m^3 s^{-1}$ throughout the record (Secretería de Infrastructura y Política Hídricia, 2018). The contemporary river is fed by rainfall and snow melt from the Andes, but was fed by meltwater direct from glaciers and/or indirectly via proglacial lakes during the cold stages of the Pleistocene (Skirrow, et al., 2021). The Río Chubut receives water supply from four tributaries: the Río Ñorquincó, Río Chico (upper) and Río Gualjaina, which are all sourced from or close to the Andes, and the Río Chico

(lower) that develops further downstream and is currently inactive (meaning, the channel was dry at the point of observation). The Río Chico (lower) is not included here as it is sourced from Lago Colhué Huapí in central Argentina and the confluence with the Río Chubut is located downstream of the study reach.

The Río Chubut passes through the Forest-Steppe ecotone at ~71.2°W at which point, *Nothofagus* and *Austrocedrus* forest turns into a dry, sparsely vegetated, steppe landscape. Precipitation and temperature follow the same pattern with a strong orographic gradient caused by the prevailing westerly winds and the rain shadow of the Andes (Fig. 3.1; Iglesias et al., 2012); mean annual precipitation is 458 mm $a^{-1}$ in the forested Andean foothills at Esquel (42.54°S, 71.18°W 655 m a.s.l. (above sea level)) (Peterson and Vose, 1997) and falls to 196 mm $a^{-1}$ east of the ecotone in the steppe at Paso de Indios (−43.82°S, −68.88°W, 460 m a.s.l.) (Peterson and Vose, 1997). Mean monthly temperature increases in an eastward direction from 4.8 / 12.8 °C (winter/summer) at Esquel to 6.7 / 16.7 °C (winter/summer) at Paso de Indios (Lawrimore et al., 2011).

## 3.2 Methods

### 3.2.1 Remotely-sensed geomorphological mapping

Geomorphological features were identified and mapped in the WGS84 geographic reference coordinate system using the ESRI™ World Imagery Layer, which provides imagery at a 0.5 m resolution (5 m accuracy) sourced from Maxar (Vivid, 21/03/2015) for the Río Chubut study reach and the wider catchment (Fig. 3.1). Contemporary and former fluvial features were digitised in ArcGIS 10.6 to a 1:5,000 scale along the 75 km reach of the Río Chubut and terrace sequences were mapped throughout the upper course catchment tributaries (Río Ñorquincó, Río Leca and Río Gualjaina). Sharp breaks in slope and shadows visible in the imagery gave an indication of relief, but digital elevation data and field mapping were also used in the mapping.

Topography was characterised using the Shuttle Radar Topography Mission (SRTM) – 30 m resolution digital elevation model (DEM) (https://www2.jpl.nasa.gov/srtm/). The resolution of the SRTM DEM highlights major terraces and breaks in slope but struggles to depict more subtle palaeo-channels and surfaces. The 16 m vertical accuracy of absolute elevation measurements means this dataset is not appropriate for calculating the absolute elevations of the catchment terrace sequences. Instead, the greater relative precision of SRTM DEM was used to plot and contrast the relative elevations of surfaces above the modern thalweg of the rivers. From this, former floodplain surfaces were grouped together as associated fragments based on

probable linkages in this sequence of terrace levels. Outliers and isolated fragments from these major groupings were left unassigned.

Satellite imagery was used to identify channels of different characteristics, some active and some inactive. As the satellite imagery portrays the landscape at a single moment in time when the photograph was taken, it was not possible in all cases to determine the activity status of each channel (i.e. active, ephemeral or abandoned). The assumption was made that gully features were ephemeral channels based on the modern desert-steppe conditions and badland landscape. Dry tributaries were identified as inactive, as their status was unknown but given that activity was conditioned by precipitation, the channels were not assumed as abandoned.

### 3.2.2 Field mapping

Low relief (<10 m above the modern river) topographic features undetectable from the SRTM 30 m DEM or satellite imagery were identified by field survey. The elevations of the lower-level terraces in the Río Chubut valley were measured using a handheld global positioning system (GPS) (5 m accuracy). Sedimentological observations were made where vertical exposures of sediment were available and accessible and followed established lithofacies and sediment landform models (e.g. Miall, 1996). Field mapping was only possible along the 75 km study reach of the Río Chubut and so we acknowledge that low relief terraces were likely present upstream of the study reach and in the connected tributaries but were not reported here.

## 3.3 Results

### 3.3.1 Higher elevation fluvial terraces

Sequences of high elevation terraces occur in the Río Chubut and tributaries: Río Ñorquincó, Río Gualjaina and Río Leca (Fig. 3.2). A total of 59 terrace fragments were observed across the four valleys and many make up clear terrace staircases that are particularly well developed in the Río Gualjaina and the Río Ñorquincó. The Ñorquincó-Chubut confluence resembled a complex multiple phase tributary fan system that has aggraded and been incised in stages to form a staircase of fan terraces. Terraces that appear to link up using their trajectory and the broad long-profile gradient of the valleys have been interpreted and grouped as associated fragments of the same terrace level (Table 3.1, Fig. 3.2). These terrace groupings are separated in elevation more widely than the uncertainties in the SRTM DEM, and so represent distinct surfaces. These groupings were associated based on elevation and trajectory of the surfaces. Terrace group (TG) 1 (~60-70 m), TG2 (~40-60 m) and TG4 (~10-20 m) included terraces that were present in more than one valley (TG1:

Ñorquincó and Chubut TG2: Gualjaina and Leca TG4: Ñorquincó, Chubut and Gualjaina) (Fig. 3.2). TG3 (~20-30 m; Río Gualjaina), TG5 (~10-15 m; Río Leca), and TG6 (~10 m; Río Gualjaina) were only present in one valley. The elevation ranges of TG5, TG4 and TG6 were similar, however, upon comparison of the elevation of terrace fragments in accordance with their downstream position they were confirmed as out of phase with the gradient profile of the other terrace groups. Although exposures (e.g. quarries or road cuttings) were not abundant, occasional degraded gully exposures into these surfaces suggested that they were mostly composed of cobble/gravel fluvial deposits. The underlying bedrock bathymetry and total thickness of these gravel deposits are not known.

Table 3.1 Key observations of the Río Chubut catchment terrace groups. Terrace groups are defined as, terraces that correspond in elevation and broadly form a pattern that parallels the long profile gradient of their respective valleys.

| **Terrace group** | **Elevation (m)** | **Valley(s) occupied** | **Comment** |
|---|---|---|---|
| TG 1 | ~60 – 70 | Ñorquincó and Chubut | No visible palaeochannels |
| TG2 | ~40 – 60 | Gualjaina and Leca | Braided planform, aggradational regime |
| TG3 | ~20 – 30 | Gualjaina | No visible palaeochannels |
| TG4 | ~10 – 20 | Ñorquincó, Chubut and Gualjaina | Unspecified multichannel planform, aggradational regime |
| TG5 | ~10 – 15 | Leca | No visible palaeochannels |
| TG6 | ~10 | Gualjaina | No visible palaeochannels |

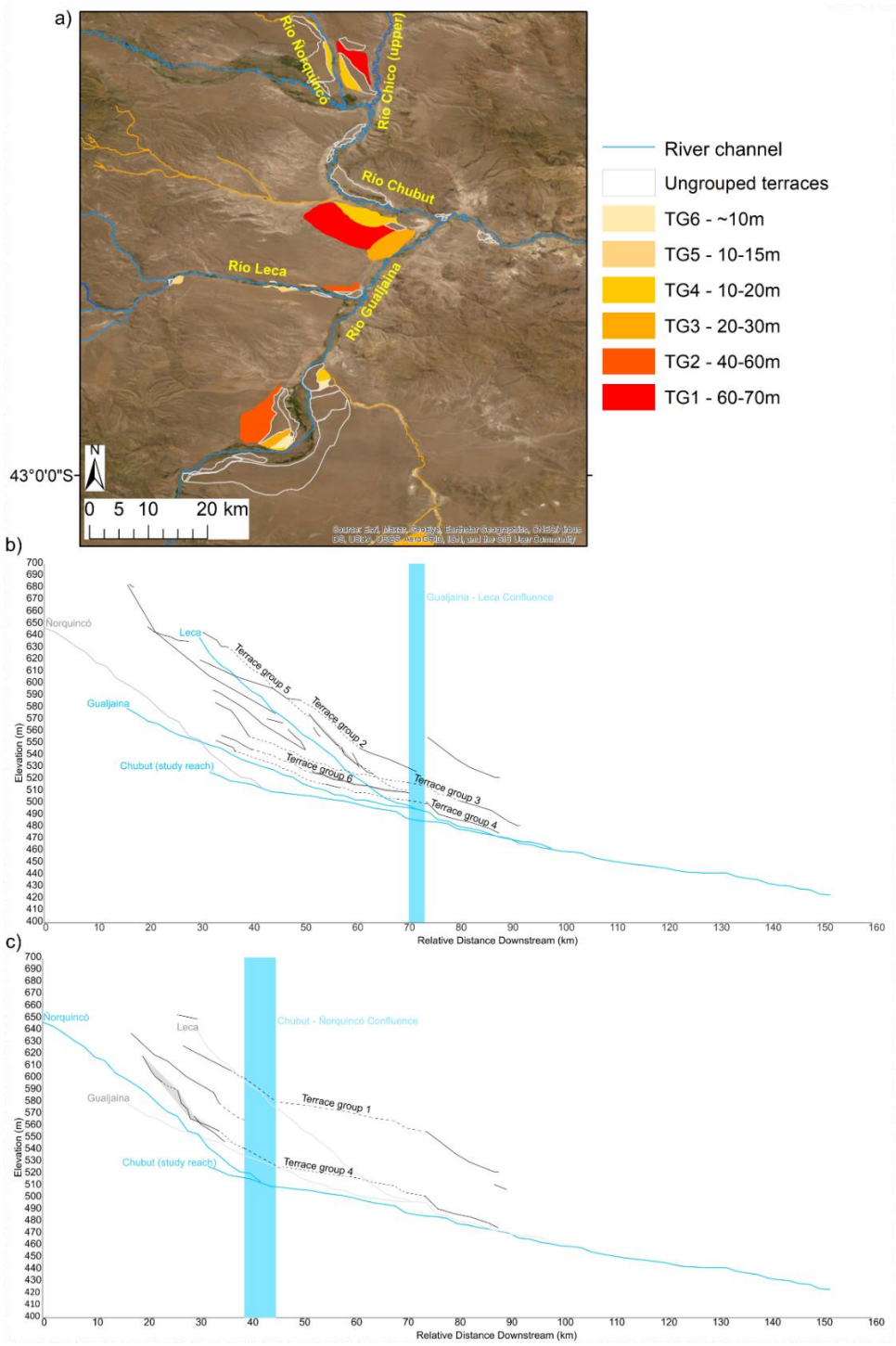


Figure 3.2. Terraces that correspond in elevation and broadly form a pattern that parallels the long profile gradient of their respective valleys are interpreted as fragments of the same former fluvial surface and are grouped as a terrace group (TG). a) Terraces located in the Río Chubut, Río Ñorquincó, Río Gualjaina and Río Leca and associated terrace groups. Lower graphs plot the elevation profiles of the rivers and the terraces. Dashed lines connect the grouped terraces and blue bars indicate the valley width at confluences. b) Includes terraces from the Río Leca, Río Chubut and Río Gualjaina valleys, c) includes terraces from the Río Ñorquincó and Río Chubut valleys.

### 3.3.2 Lower elevation floodplain geomorphology

The Río Chubut valley is flanked by an extensive badlands-style landscape with ubiquitous dendritic gullying (Fig. 3.3, 3.4b; Table 3.1). Alluvial fans occur at the confluences of these gully networks with the axial river system, sometimes connecting directly with the river, but for others the alluvial fans drape and bury the floodplain and fluvial terraces. Three inactive tributaries were identified; one draining to the Río Ñorquincó fed by slope run off, one to the Río Chubut fed by slope run off, and one to the Río Gualjaina fed by former lake drainage (Fig. 3.1).

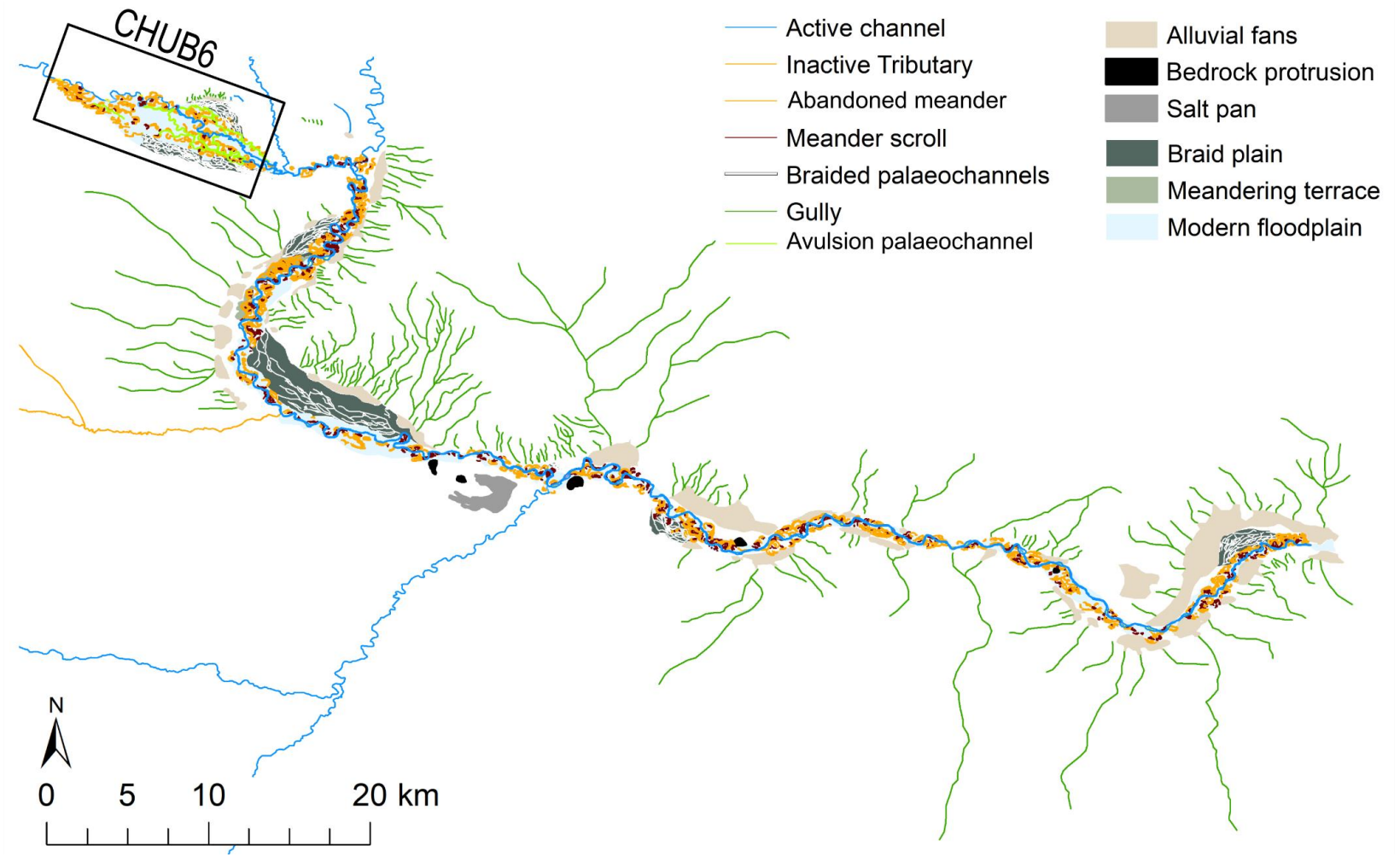


Figure 3.3. Geomorphology along the Río Chubut study reach including lower-level terraces, fluvial and landscape features. See Fig. 3.5 for smaller scale map of site CHUB6 (see Table 3.1).


Figure 3.4. Example photographs of (a) the badland landscape, (b) a bedrock protrusion along the 75 km study reach (named Piedra Parada), (c) the salt pan located at the Gualjaina-Chubut confluence, and (d) the steppe landscape dominating the study reach.

Low-level terraces and floodplain segments preserved more subtle features than the higher elevation catchment terraces. The lower-level terraces were swathed with numerous well preserved paleochannels. The highest of these lower terraces contained braided palaeochannels whilst the lower ones sustained meandering palaeochannels and scroll bars (Fig. 3.3; Table 1) – see Skirrow et al. (2021) for more detail on this braided terrain. Bedrock protrusions punctuated the valley floor floodplain, particularly in the middle section of the study reach (Fig. 3.3, 3.4a; Table 3.1). The modern floodplain contains numerous meandering palaeochannels and scroll bars, as well as an ephemeral lake/salt pan near the Gualjaina-Chubut confluence (Fig. 3.3, 3.4c; Table 3.1). The active channel follows a single thread meandering planform, but locally contains bars and islands along the course of the study reach (Fig. 3.3; Table 3.1). Bank exposures flanking the main rivers show floodplain and terrace sediments, and these comprise graded fluvial sands, some gravel beds and are capped with aeolian deposits where sediments have accumulated on the inactive fluvial terrain.

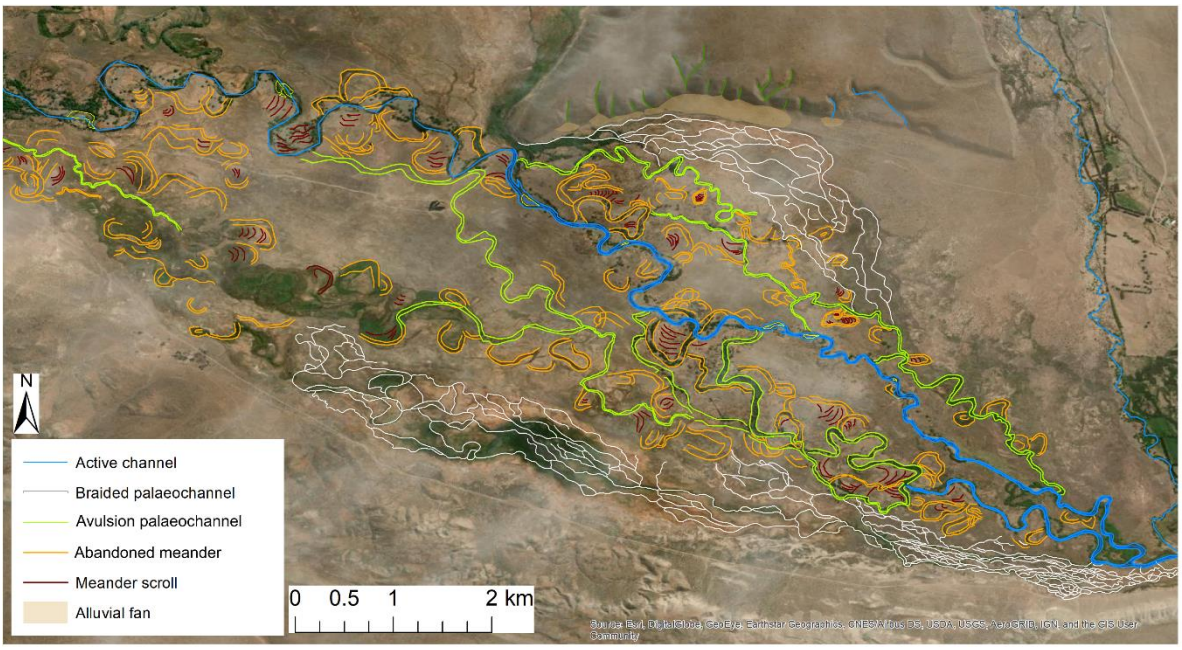


Figure 3.5. Fluvial geomorphology at site CHUB6.

At site CHUB6, the floodplain is ~6 km wide and is devoid of lower-level terraces except for the northern group of braided palaeochannels, which were positioned on a fluvial surface ~3 m above the modern channel (Fig. 3.5; Table 3.1). The wider flood basin contains multiple distinct zones of channels and floodplains that reflect different phases of activity. One of these zones consists of an apparent inactive anastomosing channel planform which is initiated from a knickpoint at the northern boundary of the upstream extent of site CHUB6. Key features including it's low energy, resistant bank material, narrow channels, little to no evidence of lateral migration and a fine grain organic channel substrate meet the specific criteria the defines an anastomosing planform that is distinct from other anabranching channels (Smith and Smith, 1980; Rust, 1981; Knighton and Nanson 1993; Nanson and Knighton,1998). The dense vegetation and partial overprinting from more recent channels make the geomorphological relationship unclear, but it is possible that channel is not an avulsion formation. There could be a connection between the anastomosing channel and the upstream wetland area on the northern periphery of the flood basin. At the time the imagery was taken this channel was not active, but the upstream wetland is densely vegetated with a visible water supply. These channel zones were typically ~1 km in width and contain channels and cut-offs. The process of the river switching to a new zone involves a substantial migration of the active channel and floodplain to a new area of the flood basin, typically ~1-2 km from the previous zone. Both zones were probably active across the transition before the establishment of a new dominant flow zone.

## 3.4 Discussion

### 3.4.1 Long-term changes in sediment balance

The high-level terraces in the Río Chubut and tributaries indicate a series of incisional and aggradational phases most likely driven by water supply outweighing the sediment supply with incision and vice versa for aggradation. The general setting outside of the maximum glacial extent in these catchments (Glasser et al., 2008) and the width of the alluvial valleys provide the potential for preservation over timescales of more than one glacial cycle. Unpaired terraces and staircases of terraces extending over ~80 m topographical extent demonstrate a long-term lowering of these rivers over time that has been punctuated by episodes of sediment aggradation. The Ñorquincó – Chubut confluence, which preserves a complex multiple phase tributary fan, has migrated laterally across an ~8 km downstream extent of the Chubut producing an extensive and complex tributary fan draining the Río Ñorquincó. This fan terrace staircase has either formed through several stages of incision lowering through the terrain, or more likely through cycles of incision and aggradation. Further downstream, the confluence of the Gualjaina and Chubut valleys also spans a significant downstream extent (6 km) of the Río Chubut, and so it is likely that the Gualjaina-Chubut confluence has also migrated over time.

Terraces that correspond in elevation and broadly form a pattern that parallels the long profile gradient of their respective valleys are interpreted as fragments of the same former fluvial surface (Gilbert, 1877; Schumm, 1977; Bull, 1991; Maddy, 1997; Kiden and Törnqvist, 1998). For the Río Chubut catchment, some of the terraces grouped by elevation (TG 1, 2 and 4) span multiple tributaries. TG1 is the highest group of multi-valley terrace fragments and assumed to be the oldest, positioned ~60-70 m above the modern river profile. The floodplain then lowered by ~20 m to TG2 at ~40-50 m, before lowering again by ~30 m to the lowest and proposed youngest multivalley terrace level, which is TG4 at ~10-20 m. Terrace staircases such as these could form over long timescales as a result of tectonic and/or climate drivers (Bridgland and Westaway, 2014; Pazzaglia, 2019). In the case of the Río Chubut, both drivers are possible given the isostatic and climate changes associated with glacial-interglacial cycles and tectonic uplift in the Andes Mountains over the Late Cenozoic (Caldenius, 1932; Ramos and Ghiglione, 2008). Deciphering these drivers requires tighter constraints on the topographical relationships, more detail on the stratigraphy associated with the terraces and a robust geochronology for the evolution of this fluvial landscape. Isolated terrace fragments situated in the sequence above TG4 lack a regional coherence, but also probably reflect episodes of aggradation in

the long-term terrace sequence of the Río Chubut. TG4 is the highest elevation and earliest group of features in the sequence, which has a catchment-wide expression as an alluvial terrace and reflects regional change (Fig. 3.2). TG5, TG3 and TG6 are not represented on the catchment scale, which could be due to a lack of preservation in other tributaries, or more localised drivers that caused the aggradation and/or incision in the respective valleys.

Previous mapping of the upper Río Chubut basin identified five levels of gravel reviewed by Martínez and Coronato (2008). In order of elevation, they are named: the Martín, Blancura, Fita Michi, Cabaña and Confluencia Formations (Volkheimer, 1963). The lowest four gravel levels have been most recently interpreted as glaciofluvial outwash from the Pleistocene, and the highest level has been interpreted as Piedmont deposits from the eastern slopes of the Andes (González Díaz, 1993a,b; González Díaz and Andrada de Palomera, 1996). The Martín, Blancura and Fita Michi Formations are higher than the terraced deposits presented here, however, the Cabaña and Confluencia formations overlap with the higher-level terraces >10 m. The high-resolution satellite imagery and the STRM 30 m DEM facilitated a higher precision to the mapping and analysis of elevations, which has led to the Confluencia formations in the Gualjaina valley to be divided here into nine stepped terrace levels. Furthermore, the grouping of the terrace fragments here, in some cases, contradict the elevation succession originally presented by Volkheimer (1963). For example, the top of the terrace staircase in the Gualjaina valley is labelled as the higher Cabaña formation, where in fact the large terrace fragment on the opposite side of the valley is higher in elevation despite being labelled as the lower Confluencia Formation. It is important to note that it is not known whether these terraces are of erosional or aggradational origin so, whilst the relative timing of terrace formation is assumed to decrease in age with elevation, the relative age of the sediment deposits may not decrease with elevation. It is not ruled out that older gravel deposits have been exposed at lower elevations from progressive valley incision without interruption of aggradational phases. Additionally, these formations could be strath terraces capped with gravel, but the lack of bedrock exposure means this not confirmed (see Chapter 2.3).

### 3.4.3 Lower-level valley features

Lower-level terraces and floodplains that are set inside the extensive reach below the TG4 terrace comprise features much closer in relative elevation, and within 3 m of the contemporary river. The terrain preserves more subtle fluvial features than the higher elevation catchment terraces. The study reach is flanked by hillslopes

sustaining Badlands-style landscapes where extensive gully networks supply ephemeral drainage to the Río Chubut during rainfall/snowmelt events and contribute sediment to alluvial fans that flank the valley. Inactive tributaries, especially the one sourced from a former lake, supplied water in the past to the Río Chubut catchment outside of the eastern extent of the Andes. The inactive, lake-fed tributary grades to the Río Gualjaina TG4 terrace level and suggests synchronicity between channel activity and the TG4 surface. The channels of the two remaining inactive tributaries (fed by precipitation run off) connect to the valley floor, which indicates that these have been active more recently. However, as satellite imagery only supplies a snapshot of the landscape at a single time, it cannot be determined if these inactive tributaries are abandoned features or are ephemeral systems sustaining flow with more substantial rainfall. It is possible that the inactive tributary fed by former lake outflow is/was active during period(s) of sustained increased precipitation to fill the lake sufficiently to feed into the Río Gualjaina tributary.

Across former floodplain and active surfaces, there is better preservation for the more recent surfaces of more subtle features like scroll bars and palaeochannels. In contrast, these features for older surfaces are more subtle and difficult to identify and map within the resolution of the remotely-sensed data. Braided palaeochannels located on a surface ~3 m above the contemporary river preserved at six locations revealed a change in planform from an earlier braided regime to the contemporary meandering system. Skirrow et al. (2021) dated this time-transgressive planform change to between 12.3 ± 1.0 ka and 9.4 ± 0.8 ka, which was associated with a weakening and southward shift in the mid-latitude storm tracks and westerlies at this time, bringing drier conditions across the headwaters.

The wide accommodation space and flat expanse of the floodplain at site CHUB6 preserves single thread palaeochannels, where the channels appear to have been abandoned through avulsion. An indication of how well-established channel belts are before being abandoned by avulsion is inferred from the development of scroll bars and density of meander cut-offs through abandoned channel belts. One channel belt displaying an anastomosing planform shows this channel planform was driven by different dynamics; specifically, low energy flow and minimal sediment transport through a floodplain substrate that is resistant to erosion and are key features in anastomosing systems (e.g. Cooper Creek (Nanson et al., 1986), the Diamantina River and others in the Channel Country (Nanson et al., 1988), Austrailia). It is not clear if this channel was part of the sequence of avulsions or if it formed a subsidiary channel sourced from the upstream wetland area. At site CHUB6, this ‘spaghetti bowl’

nature of the planform of paleochannels represents a mobile system operating in a flood basin (Bridge, 2003; Lewin et al., 2005; Ashworth and Lewin, 2012). Other features common to flood basins include the presence of extensive wetlands abundant at site CHUB6 and the evaporative lake (salt pan) near to the Río Gualjaina-Chubut confluence (Bridge, 2003; Lewin et al., 2005; Ashworth and Lewin, 2012).

The contemporary channel, floodplain and immediate terraces all display a well-established meandering system that has developed as a series of broader expanse flood basins separated by narrower sections of the valley. The sediment connectivity within the contemporary regime has not been characterised and mapped fully in this research. The present channel is largely single-thread and meandering in planform, though mid-channel bars and islands often correspond to localised areas with greater sediment supply (e.g. input from unstable banks or via tributary alluvial fans) (Hooke, 2003). The sediment deposits available for entrainment from older fluvial deposits include braided gravels composed of lithologies typical of the catchment and headwaters (Skirrow et al., 2021). The scroll bar morphology reflects lateral migration of meanders with point bar progradation through lateral erosion. Numerous abandoned meanders show processes of chute and meander neck cut-off leading to the abandonment of meander bends (Hooke, 2004); all integral processes of a mature meandering river (Charlton, 2008). Terracing of the meandering reaches show that some incision has occurred within this regime, though they are not widely separated in elevation.

### 3.5 Conclusion

The wide accommodation space typically >2 km has facilitated excellent preservation of multiple high level terrace fragments in the Río Chubut and its tributaries: the Río Ñorquincó, Río Gualjaina and Río Leca. Regional coherence to the elevation of fluvial surfaces (terraces) demonstrated a series of aggradation and incision phases in the history of the catchment that potentially spanned more than one glacial cycle. Of these terraces, six broad elevations were identified, three of which span more than one valley indicating a regional coherence and forcing of these phases of accretion and incision. Poor preservation or depiction of subtle surface features like channel planform inhibited assessment of the fluvial dynamics associated with these older surfaces. The more recent, lower-elevation valley features preserved more subtle fluvial features that revealed more detail about the fluvial dynamics, demonstrating a shift from a braided to meandering regime to between 12.3 ± 1.0 ka and 9.4 ± 0.8 ka, as well as a well-established mature meandering planform for the contemporary river. Palaeochannels indicated that key meandering processes (e.g. lateral meander

migration and channel cut-offs) were present along the study reach, in addition to processes characteristic of flood basins (e.g. whole-sale avulsion of the channel belt, endemic wetland and evaporitic lake (salt pan) formation).

**Software**

Landforms were mapped in Esri ArcGIS version 10.6 and additional formatting was carried out using Inkscape.

**Acknowledgments**

The authors would like to thank the landowners Señor Don Manuel and Señor Pascini for granting access to their land, and Laura and Daniel and Mirador Huancache, Gualjaina for their hospitality and local knowledge. This project was supported by a Natural Environment Research Council Doctoral Training Scholarship [NE/L002469/1].

# Chapter 4

## A chronology for the La Pampas Formations: Late MIS 5 and MIS 2 sandur deposits in the Río Chubut Valley (~42˚S) Argentina

This chapter looks deeper into the higher-level terrace framework that was described in Chapter 3 to understand the environmental drivers that caused the aggradation of these features (Research Question 2). Sedimentological evidence informs the type of depositional and transportation processes that characterised the aggradation of the higher-level terraces and associated tributaries (Objective 2.2) and luminescence dating is applied to understand the palaeoenvironmental conditions at the time of aggradation to investigate the environmental drivers that caused the formation of these higher-level terraces (Objective 2.2 and 2.3). These higher-level terraces represent large-scale (catchment), long-term (millennial) switches between aggradational regimes caused by glaciofluvial outwash, and incisional regimes caused by isostatic uplift and/or changes in water supply.

Grace. K. Skirrow, Rachel. K. Smedley, Richard. C. Chiverrell

To be submitted to Journal of South American Earth Sciences

**Abstract**

The origin of the extensive gravel sheets known as 'La Pampas' in the Chubut province in Argentina have been a source of debate since the pioneering field mapping by Caldenius (1932) until the early 2000s. Five levels of gravel mantles, successively decreasing in elevation (and assumed age) in an easterly direction are named from highest to lowest: the Martín, Blanura, Fita Michi, Cabaña and Confluencia Formations. Recent studies have suggested that the highest level, the Martín Formation, was a product of piedmont fluvial processes, but the lower and more easterly levels were attributed to glacial outwash. Geomorphological correlation to Late Cenozoic glacial advances have led to the tentative dating of these deposits, however, no formal geochronological methods have been applied to any of these formations. In this study, we present two new luminescence ages of a gravel deposit from the Cabaña Formation and a lower elevation gravel deposit that post-dates the Confluencia Formation in the Río Chubut valley. Our chronology shows that the top of the La Pampas Formations here were aggrading at 85.4 ± 7.8 ka (Late MIS 5) and the lower elevation Confluencia Formations in the valley had been deposited prior to

17.8 ± 1.4 ka (Late MIS 2). A re-evaluation of the younger Formations of the original La Pampas framework shows a more accurate sequence in the Río Gualjaina valley for the Cabaña and Confluencia Formations. More locally, we record a lowering of the river level by ~58 m over ~68 ka that was punctuated by periods of stability or aggradation.

### 4.1 Introduction

The Río Chubut drains a complex headwater region of ~32,000 km$^2$ (~41.3-43.6˚S) and flows ~800 km east (71.2-65.1˚W) from the Andes Mountains to the southern Atlantic Ocean (Fig. 4.1). Throughout the Quaternary, the Río Chubut headwaters have been subject to numerous glacial-interglacial cycles which changed the dominant drivers to the Río Chubut river system (Rabassa et al., 2005). During periods of glacial advance, the Río Chubut headwaters were occupied by outlet glaciers from the Patagonian Ice Sheet and drained meltwater to the Río Chubut (Glasser et al., 2008; Hein et al., 2009; Smedley et al., 2016). Glacial periods flooded the headwater valleys to form large proglacial lakes, which drained to the Río Chubut (Coronato et al., 2004, Glasser et al., 2008; Davies et al., 2020; Leger et al., 2021a). Glacial retreat saw lower elevation drainage pathways exposed to the west causing a decoupling of lakes from the Chubut catchment as they drained into the Pacific Ocean (Caldenius, 1932; Thorndycraft et al., 2019; Skirrow et al, 2021). Consequently, the Río Chubut in its contemporary state is a catchment dominated by snowmelt and run-off. Moraines suggested to be from the Great Patagonian Glaciation (GPG) in the headwater valleys of the Río Esquel and Río Corintos show that the headwaters of the Río Chubut have been influenced by glacial drainage for multiple glacial-interglacial cycles (Caldenius, 1932 and Flint and Fidalgo, 1968, González Díaz and Adrada de Palomera, 1996, Coronato et al 2004).

Extensive accumulations of gravel are situated at the flanks and foothills of the Andes in the Chubut Province, extending out into the Patagonian steppe, are known locally as ‘La Pampas’. Martínez and Coronato (2008) summarise the discussion to date on the origin of these deposits. Extensive gravel Formations are observed in five levels, at successively lower elevations in an easterly direction and have been assigned the names: Martín, Blancura, Fita Michi, Cabaña and Confluencia Formations. The La Pamapas Formations have been tentatively assigned to successive glaciations from the Great Patagonian Glaciation, but no formal chronological constraints exist. Their formation was attributed to piedmont fluvial processes in the 1960s-1980s (Volkheimer, 1963, 1964, 1965; Volkheimer and Lage, 1981; Lage, 1982 as cited in Martínez and Coronato, 2008), but more recent studies have interpreted the gravel

sheets to be of glaciofluvial origin apart from the Martín Formation which is interpretated as the product of piedmont fluvial processes (González Díaz, 1993a, b; González Díaz and Andrada de Palomera, 1996 as cited in Martínez and Coronato, 2008). Panza (2002) studied the more distal Formations located in the Río Chubut Valley (Cabaña and Confluencia) and attributed a glaciofluvial origin to these sediments. These were later mapped and classified as sandar (Glasser et al, 2008; Davies et al., 2020). Some deposits have been observed to be geomorphically connected to glacial features suggesting that they formed at a similar time. For example, the Blancura Formation has been linked to the GPG (Caldenius, 1932; Mercer, 1976; Martínez, 2002) due to its geomorphological connection to glacial till, whereas the Cabaña and Confluencia Formations have been spatially linked to known glaciofluvial features of the last glaciation (Miró, 1967). Chronostratigraphy and geomorphological interpretation has led to the estimation of the timing of deposition for the La Pampas, but formal geochronological dating does not yet exist.

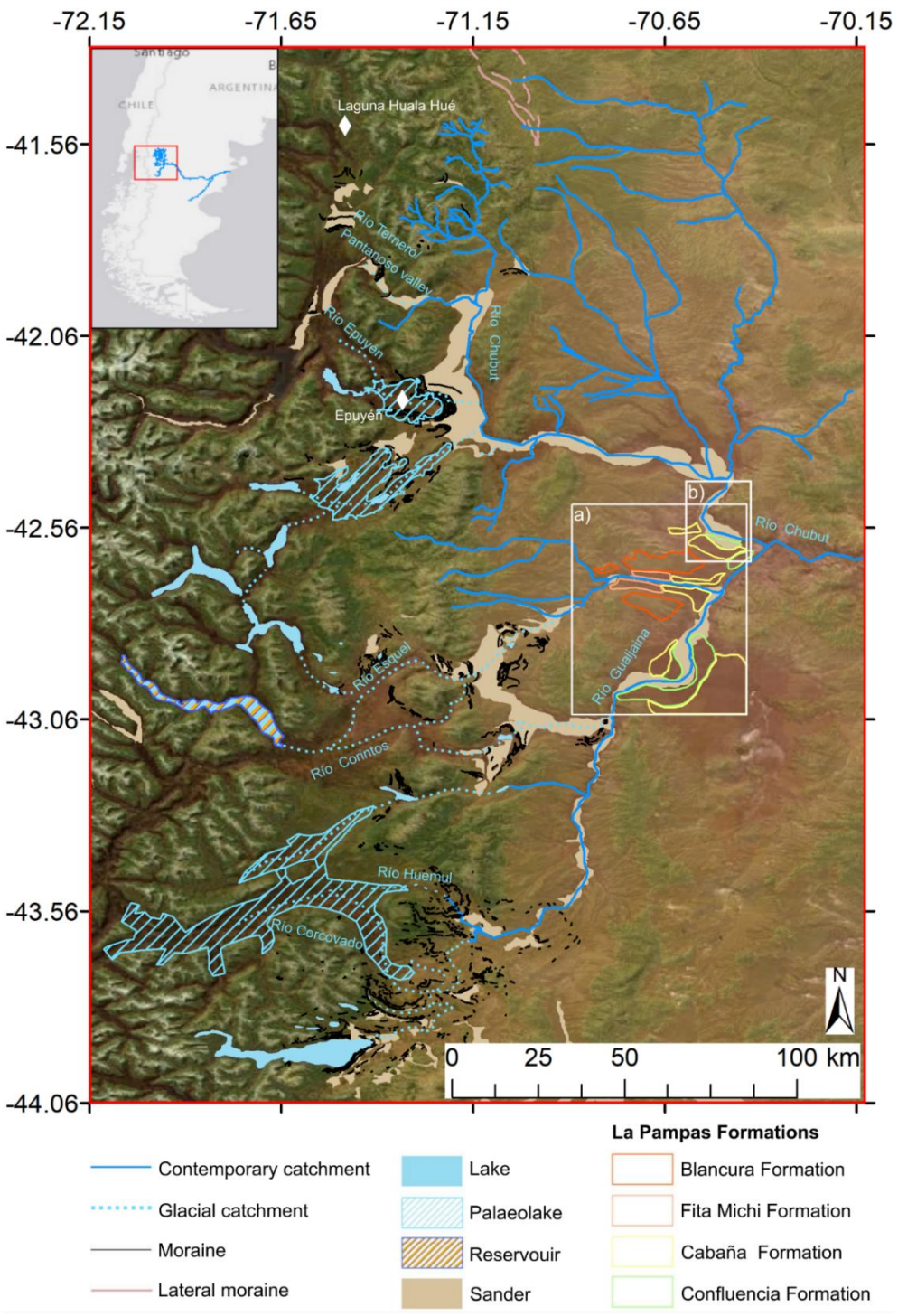


Figure 4.1. The Río Chubut catchment highlighting key differences between the contemporary catchment and former drainage pathways (Skirrow et al., 2021). White box a) marks the boundary of the maps published by Martínez et al (2008) which identify La Pampas Formations located in the Rio Gualjaina and Rio Chubut valleys. White box b) shows the study area (Fig. 4.2). Paleolake extents, Moraines and Sandur features are mapped after Leger et al., (2020) and Davies et al., (2020). White diamonds indicate places of interest cited in this paper. The basemap comprises translucent elevation imagery (STRM 30 m DEM) draped over the ESRI World Imagery Layer sourced from Maxar (Vivid, 21/03/2015).

Patagonia is recognised globally for its preservation of glacial features, in places spanning multiple glacial-interglacial cycles dating back to the Middle-Late Pliocene (Rabassa et al., 2005; Davies et al. 2020). The connecting area east of Lago Buenos Aires (46˚S, 71˚W) preserves moraines and glaciofluvial outwash from the GPG (~1.1 Ma; Springer et al., 2004), MIS 8 (~260-270 ka; Hein et al., 2017), MIS 6 (from 150±30 ka to ~110±20 ka ; Smedley et al., 2016), MIS 3 (from ~34±6.1 ka to ~30.8±5.7 ka; Smedley et al., 2016) and MIS 2 (from ~26.2±1.6 ka to ~14.7±2.1 ka; Smedley et al., 2016). The moraines and glaciofluvial outwash deposits preserved at Lago Pueyrredón constrain glacial advances from the GPG (1211±36 ka; Hein et al., 2011), MIS 15 (~600±20 ka; Hein et al., 2011), MIS 8 (~260 ka; Hein et al., 2011), the Last Glacial Maximum (LGM) (27-25 ka; Hein et al., 2010) and four subsequent advances between 23 and 17 ka (Hein et al., 2010). Lago Belgrano preserves moraine evidence of MIS 5 (~75 ka; Mendelova et al., 2020a) and the LGM (Wenzens, 2005), but beyond this, MIS 5 is poorly constrained throughout Patagonia because of the more extensive glacial advances of the last glaciation (Hein et al., 2017; Mendelova et al., 2020a). The extents and timing of the Local LGM of the Patagonian Ice Sheet is well constrained, and records show that the ice sheet reached it maximum in MIS 3, most likely between 47 ka and 30 ka across most of the region (Davies et al., 2020) prior to the global LGM, which occurred between 23 ka and 19 ka (Hughes et al., 2013).

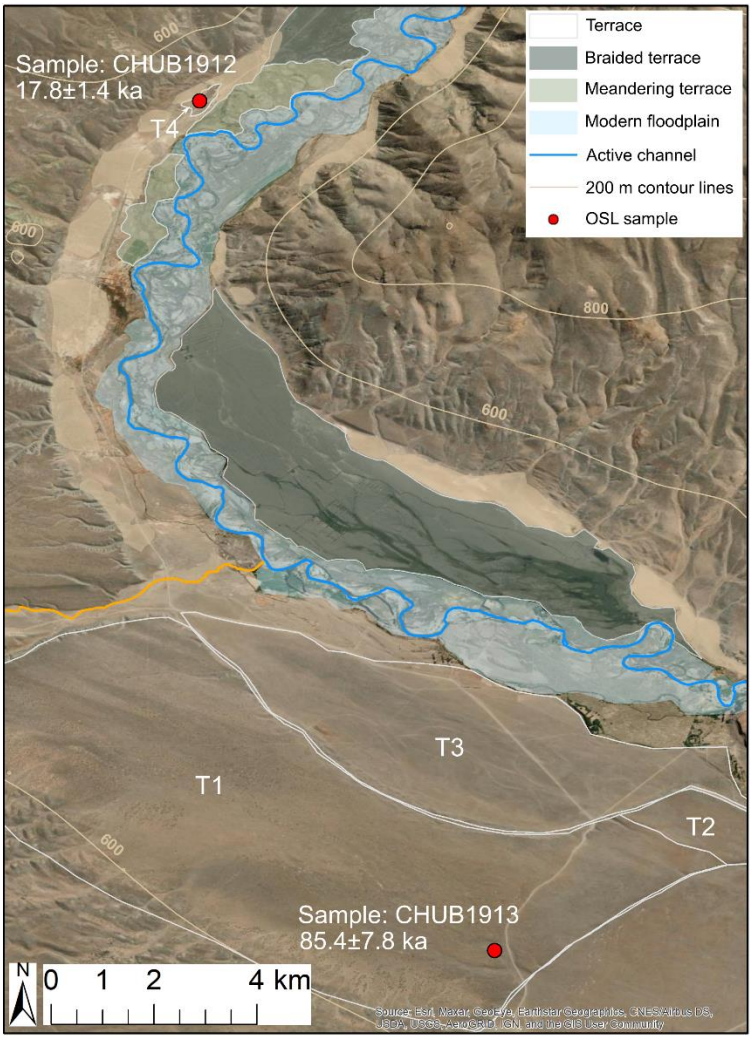


Figure 4.2. Location and age of luminescence samples in the context of valley terraces and the lower-level geomorphology (original maps by Skirrow et al., submitted).

This study presents new luminescence ages which constrain the timing of ~50 m of valley incision and the deposition of two glacial outwash deposits in the Río Chubut Valley which correspond the Cabaña and Confluencia Formations of the regional La Pampas gravels (Fig. 4.2). The new ages allow the development of gravel terraces associated with the La Pampas to be contextualised within the palaeoenvironmental and glacial conditions at that time.

## 4.2 Methods

### 4.2.1 Gravel deposit observations

The gravel deposits were initially identified in the field on the periphery of the Río Chubut valley as the sedimentology was notably different to the modern floodplain and the low-level terraces. The deposits were described, photographed, and their location was recorded using a handheld global positioning system (GPS) (~5 m

accuracy). The spatial extents and relative elevation profiles of the high-level terrace framework in the Río Chubut and tributaries - including the gravel deposits sampled here - were recorded using geomorphological mapping in the Geographic Information System (GIS), ArcMap (version 10.6) which are presented in Skirrow et al. (submitted) (see Chapter 3). Lower-level terraces, including the deposit represented by sample CHUB1912, were not included in the elevation analysis of the terrace framework as the 16 m vertical accuracy of the Shuttle Radar Topography Mission (SRTM) 30 m digital elevation model (DEM) could not resolve the low-lying topography. Topographical data for terrace level T4 (in the lower-level valley) was measured using a 30 cm resolution DEM to observe the topographical relationship between terrace level T4 and the wider terrace framework. High resolution DEMs were generated for small fragments of the lower-level valley and floodplain by collecting georeferenced imagery from an unpiloted aerial vehicle (UAV) and using structure from motion software (Agisoft Metashape version 1.6) to generate 30 cm resolution DEM imagery (~5 cm accuracy). Relative elevation values are quoted as approximations to account for the unique surface profiles of each terrace compared to the downstream profile of the modern thalweg.

Sediment samples were collected at terrace level 1 and 4 for laboratory grainsize analysis by quantifying the proportion of grainsize classes from very fine sand to large pebbles. A sub-sample of 200 g of each sample was dried and sieved at 300 µm to separate larger clasts. Grains smaller than 300 µm were sieved at 90 µm (very fine sand), 125 µm (fine sand), 150 µm (fine sand), 180 µm (fine sand), 225 µm (fine sand) and 250 µm (medium sand). Grains larger than 300 µm were classified individually into 2-4 mm (small granule), 4-8 mm (large granule), 8-16 mm (Small pebble), 16-32 mm (medium pebble) and 32-64 mm (large pebble). Composition of sediment grainsize is expressed as a percentage weight of the total sample weight.

### 4.2.2 Luminescence dating

Luminescence dating measures the time that has elapsed since a body of sediment was last exposed to sunlight (see Smedley (2018) for a review). More specifically, it is constraining the time that has elapsed since the samples were deposited and covered by overlying sediment; thus, shielded from sunlight. The samples dated here represent the time at which the respective alluvial surfaces were actively aggrading sediment. Limitations on sample accessibility and sampling equipment meant that the upper and lower boundaries of the sediment units could be not sampled, so the onset and termination of aggradation on these surfaces were not constrained. Grains of quartz and potassium (K) feldspar are globally ubiquitous and, thanks to their

composition, have the capability to accumulate a luminescence signal at a constant rate over time and store it within the crystalline structure of the grain. The natural isotopic decay of Uranium (U), Thorium (Th), Potassium (K) and Rubidium (Rb) with contributions from cosmic rays, emit electrons which become trapped at defect sites in the crystalline structure of the grain. This signal accumulates steadily over time until the trapped electrons are stimulated by sunlight, heat, or pressure at which point the electrons are emitted as photons. The process of resetting the luminescence signal of a grain is termed bleaching. If a grain is considered to have been well bleached prior to burial, its signal has been reset to zero, whereas grains with partially-bleached luminescence signals are the result of insufficient exposure to sunlight prior to burial. To measure a luminescence age, the total luminescence signal is measured in the laboratory and calibrated against known laboratory doses; this is termed the equivalent dose ($D_e$). The $D_e$ is then divided by the dose-rate ($D_r$), which is constant over time, to determine an age.

Table 4.1. Environmental dose-rate results for sedimentary samples taken from terrace level 1 (sample CHUB1913) and terrace level 4 (sample CHUB1912) along the Río Chubut study reach. ICP-MS was used to determine concentrations of K, U and Th. Dose-rates were calculated using the conversion factors of Guerin et al. (2011). Dose-rate attenuation factors were applied for alpha and beta dose-rates after Bell (1980) and Guerin et al. (2012) respectively. An Internal K-content of 10 ± 2% was used to determine the internal dose-rates. Alpha dose-rates were calculated using an a-value of 0.10 ± 0.02 (Balescu and Lamothe, 1993). Cosmic dose-rates were determined after Prescott and Hutton (1994). Water contents were estimated following laboratory measurements; water contents were estimated at 0 ± 2 % for both samples. grain size used for analysis was 180-250 µm for both samples. Environmental dose-rates were determined using the Dose-rate Age Calculator (DRAC; Durcan et al., 2015)

| Sample | Latitude (°S) | Longitude (°W) | Depth (m) | U (ppm) | Th (ppm) | K (%) | Internal dose-rate (Gy/ka) | External alpha dose-rate (Gy/ka) | External beta dose-rate (Gy/ka) | External gamma dose-rate (Gy/ka) | Cosmic dose-rate (Gy/ka) | Total dose-rate (Gy/ka) |
|---|---|---|---|---|---|---|---|---|---|---|---|---|
| CHUB1912 | -42.49175 | -70.54481 | 0.9 | 1.5±0.2 | 7.9±0.8 | 1.7±0.2 | 0.92±0.17 | 0.11±0.02 | 1.53±0.15 | 0.92±0.07 | 0.28±0.03 | 3.74±0.24 |
| CHUB1913 | -42.64062 | -70.49322 | 1.5 | 1.6±0.2 | 5.2±0.5 | 1.8±0.2 | 0.92±0.17 | 0.09±0.02 | 1.55±0.15 | 0.83±0.06 | 0.27±0.03 | 3.65±0.24 |

Samples CHUB1912 (-42.49175, -70.5448) and CHUB1913 (-42.64062, -70.49322) were collected in the field by hammering a light-tight tube horizontally into the targeted sediment unit. Coarse, unsorted sediment meant hammering was not always successful and; we found that wiggling the tube into the sediment whilst maintaining forceful contact with the vertical face to be an effective adaptation, termed scrumbling (Rhodes Pers. Comms. 2019). Field water contents (expressed at a percentage) were measured from bulk sediments in the laboratory and is considered to be

representative of the entire burial period. Internal dose-rates were estimated K-content of 10 ± 2% (after Smedley et al., 2012) and U and Th concentrations of 0.3 ± 0.1 ppm and 1.7 ± 0.4 ppm, respectively (after Smedley and Pearce, 2016). The alpha values were estimated using an a-value of 0.10 ± 0.02 (after Balescu and Lamothe, 1993). Environmental dose-rates were calculated from the U, Th and K concentrations, measured from bulk sediment using inductively coupled plasma mass spectrometry (ICP-MS). Environmental alpha, beta and gamma doses were calculated using conversion factors by Guerin et al (2011) and alpha (Bell, 1980) and beta (Guerin et al., 2012) attenuation factors. Cosmic dose-rates are calculated from the global position (latitude and longitude), elevation and burial depth (after Prescott and Hutton, 1994). Environmental dose-rates were calculated using the Dose-rate Age Calculator (DRAC; Durcan et al, 2015) and are shown in Table 4.1.

The application of luminescence dating to fluvial sediments is often characterised by partial bleaching of the luminescence signal (see Smedley and Skirrow, 2020 for review). However, by analysing single grains, partially bleached grains can be identified within the sample and the age calculated can be based only on those grains that were well bleached prior to burial (e.g. Smedley and Skirrow, 2020). The infra-red stimulated luminesce signal (IRSL) in K-feldspar was the chosen for luminescence dating in this study as quartz in Patagonia has been found to be dim in previous studies (e.g., Blombin et al., 2012; Smedley et al., 2016, Mendelova et al., 2020b). Additionally, the wavelength of infra-red light (which preferentially bleaches the luminescence signal of K feldspar) is less likely to be attenuated in a turbid water column compared to the shorter wavelengths that bleaches the optically stimulated (OSL) signal of quartz (Jerlov, 1970; Krongborg, 1983; Sanderson et al., 2007).

Bulk sediment samples were processed in the laboratory to isolate sand-sized grains of K-feldspar. Dry bulk samples were sieved at 300 µm and then wet sieved at 90 µm to remove excess material. Given the course nature of the samples, the coarsest grainsize (suitable for luminescence dating) was selected to maximise sample size for analysis so dry sieving was carried out to isolate grains between 180 µm and 250 µm. Chemical treatments of hydrochloric acid (10%) and hydrogen peroxide (10%) were applied to remove carbonate and organic matter, respectively. No etching with hydrofluoric acid was carried out after Duller (1992). K-feldspar grains were extracted from the sample using density separation with sodium polytungstate (SPT) at a density of >2.58 g $cm^{-3}$. Prepared samples of isolated K-feldspar (180-250 µm) were then mounted onto single-grain discs with a 10 x 10 grid of 300 µm diameter holes where one grain sits in each hole.

All luminescence measurements were carried out using a Risø TL/OSL DA-15 automated single-grain reader equipped with a $^{90}Sr$ beta source and focussed infra-red (IR) laser (Bøtter-Jensen et al., 2003). A single aliquot regenerative dose (SAR) protocol (Murray and Wintle, 2000) was used with a post-IR IRSL protocol (Thomsen et al., 2008) to measure the $D_e$ values for each of the grains. A stimulation temperature of 225˚C was used as the inherent bleaching rates were likely more efficient at this temperature in comparison to stimulating at 290°C, and more consistent between grains (Smedley et al., 2015). Samples were preheated for 60 s, followed by IRSL measurements at 50˚C for 100 s with IR light emitting diodes (LEDs). A test dose of 35 Gy was used. A high temperature bleach was performed at 290˚C for 200 s to remove any remaining signal at the end of each measurement cycle. Location of the discs was carried out at room temperature, rather than elevated temperatures, to mitigate thermal annealing of the IRSL signal (after Smedley and Duller, 2013). Integration limits were set for the initial 0 – 0.3 s and the background signal (1.2 – 2.0 s). $D_e$ values were accepted based on the following screening criteria accounting for the associated uncertainties: (1) recycling ratio limit (10%), (2) maximum test dose error (10%), and (3) natural test-dose signal more than 3 sigma above background.

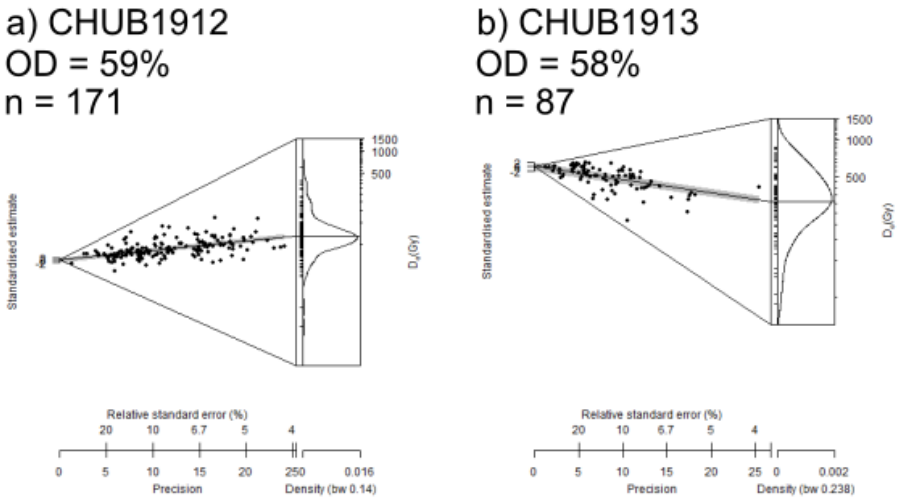


Figure 4.3. Abanico plots showing the distribution of $D_e$ values measured for each sample. The grey line shows the CAM $D_e$ value (±1σ). Also shown is the number of grains giving $D_e$ values for each sample.

Dose recovery and residual dose experiments showed that the SAR protocol was appropriate for the analysis of these samples where an intrinsic overdispersion value was measured to be 22 ± 0.01% for sample CHUB1913. Anomalous fading is a

process that can impact upon some K-feldspar samples whereby the IRSL signal depletes over time athermally, without exposure to light (Wintle, 1973). Fading measurements were carried out using three multiple-grain aliquots following the procedure of Huntley and Lamothe (2001) with a maximum time delay of 10 hours and a given dose of 35 Gy. G-values (normalised to 2 days) were calculated from the weighted mean and the standard error for each sample and were found to be consistent to that of quartz (Thiel et al., 2010). Therefore, these samples are considered not to have been subject to anomalous fading. The high $D_e$ value for sample CHUB1913 presented the possibility that the luminescence signal of some grains could be approaching saturation or saturated, whereby burial continues after the available electron traps in grains are filled, meaning that the luminescence signal ceases to grow. If the luminescence signal is saturated, the $D_e$ values determined for those grains does not reflect the burial age as it is underestimated. $D_e$ values are considered unreliable if it is $>2D_0$ (Wintle and Murray, 2006), although it is important to note that this limit is somewhat arbitrary. For sample CHUB1913, the ratio of $D_e$ values to $2_{D0}$ was 0.5 ± 0.3 and so this sample was not deemed to be saturated. The measured $D_e$ values for both samples are presented in abanico plots (Fig. 4.3). The central age model (CAM) was used for both samples (sample CHBUB1912 and CHUB1913) because the distribution of $D_e$ values was symmetrical; thus, considered to be well bleached before deposition and burial, or that the proportion of scatter in the $D_e$ distribution caused by partial bleaching prior to burial was small in comparison to the dose accumulated throughout burial.

## 4.3 Results

### 4.3.1 Sediment description

Both terrace deposits studied here were characterised as poorly-sorted, gravel-dominated deposits with a coarse-sand matrix. The ~60 m gravel deposit (sample CHUB1913) was overlain with a sharp boundary by a unit (~50 cm) of sediment that reflected the same clast characteristics as the lower unit, but the matrix was consolidated with finer grained material (making it impossible to sample with the equipment available). Both samples had limited exposure to the in-situ sediment as scree slopes covered much of the vertical faces. The lower-level gravel deposit (sample CHUB1912) was massive and had no visible stratification of sedimentary units. Cobble-sized clasts were less frequent than gravel but present in both deposits (Fig. 4.4 and 4.5). Grainsize analyses of bulk sediment samples in the laboratory do not include cobble clasts due to transport limitations, but still reveal that the deposits comprised quite different grainsize assemblages. Sample CHUB1913 was comprised

of 96% of gravel; the matrix, characterised by medium and small pebbles, and supports frequent clasts of large pebbles. This sediment unit is considered to be poorly sorted because of the variety of gravel grainsizes between 4 and 32 mm. Sample CHUB1912 was also comprised mostly of gravel (83%), particularly large pebbles (41%). This sample contained a greater fraction of sand in its matrix (17%) compared to sample CHUB1912 (4%) and is considered to be very poorly sorted given the greater distribution of grainsizes in its composition (90 µm – 32 mm) (see supplementary material; Fig. S1). Both samples were characterised by rounded to well-rounded clasts with a mixture of low and high sphericity (Fig 4.4 and 4.5). Both samples also contained mixed lithologies that was identified from the variation of colours and textures amongst the grains, and igneous rocks were frequent in both samples.

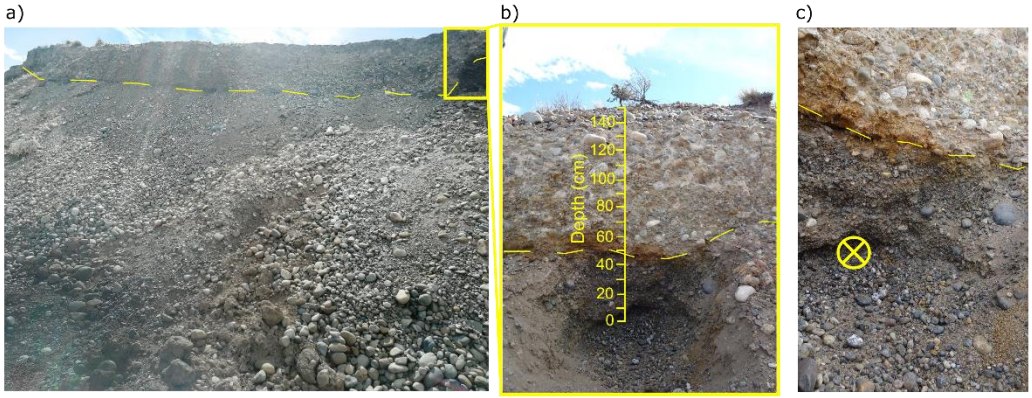


Figure 4.4. Field photographs of the location of sample CHUB1913. The yellow dashed lines indicates the sharp boundary between sedimentary units, while the yellow crossed circle indicates the sampling location for luminescence dating and grainsize analysis.

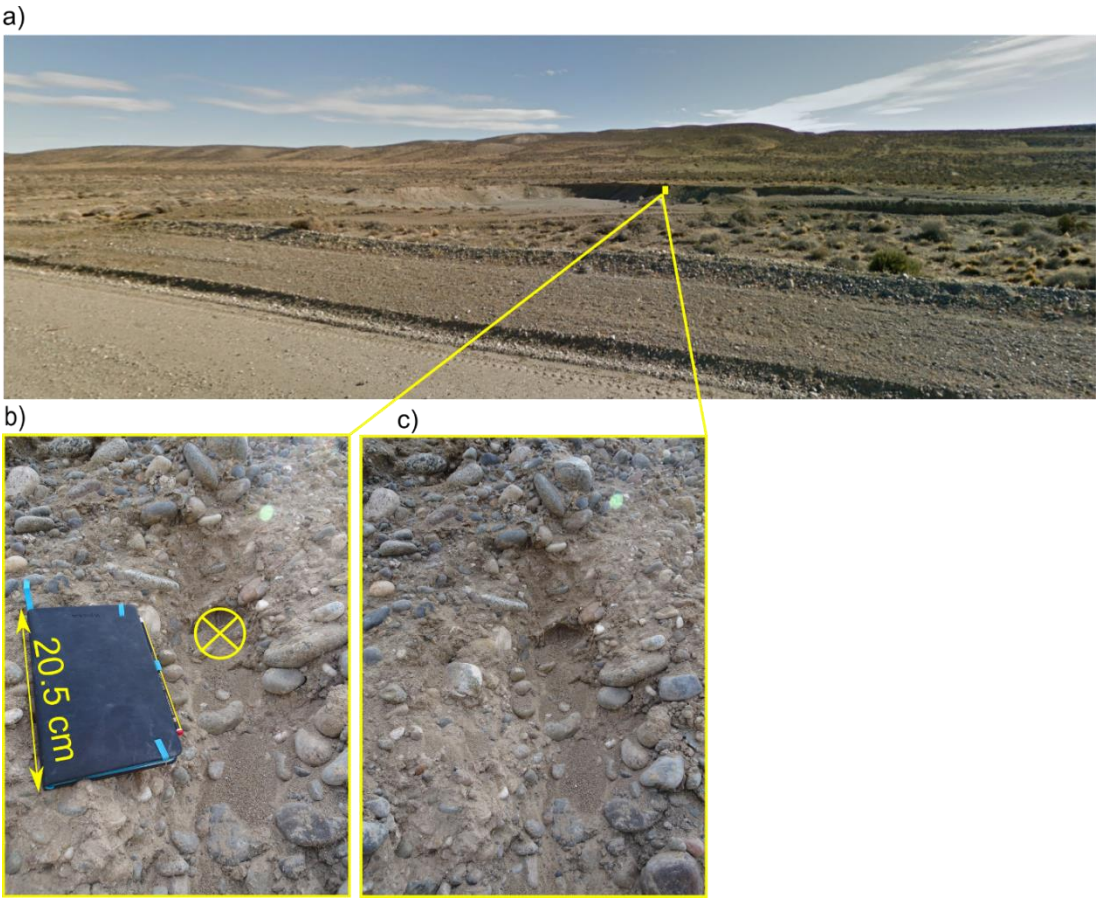


Figure 4.5. Field photograph of the location of sample CHUB1912. a) Image sourced from Google Street View [Image capture: May 2014], shows wider location of sample site in a small quarry on the periphery of the Río Chubut valley. b) shows the sample location (with notebook pictured for scale) where the yellow crossed-circle indicates the location of samples for luminescence dating and grainsize analysis. c) A photograph of the in-situ sediment around the sample site.

### 4.3.2 Terrace levels

The addition of elevation data for Chubut T4 to the Río Chubut valley terrace framework (Skirrow et al., submitted) shows a difference in elevation of ~55 m between terrace levels T1 and T4 (Fig. 4.6). The river lowered by ~21 m from the highest terrace level T4 (~59 m above the modern river) to aggrade to terrace level T2 (~38 m), the river then lowered by ~29 m to aggrade to terrace level T3 (~9 m) and then lowered by ~5 m to aggrade terrace level T4 (~4 m; measured from the DEM with 30 cm resolution).

### 4.3.3 Luminescence dating

The luminescence ages constrain the timing of the latest (accessible) deposition on this fluvial surface (CHUB1912 and CHUB1913). Deposition forming the gravel deposit located in the lower-level Río Chubut valley (CHUB1912) was active during

the end of the last glaciation at 17.1 ± 1.4 ka. The ~59 m gravel deposit (T1) was actively aggrading sediment at 85.4 ± 7.8 ka, between Marine Isotope Stage 5a (82 ka; peak interglacial sub-stage) and 5b (87 ka; peak glacial sub-stage) (Lisiecki and Raymo, 2005).

Table 4.2. Luminescence dating results for sedimentary samples taken from terrace level 1 (T1; sample CHUB1913) and terrace level 4 (T4; sample CHUB1912) along the Río Chubut study reach. The *g*-values (%/decade) were measured for three aliquots of K-feldspar per sample using the $pIRIR_{225}$ signal, were normalised to 2 days and are presented as weighted means and standard errors. The number of grains used to determine the $D_e$ (n) are presented as a fraction of the total grains measured (N). The CAM was used to determine the $D_e$ for both samples because they showed symmetrical distributions deemed to have been well bleached. The $\sigma_b$ value (0.3) was estimated by combining overdispersion from internal and extrinsic sources in quadrature.

| Sample | Total dose-rate (Gy/ka) | g-value (%/dec.) | n/N | Overdispersion (%) | Age model chosen | $\sigma_b$ | $D_e$ (Gy) | Age (ka) |
|---|---|---|---|---|---|---|---|---|
| CHUB1912 | 3.74±0.24 | -0.8±0.9 | 171/1000 | 59 | CAM | 0.31 | 66.4±3.1 | 17.8±1.4 |
| CHUB1913 | 3.65±0.24 | 1.6±0.9 | 87/1000 | 58 | CAM | 0.31 | 311.5±20.4 | 85.4±7.8 |

## 4.4 Discussion

The poorly sorted and rounded nature of the sediments comprising terrace levels T1 and T4 suggest turbid, high-energy, fluvial transport with abundant exposure to attrition. The sand and gravel grainsize indicate that these sediments were transported through traction and saltation in the bed load of the river systems. The Río Chubut glacial history and the geomorphological relationship to the moraines and sandur deposits of the glaciers formerly occupying the Río Epuyén (42.2˚S) and Río Ternero/Pantanoso (42.0˚S) valleys, mean that the origin of the dated deposits is interpreted as glaciofluvial outwash. These sediment descriptions match those of existing studies (González Díaz and Adrada de Palomera, 1996; Panza, 2002; Martínez et al., 2014) who also conclude a glaciofluvial origin to the sediments comprising the La Pampas Formations in the Río Chubut headwater region. Furthermore, mapping by Glasser et al., (2008) and Davies et al., (2020) also report extensive sandur deposits in the Río Chubut valley and La Pampas region.

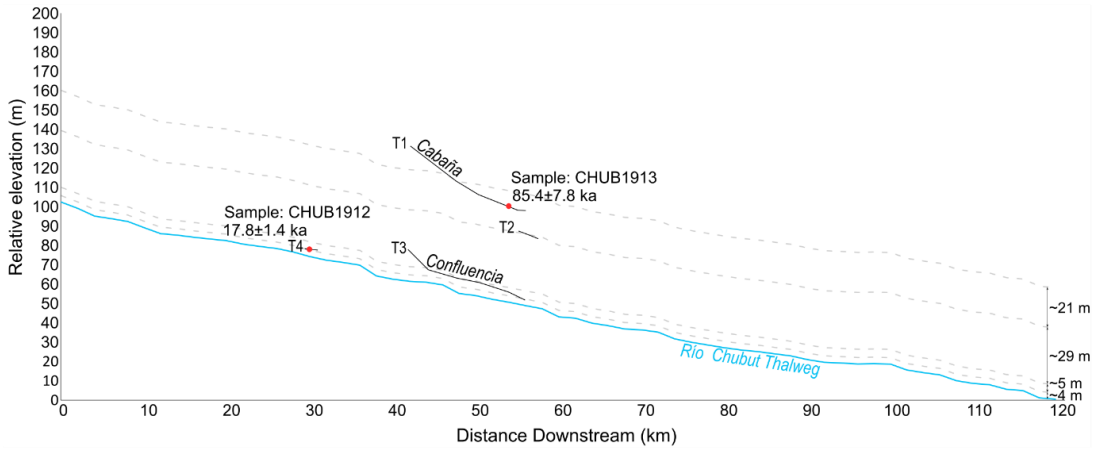


Figure 4.6. Relative terrace elevation inferred from downstream profile of the modern river thalweg (75 km study reach) after Skirrow et al. (submitted), Elevation data for terrace level T4 measured from 30 m DEM. Cabaña and Confluencia annotations indicate the terraces characterised as La Pampas formations (Volkheimer, 1963, 1964 and 1965).

The Río Chubut valley is considered an underfit valley whereby the river once operated on a much larger scale in order to carve the valley it now flows through (Thorndycraft et al., 2019). The high elevation terraces in the Chubut valley and tributaries (Skirrow et al., submitted) are relics from a point in time where the river operated >60 m above the modern channel. The chronology presented here shows that the lowering of the river level by ~55 m occurred over ~68 ka between MIS 5b, prior to onset of the last glacial (85.4 ±7.8 ka) and during the last deglaciation of MIS 2 (~17.8±1.4 ka) (Fig. 4.6). The two preserved terrace levels in the Chubut valley between these geochronological markers (T2, ~40 m and T3, ~8 m) indicate former switches between aggradation and incision (Fig. 4.6). The chronology indicates that the terraces were aggradational rather than erosional forms because the younger deposit is situated lower in the valley and was therefore, aggraded after the incision that led to the abandonment of the older T1 terrace level. Terrace level T1 forms part of the catchment terrace group TG1 presented in Skirrow et al. (2021) where terrace fragments that broadly follow the downstream profile of the modern river were grouped as fragments of the same fluvial surface (Fig. 4.7). Broad age constraints are applied to the Río Chubut and tributaries terrace framework whereby terraces higher than the ~60-70 m terrace group (TG1) were older than 85.4±7.8 ka and those lower were constrained to between 85.4±7.8 ka and 17.8±1.4 ka (Fig. 4.7).

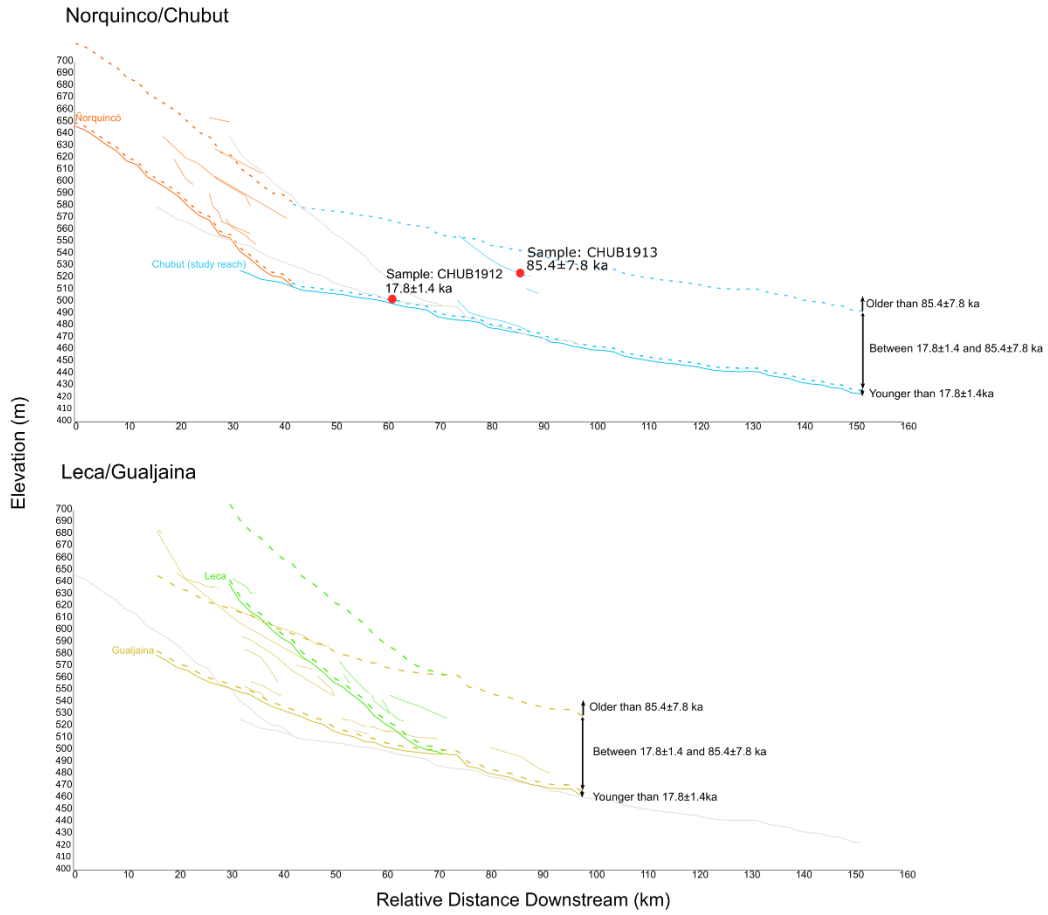


Figure 4.7. Suggested depositional age constraints for the Río Chubut and Tributaries higher-level terrace framework (Skirrow et al., submitted).

Terrace levels T1, T2 and T3 have been described previously as part of the extensive La Pampas gravel sheets and were considered part of the glaciofluvial Confluencia (T3) and Cabaña (T1) Formations (Volkheimer, 1963, 1964, 1965). Correlations of the geomorphology to glaciofluvial outwash deposits in Cordón El Maitén led to suggestions that these deposits formed during the last glacial (Miró, 1967). However, our chronology shows that terrace level T1 (part of the Cabaña Formation) was still aggrading >10 ka prior to the onset of the last glacial period, in the later stages of MIS 5 (Lisiecki and Raymo, 2005). No direct dating of the Confluencia Formation in the Río Chubut was carried out but dating of the T1 and T4 terrace levels constrained the formation of the T3 Confluencia deposit in the Río Chubut valley to between 17.8±1.4 ka and 85.4±7.8 ka (i.e. last glacial period or late MIS 5). It is plausible that Isostatic uplift was a factor in the abandonment of higher-level terraces at the end of the last glaciation as ice retreated from the region and the land rebounded; ~130 m of uplift is estimated to have occurred since ~18 ka at Palena (43˚S) (Leger et al., 2021b),

hence similar uplift nearby in the Río Chubut headwaters could have occurred impacted the study site.

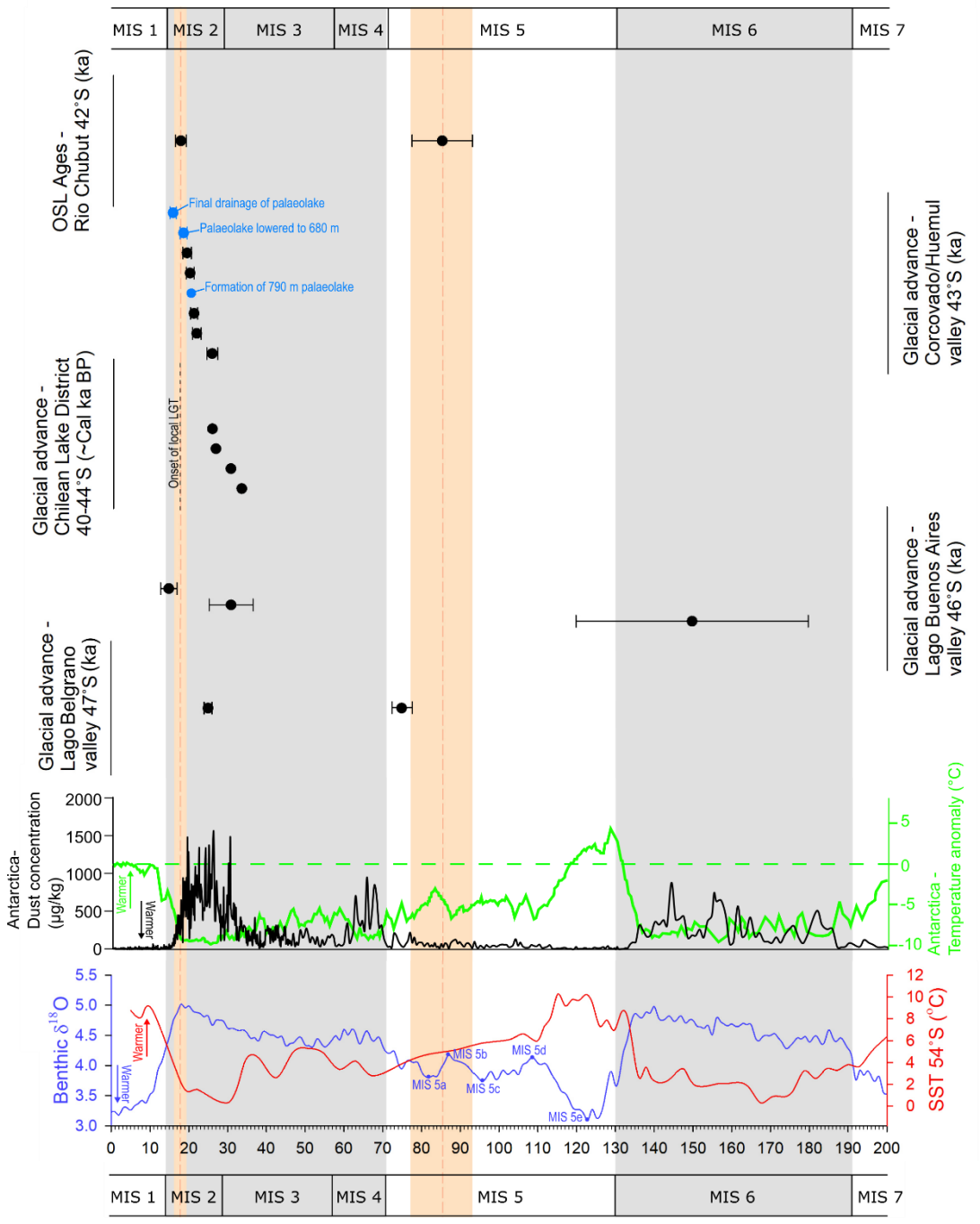


Figure 4.8. Luminescence ages representing glaciofluvial outwash aggradation plotted alongside the cosmogenic nuclide ages for ice margins in the Corcovado valley (Leger et al., 2021a) Chilean Lake District (Moreno et al., 2015), and Lago Belgrano (Mendelova et al., 2020a (age errors quoted in Mendelova et al., 2020b)) and the Luminescence chronology for Ice margins at Lago Buenos Aires (Smedley et al., 2016). Palaeoenvironmental records including the dust record (Dust abundance correlates with colder conditions) (Lambert et al., 2008) and temperature anomaly reconstruction (Jouzel et al., 2007) from the EPICA Dome C

Ice Core, Antarctica show climatic variability on millennial timescales over the last two glacial cycles. Global ice volume and Sea surface temperature reconstructions were sourced from the Benthic $\delta^{18}O$ marine stack (Lisiecki and Raymo, 2005) and marine core PS75/034-2 from the Pacific sector of the Southern Ocean (Ho et al., 2012), respectively. Grey, vertical bars indicate glacial periods, peach dashed lines indicate the OSL ages presented in this study and the peach vertical bars mark their error range.

The dating of terrace level T4 in this study focusses on a locality upstream of the confluence with the Río Gualjaina, and so the aggradation of sediments here was fed by the northern reaches of the complex headwater catchment. The new ages for the glaciofluvial outwash deposit comprising terrace level T4 suggests that the river was still affected by glacial outwash by 17.8±1.4 ka, post-dating the final advances recorded in the Belgrano Valley, Chilean Lake District and the Río Corcovado/Río Huemul valleys (Fig. 4.8). There are few records constraining the timing of deglaciation in the headwater valleys of the Río Chubut, however, this timing coincides with the last glacial terminus observed in the Chilean Lake District (~17.8 cal. ka BP), whereafter the ice sheet in this region retreated (Moreno et al., 2015; Fig. 4.8). Laguna Huala Hué in the Río Manso valley (Fig. 4.1) is situated in the northern reaches of the Río Chubut headwaters. The lake basin was exposed when the valley deglaciated and the palaeoenvironmental record demonstrates that the ice had retreated from the valley by 13.5 cal. ka BP (Iglesias et al., 2012). Geomorphological mapping of the Lago Epuyén Valley shows that a proglacial lake formed when the Epuyén glacier retreated from its maximum (Coronato et al., 2004). The formation of proglacial lakes interrupts the drainage regime and traps inflowing glacial sediment; thus, prohibiting the aggradation of sandur. Although glacial lake drainage would mobilise and potentially redistribute sediments present within the fluvial system, it is possible that there was still a land-terminating ice lobe at Epuyén when the T4 terrace level was aggrading, but the numerous valleys feeding the Río Chubut means that this cannot be confirmed without further chronological and geomorphological investigation. Records from the south of the catchment contrast this narrative as the Río Corcovado and Río Huemul proglacial lake(s) (Fig. 4.1) (formerly draining into the Río Gualjaina tributary) were formed ~3 ka earlier (Leger et al., 2021; Fig. 4.8). The asynchrony of changes to the Río Chubut headwater valleys demonstrates the variability and sensitivity of localised valleys to widespread climate change such as the end of the last glaciation. The transition in the Río Chubut from glacial, to lacustrine, to precipitation feeders, although directional in response to regional drivers (Skirrow et al., 2021), was likely not synchronous across the headwater catchment during the last glacial-interglacial transition.

The luminescence sample CHUB1913 constrains the later stages of aggradation of terrace level T1 as the unit was sampled as close to the upper boundary as possible, so we infer that aggradation of this surface began prior to 85.4±7.8 ka and the overlying 1.5 m of sediment aggraded afterwards. The overall thickness of the T1 deposit is unknown as scree slopes concealed most of the sediment exposure. The ~60 m elevation above the modern river is not an indication of sediment thickness in this instance as there is likely bedrock higher than the modern river over which the T1 deposit is draped (as incision into the bedrock is observed elsewhere in the valley). Paleoenvironmental records for MIS 5 are poorly preserved for the Patagonia region because of the more extensive glacial advances of MIS 2 and 3 (Zech et al., 2011; Moreno et al., 2015; Leger et al 2021a), which restricts our understanding of the conditions existing when terrace level T1 was deposited. However, the T1 terrace level was an actively aggrading sandur surface at 85.4±7.8 ka, which indicates that the Río Chubut was fed predominantly by glacial drainage at this time; a challenging concept when the sea surface temperature difference between the aggradation of terrace level T4 and T1 is equal to ~50% of the total sea surface temperature range between the LGM and the onset of the Holocene (Fig. 4.8). Possible explanations for the timing of this aggradation include firstly that the Patagonian Ice Sheet could have been occupying the headwaters at this time supplying the Chubut catchment with glacial meltwater and outwash sediment. Despite the persistently warmer conditions throughout the last interglacial compared the last glacial, there was a cooler phase during MIS 5b where summer insolation and $\delta^{18}O$ were comparable to the warmest phase of the last glacial period (Fig. 4.8). It could be that glaciers were able to establish in the headwaters of the Río Chubut around the cooler peak of MIS 5b. Although MIS 5 records are uncommon in Patagonia, there is evidence of an MIS 5 glacial advance in the Belgrano valley (47.6˚S) (Mendelova et al., 2020a) at ~75 ka. This advance occurred ~10 ka later than the glaciofluvial aggradation in the Chubut valley and was interpreted as glacial advance during the early stages of the last glacial (Mendelova et al., 2020a).

Alternatively, the deposition of glacio-fluvial outwash could have been initiated by a land terminating glacier injecting meltwater and sediment into a river (Slaymaker, 2009), where paraglacial adjustment can occur for millennia after deglaciation and glacially-derived sediments (now decoupled from their source) continue transportation downstream. Braided, sandur systems can persist until the available glacial sediments are exhausted and the river reaches its interglacial regime (Ballantyne, 2002). It could also be that the basal sediments of the terrace levels T1

and T4 deposits represent active glacial drainage to the Río Chubut. However, paraglacial adjustment could have transported the glacial outwash downstream to its current position after decoupling from the ice sheet. A study of the post-glacial regime and planform shift around the onset of the Holocene by Skirrow et al., (2021) demonstrated that paraglacial adjustment in the Río Chubut was dependent upon sustained water supply from climate systems such as the southern westerlies and mid-latitude storm tracks. The southward shift of the southern westerlies around the onset of the Holocene led to a decrease in water supply (Whitlock et al., 2007; Markraf and Huber, 2010; Moreno et al., 2010; Iglesias et al., 2016), which lessened the competency of the Río Chubut leading to the abandonment of the paraglacial braided planform for a lower energy meandering planform (Skirrow et al., 2021). The position of the southern westerlies and mid-latitude storm tracks has not been constrained for MIS 5 at the latitude of the Río Chubut catchment. Alternatively, a 120 ka dust record from 27˚S reconstructs relative aridity near the Atacama desert (Stuut and Lamy, 2004), however, the northerly position of this record means it is not latitudinally representative of the Chubut catchment (~41.3-43.6˚S).

The phase of glacial advance that initiated the deposition of the terrace level T1 deposit is unknown because of the lack of glacial records prior to the last glacial and the inaccessibility of the basal sediments for dating. It is possible that the causal glacial advance occurred during the MIS 6 glaciation and paraglacial adjustment persisted through the MIS 5 interglacial. Observations from the last glacial-interglacial transition shows that paraglacial sandur is dependent on sustained water supply from key climate drivers in the headwaters of the Río Chubut (Skirrow et al., 2021) – particularly the southern westerlies - and so this scenario implies that sufficient precipitation was sustained for at least ~45 ka after the end MIS 6 to sustain the sandur river regime. Contrary to this, MIS 5 is characterised by climatic variability as evidenced by the Antarctic ice core records including dust (Lambert et al., 2008) and temperature anomaly (Jouzel et al 2007) reconstructions (Fig. 4.8), but conclusive precipitation reconstructions for MIS 5 at this latitude have not been recorded. An alternative, shorter-term, scenario could be that glacier expansion occurred during a cooler peak of MIS5 (as discussed above) and paraglacial adjustment followed up to and after 85.4 ± 7.8 ka. However, the similarity in timing of the MIS 5b peak and the dated aggradation on terrace level T1 do not account for millennial timescale paraglacial adjustment, however, it can be accounted for by the multi-millennia scale uncertainties associated with the luminescence ages. The lack of access to basal sediments means that we cannot constrain the timing of the ice advances that initiated

the aggradation of these deposits, but we can constrain periods in time when these surfaces were aggrading.

Glaciofluvial outwash fans that are geomorphologically linked to moraines and proximal to former ice limits have been favoured over moraines for constraining the age of pre-LGM glacial advances and still stands across Patagonia (Hein et al., 2009; 2011; 2017; Smedley., 2016; Mendelova et al., 2020a; Leger et al., 2021a) to overcome the challenges associated with dating older moraine deposits (Hein et al., 2009; Thrasher et al., 2009). The glaciofluvial outwash identified in terrace level T1 and T4 are ~ 75 km and ~90 km downstream of the nearest former ice front at Epuyén and are not in direct contact with moraines or associated with a specific glacier. Whilst the timing of ice advance in particular valleys cannot be constrained from these distal deposits, the study reach reflects a regional signal from the headwaters, including water/sediment supply systems and climate drivers. When applied to the palaeoenvironmental context, the evidence from these deposits shed light on the timing of preferential drainage from land-terminating glaciers to the northern Río Chubut headwaters between 41.4˚S and 42.3˚S.

### 4.5 Conclusion

Luminescence dating constrains the timing of sediment deposition of Terrace level 1 (T1) and Terrace level 4 (T4) to 85.4 ± 7.3 ka and 17.8 ± 1.4 ka, respectively. It places the lowering of the river level by ~55 m over ~68 ka to between 85.4 ±7.8 ka (Late MIS 5, prior to onset of last glacial) and 17.8±1.4 ka (Late Glacial) where the Río Chubut incised and aggraded four terrace levels at ~59 m (T1), ~38 m (T2), ~9 m (T3) and ~4 m (T4). Sedimentary observations of the gravels in terrace level T1 and T4 agree with existing studies that these are of glaciofluvial origin. Two of the Chubut valley terraces correspond to the Cabaña (T1) and Confluencia (T3) Formations, previously undated but were interpreted to have formed in the last glaciation. Our luminescence chronology suggests that the top of the Cabaña Formation in the Río Chubut (T1) was actively aggrading ~10 ka prior to the onset of the last glacial period, in the later stages of MIS 5, but the basal sediments of this terrace level may have begun aggrading prior to this. The lower glacial outwash deposit preserved at terrace level T4 was active at 17.8±1.4 ka suggesting that the northern Río Chubut catchment could still have been dominated by glacial drainage at this time.This post-dates the final advances recorded in the Belgrano valley, Chilean Lake District and the Río Corcovado/Río Huemul valleys. The findings of this study show that the higher-level terraces in the Río Chubut valley preserve evidence of fluvial and glacial conditions from the poorly understood late glacial in the northern headwaters and from the

regionally poorly understood MIS 5. The upper-middle course of the Río Chubut has previously been sensitive to large-scale, long-term changes in the headwater region, which were driven by former expansions of the Patagonian Ice Sheet.

**Acknowledgements**

The authors extend their thanks to the landowners for granting permission to their land including Señor Don Manuel and Señor Pascini, and to Laura and Daniel at Mirador Huanache, Gualjiana for their hospitality and local knowledge. We are grateful to Dr. Martínez for sharing his expertise on the La Pampas Region, Dr. Geiger and Dr Ferri for their assistance in locating locally available literature, Dr. Olive for her efficient ICP-MS measurements and to Mr. Fitter his assistance enhancing photographs for this manuscript. This research is supported by a Natural Environment Research Council Doctoral Training Scholarship [NE/L002469/1].

*"Her name is Rio and she dances on the sand,*
*just like that river twisting through a dusty land" – Duran Duran*

# Chapter 5

## Planform change of the Río Chubut (~42°S, ~70°W, Argentina) in response to climate drivers in the southern Andes.

This Chapter investigates environmental drivers of the braided to meandering planform shift that was identified from geomorphological evidence in Chapter 3 (Research Question 3). Luminescence dating constrains the timing of this shift in river regime (Objective 3.1) which facilitate the interpretation of environmental drivers from palaeoenvironmental reconstructions (Objective 3.3). Sedimentological evidence discerns the changes in depositional environment during the waning and abandonment of the braided planform (Objective 3.2). This planform shift represents resilience of the braided planform to deglaciation of the headwaters but sensitivity to changes in water supply driven by the strength and position of the southern westerlies.

G.K. Skirrow, R. K. Smedley, R.C. Chiverrell, J. M. Hooke

Published in Geomorphology 2021

**Abstract**

The Río Chubut (southern Argentina) displays complex geomorphological and sedimentological responses to long-term variations in hydrology and sediment supply. A 75 km study reach located 65 km downstream of the former ice margin and proglacial lake (Lago Epuyen) at the foothills of the Andes shows that the river has previously undergone large-scale planform changes from a braided to a meandering regime. The new luminescence chronology presented here constrains the timing of changes in fluvial characteristics in the Chubut valley, including the waning and abandonment of a braid plain dated at four locations, the minimum age for the shift to the modern meandering regime, and the timespan of activity for an alluvial fan. Sedimentology, geomorphology and geochronology findings show that the Río Chubut maintained a braided planform during the last deglaciation until the water supply to the headwaters in the Andes decreased because the mid-latitude storm tracks and westerlies in the Southern Hemisphere weakened and shifted southwards causing drier conditions across Patagonia. This encouraged a time-transgressive

shift in the Río Chubut between 12.3 ± 1.0 ka and 9.4 ± 0.8 ka from a braided planform to the meandering system active today. These findings highlight that modern braided rivers (e.g., the Rakaia River, New Zealand) that are experiencing a reduction in discharge could be vulnerable to similar large-scale planform changes with the potential to impact upon unique habitats and ecosystems.

**Keywords:** fluvial, braiding, geomorphology, planform, luminescence dating, Patagonia, Southern westerlies

### 5.1 Introduction

Patagonia is a climatically-important land mass that is uniquely situated across a large latitudinal transect in the ocean-dominated Southern Hemisphere (Fig. 5.1). During the last glaciation, the southern Andes hosted a large ice sheet extending from 37°S to 56°S (e.g., Caldenius, 1932; Rabassa et al., 2011; Davies et al., 2020). The ice margin was largely marine-terminating in the western portion and land- or lake-terminating in the eastern portion (Glasser et al., 2008), extending to its maximum at ca. 30 ka with a volume of 597.5 x $10^3$ $km^3$ (Davies et al., 2020). Past, present and future environmental change in Patagonia is influenced by key climate systems such as the ENSO, which was weak or non-existent prior to ca. 7 ka (Moreno, 2004), and the mid-latitude storm tracks and the westerlies, which vary in latitudinal extent and intensity in response to changing meridional temperature gradients (e.g., Lamy et al., 2010). This includes the southward shift observed with anthropogenic climate change over recent decades (Swart and Fyfe. 2012, Stevenson et al., 2012, Wu et al., 2011). The recent work of Denton et al. (2021) suggest that the influence of the Zealandian Switch can induce millennial-scale climate shifts across both hemispheres as a result of changes in the southern westerlies, and was prevalent through the last glacial-interglacial transition. Large-scale climate shifts have occurred since the Last Glacial Maximum (LGM) and the terrestrial response to these is well documented in lacustrine (e.g., Iglesias et al., 2014, 2016; Markgraf and Huber, 2010; Bendle et al., 2017a; Moreno, 2004; Moreno et al., 2018, Davies et al., 2020) and glacial archives (e.g., Smedley et al., 2016; Sagredo and Lowell. 2012; Glasser et al., 2008; Bendle et al., 2017b; Hein et al., 2010, Davies et al., 2020). However, we lack any studies investigating how the large river systems draining the eastern margin of the former Patagonian Ice Sheet and the southern Andes today responded to past environmental change.

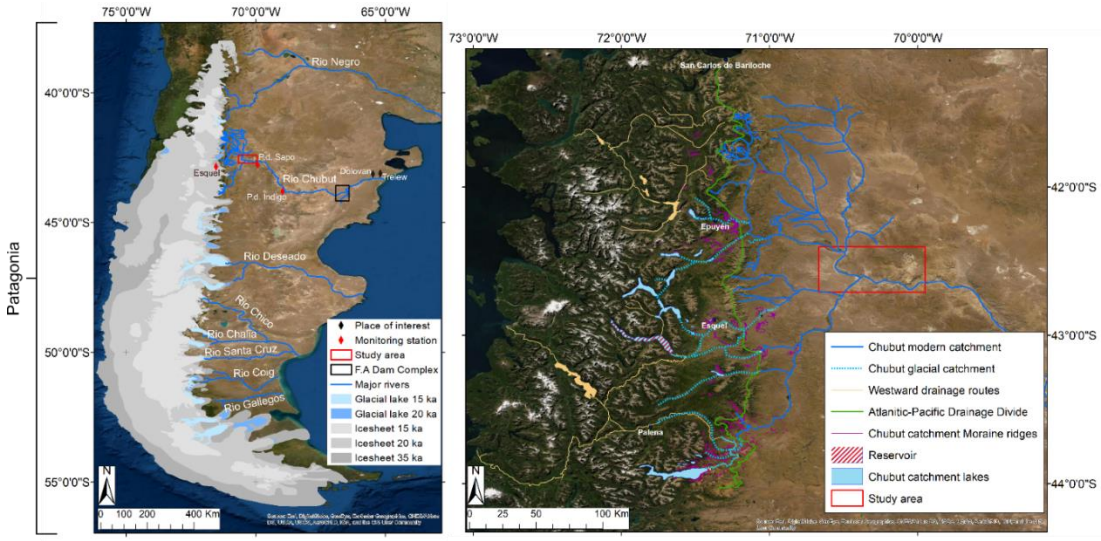


Figure. 5.1. Location of Río Chubut catchment in context of the major southern South American rivers overlain by PATICE ice sheet and glacial lake reconstructions (Davies et al., 2020). Locations of places of interest and monitoring stations mentioned in this article (left). P.d. Sapo and P.d. Indigo refer to the small settlements Paso del Sapo and Paso del Indios, respectively. F.A Dam complex refers to the Florentino Ameghino Dam Complex (left). The study reach is shown (right) in context of the wider Río Chubut catchment and the study area (red box) corresponds to the area shown in Fig. 5.2. The major tributaries of the Río Chubut are labelled (right). Moraine ridges (Davies et al., 2020 [northwest of Palena]; Leger et al., 2020 [southwest of Palena]) and Atlantic-Pacific drainage divide (southwest of Palena mapped by Leger et al., 2020) presented in context of the modern and glacial drainage regimes. The satellite imagery basemaps are from the ESRI Global Basemap (ESRI, 2009).

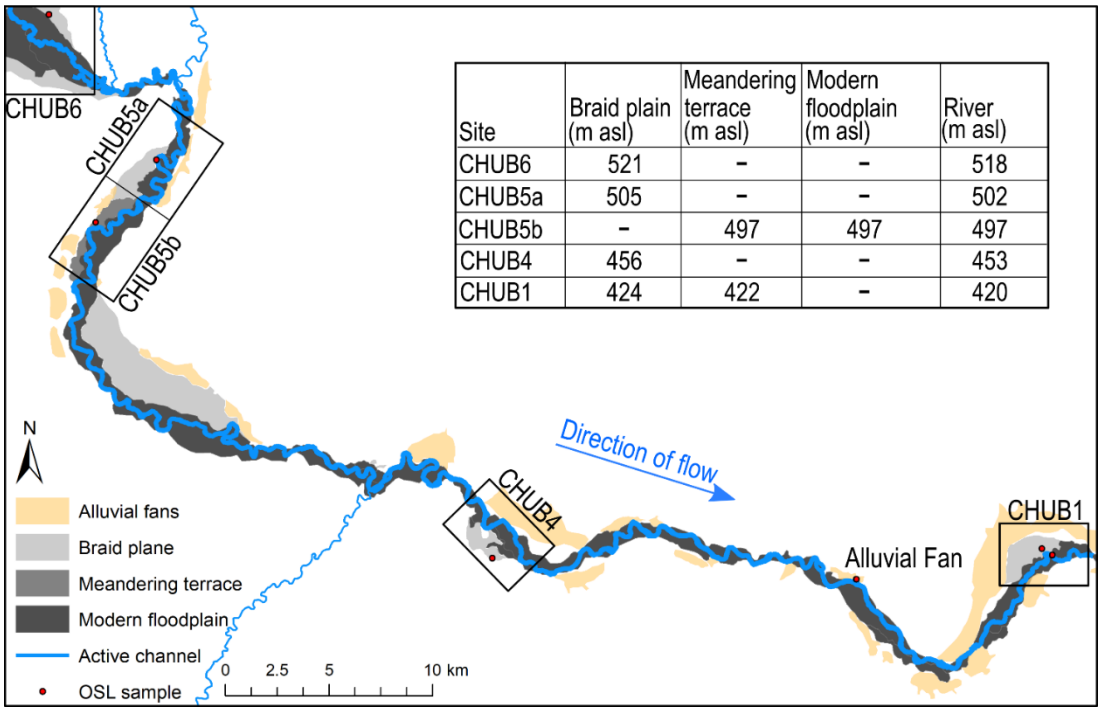


| Site | Braid plain (m asl) | Meandering terrace (m asl) | Modern floodplain (m asl) | River (m asl) |
|---|---|---|---|---|
| CHUB6 | 521 | - | - | 518 |
| CHUB5a | 505 | - | - | 502 |
| CHUB5b | - | 497 | 497 | 497 |
| CHUB4 | 456 | - | - | 453 |
| CHUB1 | 424 | 422 | - | 420 |

Figure. 5.2. Geomorphological map of the study reach along the Río Chubut demonstrating the elevation of the lower level terraces and position of alluvial fans in relation to the modern-day channel. Remote mapping scale 1:20,000 supplemented with field observations.

Eight major river systems occupy Argentina, which drain water eastward across the Patagonian steppe of Argentina and into the southern Atlantic (Fig. 5.1). During glacial periods, these rivers drained meltwater from the former Patagonian Ice Sheet and proglacial lakes. During deglaciations of the Quaternary, these rivers would have carried vast amounts of freshwater from the retreating ice sheet and injected it into the southern Atlantic, which was likely to have impacted ocean circulation similar to that of the Younger Dryas and the 8.2 ka event observed in the Northern Hemisphere (Glasser et al., 2016; Thorndycraft et al., 2019). The eastward draining river systems today (except for the Río Santa Cruz and Río Negro) are considered underfit rivers, whereby the rivers, under their current regimes, would struggle to incise the valleys in which they flow (Thorndycraft et al., 2019). The size of the valleys indicate that these rivers were previously larger and had more erosional power to carve valleys of this scale. During the last deglaciation, these rivers were subject to a variety of forcing parameters including changing climate, the decoupling from glacier input and proglacial lakes, and they experienced reversals in drainage as westward flow paths became available with ice retreat higher into the southern Andes (Garcia et al., 2014; Thorndycraft et al., 2019; Turner et al., 2005).

Rivers are sensitive to a multitude of environmental conditions including discharge, sediment supply and vegetation cover. These factors combine to dictate a sediment-water balance that influences the planform of the channel. Braided river planforms are common in glacial settings as there is a high production of sediment from glacial processes and high discharge from glacial meltwater (Malard et al., 2006). During periods of glacial retreat, more water is available to the system as the rate of ice melt is accelerated. Hydrological and sediment inputs to the major Patagonian eastern river systems underwent significant change after the onset of the deglaciation ~18 ka when the climate and environment was unstable (Moreno et al., 2015; Iglesias et al., 2016; Davies et al., 2020). As the ice sheet retreated, the headwaters shifted from being dominated by glacial and lacustrine to precipitation and snowmelt sources as the rivers decoupled from the retreating ice sheet in the Late Glacial. Studies have also suggested that some of these rivers were subject to glacial lake outburst floods during this extended period of environmental instability (Glasser et al., 2016), prior to the Atlantic-Pacific drainage reversals that occurred during the deglaciation (Garcia et al.,2014; Thorndycraft et al., 2019; Turner et al., 2005).

This study aims to provide the first chronological constraints on the fluvial response to environmental change in the eastward-draining river systems of the southern Andes (Argentina). The objectives of this study are (1) to use high-resolution mapping of the lower relief fluvial landforms to observe and record evidence of past shifts in fluvial dynamics such as planform change, (2) to study the sedimentology and stratigraphy of abandoned fluvial surfaces and floodplains to infer past changes in the depositional environment, and (3) to develop a new chronology (based on eight luminescence ages) for this sediment-landform sequence to constrain the timing of past shifts in fluvial dynamics. These data reveal the timing and environmental drivers for major changes in the fluvial evolution of the Río Chubut.

## 5.2 The Río Chubut catchment

### 5.2.1 Present-day environmental conditions

The Río Chubut (~42°S, 71-65°W) drains an area of ~32,000 km$^2$ and flows ~800 km east from the Andes, through the Patagonian steppe, to Bahía Engaño where it meets the Atlantic Ocean. The headwater vegetation is dominated by *Nothofagus* and *Austrocedrus* forests (Iglesias et al., 2012), which contrasts with the dry and sparsely vegetated steppe that dominates east of the Andes, owing to the prevailing westerly winds and precipitation and Andes rain shadow. The Río Chubut is a single channel sand and gravel-bedded wandering to meandering river, with water discharges fed by snowmelt and rainfall from the Andes to the west. In the study reach at Paso Del

Sapo (42.74083°S, 69.59472°W; station 2138, Fig. 5.1), the Río Chubut from 4/2018 to 2/2020 varied around an average annual daily maximum discharge of 29.9 $m^3 s^{-1}$, 10% exceedance of 52.2 $m^3 s^{-1}$ and maximum discharge of 75.7 $m^3 s^{-1}$ (Secretería de Infraestructura y Política Hídricia, 2018). The Río Chubut catchment displays a strong orographic rainfall gradient with mean annual precipitation in the Andean foothill headwaters of 458 mm $a^{-1}$ at Esquel (Fig. 5.1; Peterson and Vose, 1997) but much drier at 196 mm $a^{-1}$ in steppe conditions of the study reach at Paso de Indios (-43.82°S, -68.88°W, 460 m above sea level (a.s.l.), Fig. 5.1) (Peterson and Vose, 1997). Mean monthly temperature ranges increase moving downstream from 12.8°C (summer) and 4.8°C (winter) at Esquel (42.54°S, 71.18°W 655 m a.s.l.) (Lawrimore et al., 2011), to 16.7°C (summer) and 6.7°C (winter) farther east at Paso de Indios (Lawrimore et al., 2011).

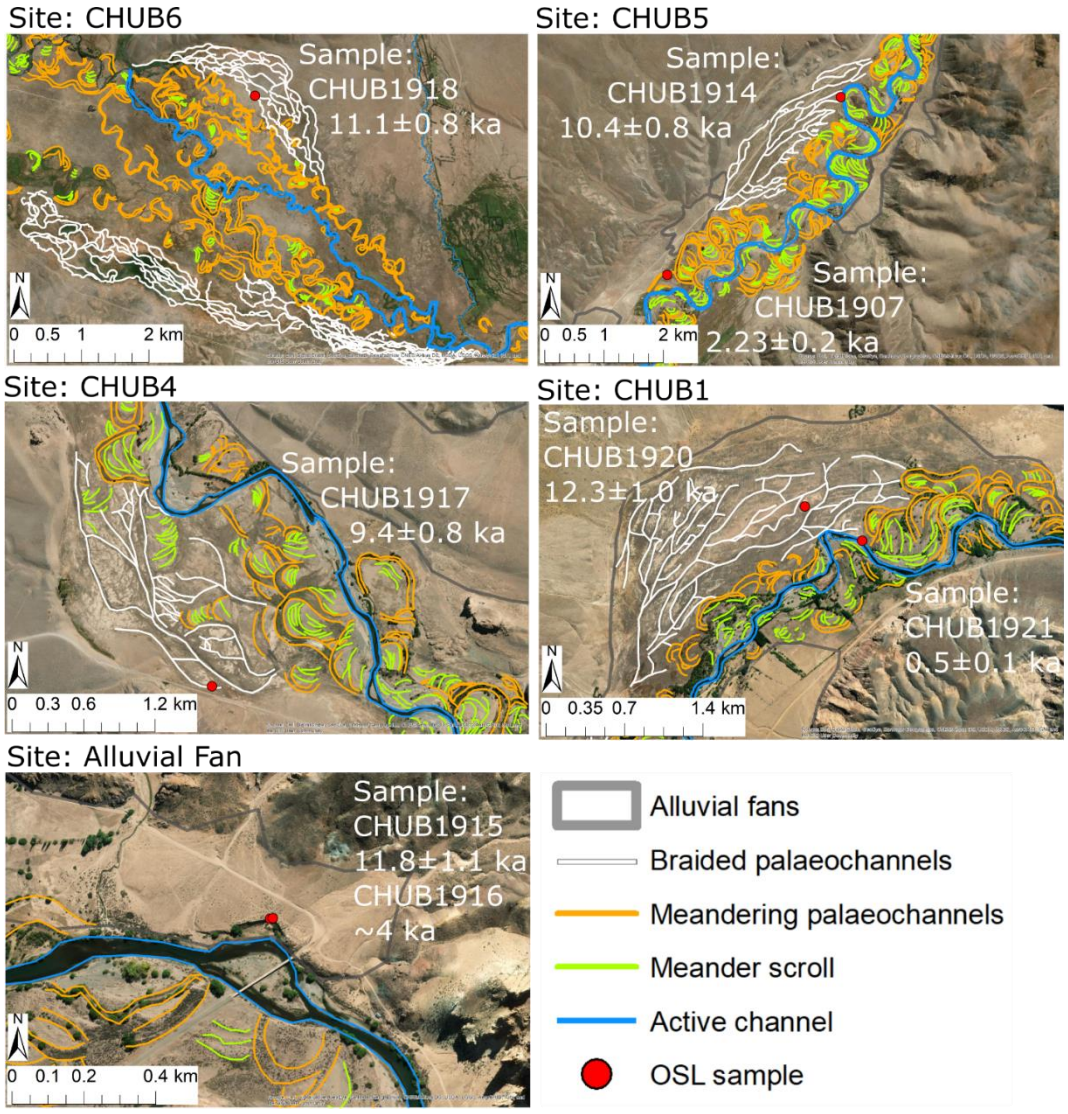


Figure. 5.3. High resolution geomorphological mapping (1:8000) identifying landforms sampled for luminescence dating, including braided samples CHUB1918 (site CHUB6),

CHUB1914 (site CHUB5), CHUB1917 (site CHUB4), CHUB1920 (site CHUB1), meandering samples CHUB1907 (site CHUB5) and CHUB1921 (site CHUB1) and alluvial fan samples CHUB1915 and CHUB1916.

The study area here is a 75 km stretch of the Río Chubut that flows through the Patagonian Steppe, beginning 65 km east of Esquel and extending downstream close to Paso Del Sapo (Fig. 5.1). The entire drainage area of the Río Chubut headwaters (~20,000 $km^2$) are encompassed in the study reach as all major tributaries join the river along this stretch. The valley comprises a badlands style landscape where the flanking slopes are excessively incised by ephemeral streams to form extensive dendritic gully networks (Fig. 5.3). Vegetation is sparse, where small, drought-tolerant shrubs occupy the floodplains and terraces, and riparian Poplar trees (*Populus*) line the riverbanks where moisture is more readily available.

The geology of the Río Chubut differs between its headwaters and the study region. Cretaceous-Tertiary volcanic, Palaeozoic intrusive and Precambrian undifferentiated bedrock dominates the northern headwaters of the river and Quaternary/Tertiary sedimentary bedrock occupies the study area (Schenk et al., 1999). The Patagonian Andes have continued to experience glacio-isostatic uplift since the last deglaciation, however, the rate of uplift north of 46.5°S is <8 mm $a^{-1}$, so the Río Chubut catchment is not subject to rapid crustal uplift during the timeframes studied here (Dietrich et al., 2010).

### 5.2.2 Headwaters and Quaternary history

The eight major river systems that drained the eastern ice margin of the former Patagonian Ice Sheet during the last glaciation mostly drained discrete catchment areas associated with a large proglacial lake or terrestrially-terminating ice lobes, e.g., Río Santa Cruz (Fig. 5.1). However, the Río Chubut has a more complex catchment that spans a large area (~32,000 $km^2$) between 41°S and 44°S where water has been sourced from multiple lakes and formerly glaciated valleys (Fig. 5.1), which changed in extent over time between glacial and interglacial cycles (e.g., Davies et al., 2020). During glaciations, the Río Chubut likely received discharge contributions from glacial meltwater and proglacial lake drainage (Fig. 5.1). The proglacial lakes that drained into the river include Lago Epuyen and Lago Palena, which each show clear drainage channels into the Río Chubut that are no longer active. A key event suggested to have impacted the tributaries of the Río Chubut was the Pacific-Atlantic drainage reversal, where the retreating ice sheet exposed lower elevation cols, which redirected the lake drainage west into the Pacific Ocean (Caldenius, 1932; Thorndycraft et al., 2019). Phases of lake drainage and drainage reversal are not yet

constrained for Lago Palena or Lago Epuyen, however, records throughout Patagonia suggest these events occurred during a period of deglaciation before the region experienced interglacial conditions (e.g., Bendle et al., 2017; Garcia et al 2019; Thorndycraft et al., 2019; Hein et al., 2010). Radiocarbon dating of geomorphological and stratigraphic markers of ice extents indicate that the deglaciation – at the same latitude as the Rio Chubut catchment – began at 17.8 ka cal. BP (Chilean lake district, 40°S - 44°S) (Moreno et al., 2015). This is supported by palaeoenvironmental reconstructions from lake records in the Chilean Lake District, which indicated that the spread of thermophilous vegetation and lake level lowering was at 17.8 ka cal. BP (Moreno et al., 2018). As definitions of the catchment area vary greatly between glacial and interglacial conditions, the catchment is termed the 'glacial catchment' when referring to the catchment under glacial conditions and termed the 'contemporary catchment' when referring to the catchment under post-glacial and interglacial conditions. Note that the change from a 'glacial catchment' to 'contemporary catchment' was potentially time-transgressive because of the complex pattern of tributaries for the Rio Chubut and multiple proglacial lakes that may have drained asynchronously.

Today, these westward drainage routes are still draining the Andes and are visible from satellite imagery (Fig. 5.1). Given the absence of glaciers and proglacial lakes after the Pacific-Atlantic drainage reversal at the end of the last glaciation, the discharge contribution of lake drainage to the Río Chubut in the contemporary catchment is negligible. The headwaters of the Río Chubut extend north towards San Carlos de Bariloche in the Río Negro province and are fed predominantly by precipitation and snowmelt runoff. In the south, the Río Chubut catchment extends as far as the Palena region, with the Río Tecka feeding the tributary Río Gualjaina, and joins the Río Chubut between two sample sites in this study, CHUB5 and CHUB4 (Fig. 5.1).

Extensive gullying in the semi-arid badland hillslopes feeds sediments to numerous alluvial fans along the length of the study reach. Flow in these gullies is ephemeral, and they primarily contribute water supply during seasonal snowmelt and in heavy local precipitation events usually associated with easterly atmospheric systems (Agosta et al., 2015; Garreaud et al., 2013). The sediments deposited in the alluvial fans have locally been eroded by the modern channel.

### 5.2.3 Human activity and land use

Eastward draining palaeochannels show that this system is part of the Río Chubut glacial catchment, but now drains west to the Pacific Ocean after undergoing a drainage reversal. Therefore, in postglacial times the Río Chubut headwaters maintained a natural discharge regime that was unaffected by the construction of dams. The Florentino Ameghino Dam is located in the lower reaches of the Río Chubut downstream of the confluence of the Río Chico (Fig. 5.1). The Río Chubut floodplain is mostly occupied by small settlements of livestock farmers and small holdings. There is evidence that the dry floodplains are periodically irrigated by farmers by building irrigation channels to divert water from the main river channel for vegetation growth. Satellite imagery shows that farther downstream, eastwards toward the coast and beyond the study area, large areas of the Río Chubut floodplains have been irrigated to support arable farming between Dolavon and Trelew. These farming practices utilising the water resources provided by the Río Chubut emphasises the reliance of local people on the river's water levels and behaviour.

## 5.3 Geomorphology and stratigraphy

### 5.3.1 Methods

The geomorphology and stratigraphy along the study area of the Río Chubut was used to identify and document any changes in planform over time. Geomorphological maps were made in ArcGIS 10.6 of the lower level valley in the Río Chubut study reach from satellite imagery from the ESRI Global Basemap (ESRI, 2009). The modern meandering system was mapped including the active channel and palaeochannels on the floodplain to a scale of 1:8000. Terraces containing suspected braided palaeochannels were identified by the characteristic multichannel planform separated by mid-channel bars and were mapped at the same scale. Satellite imagery and the ALOS PLANSAR (ASF DAAC, 2011) dataset digital elevation models (DEM) were limited in their resolution to depict smaller scale topography such as river terraces, so aerial imagery was collected from an uncrewed aerial vehicle (UAV) on site for the generation of high-resolution orthographic imagery and DEMs for the refinement of geomorphological analysis (Westoby et al., 2012). UAV surveys took place at sample sites and areas of key interest. River terraces were identified and mapped where possible along the 75 km study reach using satellite imagery to a scale of 1:20,000, localised high resolution DEMs and field observations.

Descriptions and interpretations of past fluvial changes were based on established lithofacies and sediment landform models (e.g., Miall, 1996). Regional mapping of the glacial and lacustrine features by Leger et al. (2020), Davies et al. (2020) and Glasser

et al. (2008) provide a basis for contextual interpretations of the fluvial features observed in the Rio Chubut study reach. Stratigraphic descriptions were obtained at riverbank exposures, or when augering through the floodplain to identify changes in grain size that were indicative of a changing depositional environment between higher energy and lower energy settings. Basal sediments extended below the exposure of the river bank sections and were not penetrable by the augering equipment, therefore, the thickness of the basal sediments could not be measured.

### 5.3.2 Results

Geomorphological mapping of the lower level Chubut valley identified: (1) a mature-meandering single thread modern-day river; (2) meandering palaeochannels on the active floodplain; (3) terraces ~3 m above the modern river channel displaying braided palaeochannels (Fig. 5.2); and (4) a skirt of alluvial fans that line the valley. The modern-day planform displays a mature meandering system with meander bends, scroll bars and meander cut off chute channels, as well as terraces in localised areas (Figs. 5.2 and 5.3). Field observations found a high availability of sands and gravels on the meandering floodplain and in localised terraces both on the surface and buried within the terrace stratigraphy. Vertical exposures of the floodplain and meander scrolls at site CHUB5 display a stratigraphy consisting of sand and gravel beds. One of the deposits was topped with a fine-grained massive clay/silt unit (Fig. 5.4c). Samples were taken for luminescence dating from the top of the uppermost gravel unit to constrain the timing of the most recent channel activity of a preserved meander palaeochannel. These deposits are represented by samples CHUB1907 (Fig. S7) and CHUB1921 (Fig. S8) The terraces located ~3 m above the modern river channel were found to preserve palaeochannels from past activity of the Río Chubut. These channels display a large-scale braided planform, with channels up to ~50 m wide and bars up to ~500 m wide and ~100 m in length, which differs from the modern meandering regime (e.g., Fig. 5.5). These braided terraces are found along a 75 km reach of the river and persist upstream and downstream of the tributaries, Río Ñorquincó, Río Chico and Río Gualjaina. Basal sediments of the terrace stratigraphy are rounded fluvial gravels of mixed lithology, which are graded to sand/silt deposits (~1 m thick). These fluvial sediments are overlain by a thick surface unit (up to 2.6 m) of fine-grained massive clay/silt material (identified as loess) with a sharp lower boundary (see Fig. 5.6). Samples were acquired for luminescence dating from the top of the abandoned braid plain deposits (Fig. 5.6) to constrain the most recent braiding activity in the Río Chubut study reach; this likely represents the maximum age for the transition between planforms. These deposits are represented by samples

CHUB1914 (Fig. S1), CHUB1917 (Fig. S2), CHUB1918 (Fig. S3) and CHUB1920 (Fig. S4). No luminescence samples were collected from the aeolian sediments as the grain size is too small for single-grain luminescence dating, which was essential for identifying modern contamination that may have been introduced during the sampling approach.

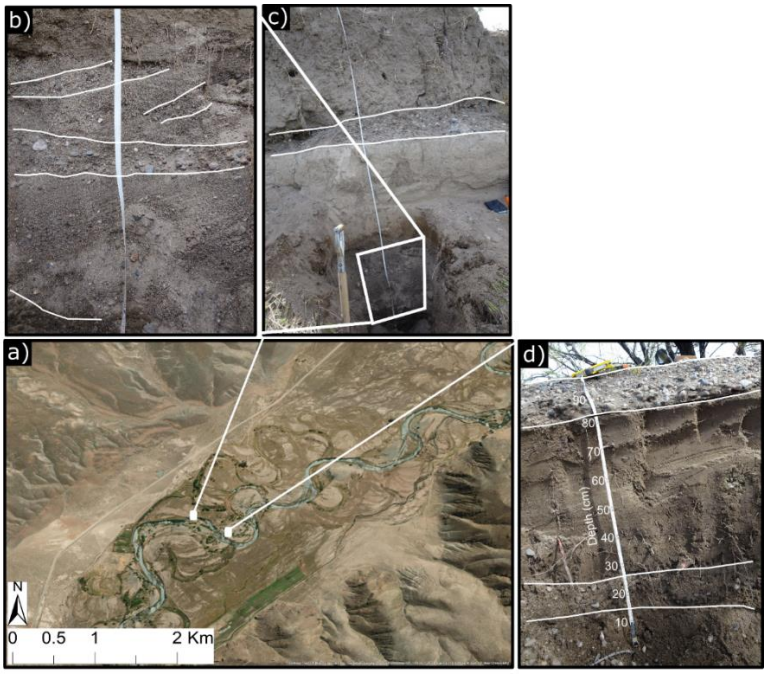


Figure. 5.4. Sand and gravel deposits observed on the surface and buried on the modern, meandering floodplain at site CHUB5 along the Río Chubut. White line annotations indicate gravel beds in the stratigraphy. (a) The location of stratigraphic observations at site CHUB5. The satellite imagery basemaps are from the ESRI Global Basemap (ESRI, 2009). (b) Section of the river bank comprising sands and gravel with gravel beds. (c) The full river bank exposure indicating the location photographed in image (b). (d) The surface gravels and buried gravel bed comprising a meander scroll proximal to the active channel.

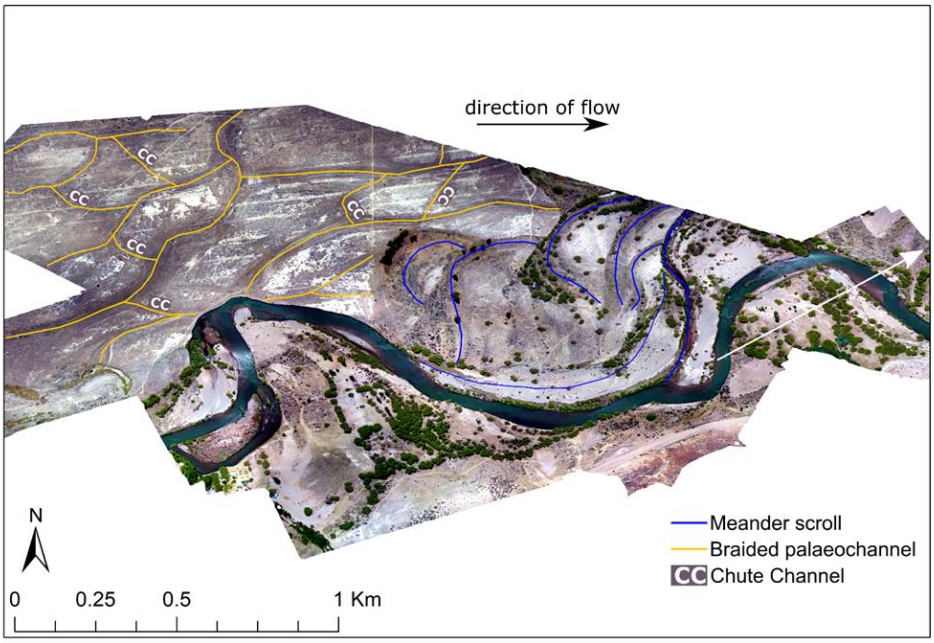


Figure 5.5. Aerial imagery obtained from the UAV survey at site CHUB1 demonstrating the contrast between the palaeo-braided planform and modern meandering channel.

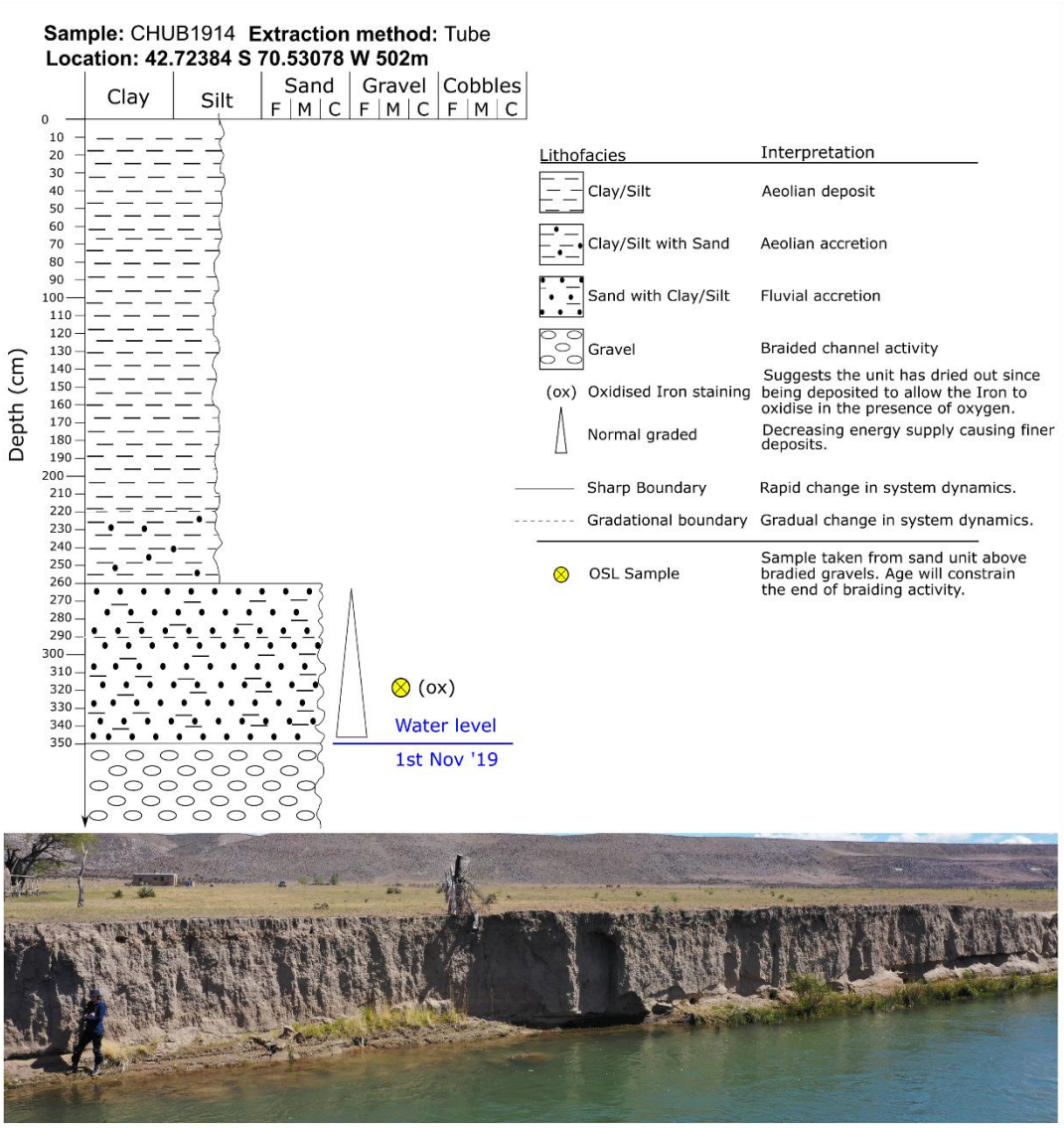


Figure 5.6. Example of stratigraphic sequence found in braided samples with a corresponding photograph of a section exposed at site CHUB5 along the banks of the Río Chubut.

Alluvial fans frequently line the valley along the study reach, and prograde over the braided terraces where present and are eroded by the modern channel where they are in contact. Sediments from the top and bottom of an alluvial fan were sampled to constrain the timing of activity for that gully/alluvial fan system (CHUB1915, Fig. S5 and CHUB1916, Fig. S6, respectively). The stratigraphy alternated between finer and coarser-grained sediment units of the same lithology. The finer-grained units consisted of well sorted silt/sand and the coarser units, comprising poorly sorted silts, sands and gravels, were matrix supported with (sub)angular gravel clasts (~2 cm).

## 5.4 Luminescence dating

### 5.4.1 Methods

Luminescence dating can determine the time that has elapsed since mineral grains (quartz or K-feldspar) were last exposed to sunlight (see Smedley (2018) for a review). For the samples from the braided plains, luminescence dating was used to determine the time elapsed since grains in the braided planform sediments were exposed to sunlight during the latest stages of braid plain activity, and then buried by floodplain accretion (i.e., shielding the grains from sunlight). For the samples from the meandering floodplain/terrace, luminescence dating was used to determine the age of the meandering regime preserved by the geomorphology. However, the characteristic mobility of meandering rivers meant that the oldest palaeochannels have likely been overprinted by younger migrating meander bends. Therefore, these luminescence ages reflect a minimum age for the modern meandering regime in the Río Chubut. For the samples from the alluvial fan, luminescence dating constrained the time elapsed since that sector of the alluvial fan was active and depositing the sampled sediment. Upon exposure to sunlight, the luminescence signal of a grain is reset to zero, which is termed well bleached. Once buried, the luminescence signal accumulates in grains because of natural radiation in the form of radioactive decay of K, U and Rb, in addition to a contribution from the cosmic rays. Electrons are trapped at defect sites within the crystalline structure of the grains and stored over time. To determine a luminescence age, the total luminescence signal accumulated within the grain is measured in the laboratory, termed the equivalent dose ($D_e$). The $D_e$ is then divided by the environmental dose rate, which is constant over time.

Table 5.1. Environmental dose-rate results for the sedimentary samples taken from the Río Chubut, Argentina. Environmental dose-rates were determined using ICP-MS to determine K, U and Th concentrations. The dose-rates were calculated using the conversion factors of Guerin et al., (2011) and alpha (Bell, 1980) and beta (Guerin et al., 2012) dose-rate attenuation factors. Water contents were estimated following measurement in the laboratory; these values are expressed as a percentage of the mass of dry sediment. An internal K-content of 10 ± 2% (Smedley et al., 2012) were used to determine the internal dose-rates. An a-value of 0.10 ± 0.02 (Balescu and Lamothe, 1993) was used to calculate the alpha dose-rates. Cosmic dose-rates were determined after Prescott and Hutton (1994). Dose-rates were calculated using the Dose Rate and Age Calculator (DRAC; Durcan et al., 2015).

| Sample | Latitude (°S) | Longitude (°W) | Depth (m) | Grain size (µm) | Water content (%) | U (mg kg-1) | Th (mg kg-1) | K (%) | Internal dose-rate (Gy/ka) | External alpha dose-rate (Gy/ka) | External beta dose-rate (Gy/ka) | External gamma dose-rate (Gy/ka) | Cosmic dose-rate (Gy/ka) | Total dose-rate (Gy/ka) |
|---|---|---|---|---|---|---|---|---|---|---|---|---|---|---|
| CHUB1918 | -42.40465 | -70.56822 | 3.4 | 180-250 | 25±2 | 1.5±0.2 | 5.8±0.6 | 1.6±0.2 | 0.92 ±0.17 | 0.07±0.01 | 1.14±0.10 | 0.66±0.04 | 0.24±0.02 | 3.02±0.20 |
| CHUB1914 | -42.46844 | -70.50665 | 3.0 | 180-250 | 31±2 | 1.2±0.1 | 5.8±0.6 | 1.5±0.2 | 0.92 ±0.17 | 0.06±0.01 | 0.97±0.08 | 0.57±0.04 | 2.24±0.02 | 2.75±0.20 |
| CHUB1917 | -42.64326 | -70.31312 | 2.1 | 180-250 | 16±2 | 1.1±0.1 | 3.9±0.4 | 1.3±0.1 | 0.92 ±0.17 | 0.05±0.01 | 1.01±0.09 | 0.54±0.04 | 0.25±0.03 | 2.77±0.20 |
| CHUB1920 | -42.64231 | -69.98988 | 4.6 | 180-250 | 30±2 | 2.4±0.2 | 6.4±0.6 | 1.6±0.2 | 0.92 ±0.17 | 0.09±0.01 | 1.19±0.09 | 0.72±0.04 | 0.22±0.02 | 3.14±0.20 |
| CHUB1907 | -42.49494 | -70.54292 | 2.2 | 212-250 | 19±2 | 2.0±0.3 | 9.2±0.3 | 1.2±0.3 | 0.97±0.15 | 0.11±0.02 | 1.07±0.18 | 0.79±0.07 | 0.25±0.03 | 3.19±0.25 |
| CHUB1921 | -42.64511 | -69.98370 | 3.8 | 212-250 | 54±2 | 2.1±0.3 | 0.8±0.3 | 1.0±0.3 | 0.97±0.15 | 0.07±0.01 | 0.70±0.13 | 0.54±0.05 | 0.23±0.02 | 2.50±0.21 |
| CHUB1915 | -42.65471 | -70.09927 | 2.3 | 212-250 | 6±2 | 0.5±0.2 | 5.1±0.5 | 1.5±0.2 | 0.97±0.15 | 0.07±0.01 | 1.31±0.11 | 0.74±0.05 | 0.25±0.03 | 3.34±0.20 |
| CHUB1916 | -42.65470 | -70.09917 | 0.4 | 212-250 | 6±2 | 1.3±0.1 | 5.0±0.5 | 1.6±0.2 | 0.97±0.15 | 0.07±0.01 | 1.42±0.12 | 0.77±0.05 | 0.29±0.03 | 3.52±0.20 |

Samples were collected in the field using two techniques: (1) a light-tight tube was hammered horizontally into a vertical exposure to ensure the sample was shielded from sunlight within the tube; or (2) a borehole was extracted using an Edelman type auger with a 20 cm chamber, ensuring the sediment remained light-tight during sampling (see the Supplementary Information for details). The environmental dose rate was calculated from the U, Th and K concentrations for bulk sediment from each sample, which was measured using inductively coupled plasma mass spectrometry (ICP-MS). The conversion factors by Guerin et al (2011) and the alpha (Bell, 1980) and beta (Guerin et al., 2012) attenuation factors were applied to determine the environmental alpha, beta and gamma dose rates. Field water contents were measured in the laboratory and are expressed as a percentage of the bulk sediment; the values measured were representative of the entire burial history. Internal dose rates were determined using an internal K-content of 10 ± 2% (Smedley et al., 2012) and internal U and Th concentrations of 0.3 ± 0.1 mg $kg^{-1}$ and 1.7 ± 0.4 mg $kg^{-1}$ (Smedley and Pearce, 2016). The alpha values were calculated using an a-value of 0.10 ± 0.02 (after Balescu and Lamothe, 1993). Cosmic dose-rates were calculated (after Prescott and Hutton, 1994) using the latitude, longitude, elevation and burial depth. Environmental dose-rates were calculated using the Dose Rate Age Calculator (DRAC; Durcan et al, 2015) and are shown in Table 5.1.

Luminescence dating of fluvial sediments is often characterised by partial bleaching (see Smedley and Skirrow, 2020 for review), where the luminescence signals of only a proportion of the grains in the sample are completely reset prior to burial. Single-grain analysis allows the luminescence signal to be measured in individual grains meaning that partial bleaching can be identified and overcome (e.g., Smedley and Skirrow, 2020). Furthermore, single-grain analysis was also applied to detect any modern contamination of grains incorporated from modern wind transport during augering. To date, K-feldspar grains have been preferred for single-grain analysis in Patagonia (e.g., Blondin et al., 2012; Smedley et al., 2016, Mendelova et al., 2020b) as previous studies have found the quartz in this region to be dim (e.g., Duller, 2006). Moreover, it has been reported that the wavelengths that more efficiently bleach the infrared stimulated luminescence (IRSL) signal in K-feldspars are less likely to be

attenuated through a turbid water column in comparison to the shorter wavelengths that bleach the OSL signal quartz more efficiently (Jerlov, 1970; Krongborg, 1983; Sanderson et al., 2007).

A standard procedure for laboratory sample preparation was followed to isolate the K-feldspar sand-sized grains. The coarsest grain size possible (suitable for single-grain dating) was used as the braided sediments in the Río Chubut terraces were composed of coarse sand and gravel. Bulk sediment was wet sieved at 90 µm and 300 µm to remove the coarsest (>300 µm) and finest material (<90 µm). Once dried, the samples were dry sieved to isolate the 180-250 µm or 212-250 µm fraction, which was then subjected to hydrochloric acid (10%) and hydrogen peroxide (10%) to remove any carbonates and organics, respectively. Density separation with sodium polytungstate was used to isolate the K-feldspar (<2.58 g $cm^3$) fraction, which was not etched with hydrofluoric acid (after Duller, 1992). Finally, the K-feldspar grains were mounted into single-grain disc holders containing a 10 x 10 array of 300 µm diameter holes, whereby one grain would be in each hole.

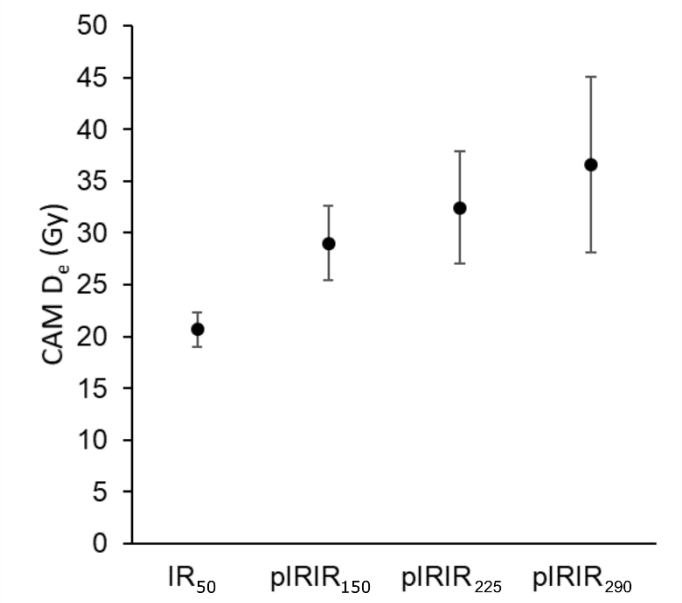


Figure 5.7. Multiple stimulation and preheat temperature plateau test results for sample CHUB1917.

All luminescence measurements were performed on a Risø TL/OSL DA-15 automated single-grain reader equipped with a $^{90}Sr$ beta source and focussed infra-red (IR) laser (Bøtter-Jensen et al., 2003). A single aliquot regenerative dose (SAR) protocol was used (Murray and Wintle, 2000) to determine $D_e$ values using the post-IR IRSL protocol (Thomsen et al., 2008). A preheat-stimulation temperature plateau test (Roberts, 2012) using the IRSL signals measured at 50°C ($IR_{50}$), 150°C

($pIRIR_{150}$), 225°C ($pIRIR_{225}$) and 290°C ($pIRIR_{290}$) signals was performed on sample CHUB1917 to determine the most suitable IRSL signal for analysis. Note that the $IR_{50}$, $pIRIR_{150}$ and $pIRIR_{225}$ signals were performed using a preheat temperature of 250°C, while the $pIRIR_{290}$ signal was measured using a preheat temperature of 320°C (Fig. 5.7). The results showed that the $IR_{50}$ measured the lowest $D_e$ value likely caused by anomalous fading, while the $D_e$ values determined using the $pIRIR_{150}$, $pIRIR_{225}$ and $pIRIR_{290}$ signals were consistent within uncertainties. Consequently, the $pIRIR_{225}$ signal was used for analysis as the inherent bleaching rates of the $pIRIR_{225}$ signal for individual grains were likely more efficient and more consistent between grains than the $pIRIR_{290}$ signal (Smedley et al., 2015). Therefore, for dating analysis, a preheat temperature of 250°C for 60 s was used and the IRSL measurement performed at 50°C was performed using the IR light emitting diodes (LEDs) for 100 s. A test-dose of 35 Gy was used and an elevated temperature bleach at 290°C for 200 s removed any remaining IRSL signal at the end of each measurement cycle. The location of single-grain discs was performed at room temperature, rather than elevated temperatures, to prevent thermal annealing of the IRSL signal (after Smedley and Duller, 2013). Integration limits were set for the initial (0 - 0.3 s) and the background IRSL signals (1.2 – 2.0 s). $D_e$ values were only accepted for a grain if it passed the following screening criteria, accounting for the associated uncertainties: (1) recycling ratio limit (10%), (2) maximum test dose error (10%), (3) natural test-dose signal more than 3 sigma above background, (4) the $D_e$ value was not identified by the finite mixture model (FMM) as a low dose component consistent with a modern age (i.e., 0 Gy). Note that contaminating low dose components were only found in two samples (CHUB1917 and CHUB1918), and accounted for only 0.5% and 2.4% (respectively) of the grains giving a $D_e$ value. Dose-recovery and residual dose experiments showed that the SAR protocol used for analysis was appropriate and determined the intrinsic overdispersion in these samples (27.8 ± 0.4% for sample CHUB1917; Fig. S10). Anomalous fading occurs in some K-feldspar samples where a portion of the luminescence signal in the grains depletes athermally over time without exposure to light. Three aliquots per sample were measured following the procedure of Huntley and Lamothe (2001) with a maximum time delay of 10 h, a given dose similar to the natural $D_e$ (35 Gy) and a repeated prompt measurement was used to assess reproducibility. G-values (normalised to two days) were determined from the weighed mean and standard error for each sample. G-values for the $pIRIR_{225}$ signal were consistent with the non-fading signal of quartz (Thiel et al., 2010), and so these sample are considered to have not been subject to anomalous fading.

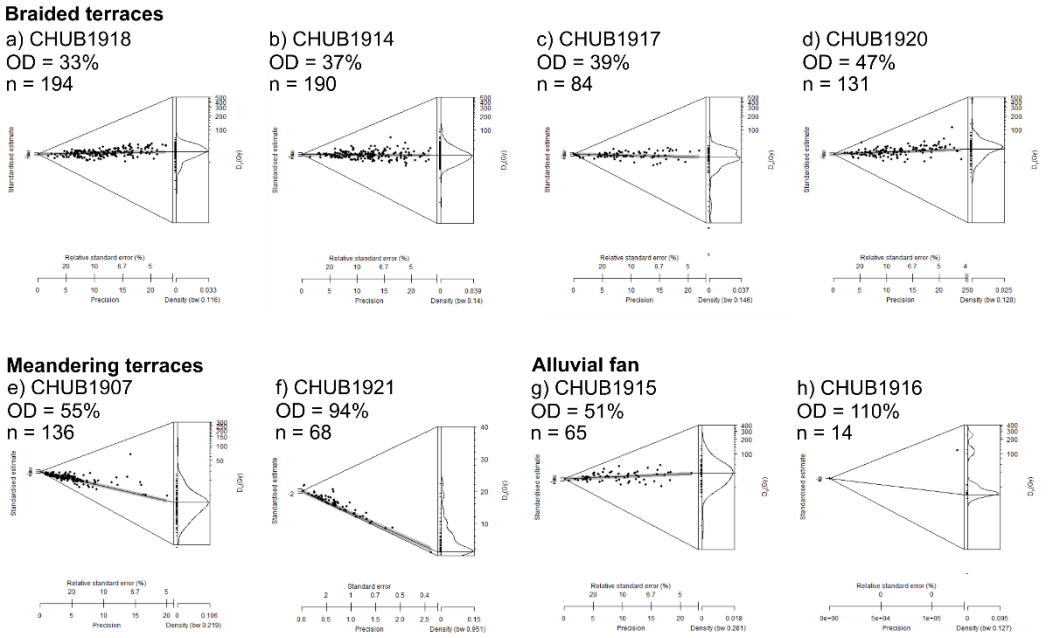


Figure 5.8. Abanico Plots showing the distribution of single-grain $D_e$ values measured for each sample. The grey line shows the CAM or MAM $D_e$ value (±1σ). The unlogged-MAM was used for sample CHUB1921 and so is presented on an unlogged scale, unlike the rest of the samples. Note that an approximate age was calculated for CHUB1916 because of the very low yield of $D_e$ values from grains of this sample.

Table 5.2. Luminescence dating results for the sedimentary samples taken from the Río Chubut Argentina. The *g*-values (%/decade) were measured using the $pIRIR_{225}$ signal for three aliquots of K-feldspar for each sample, normalised to 2 days and are presented as weighted means and standard errors. The number of grains that were used to determine a $D_e$ value (n) are shown as a proportion of the total grains measured (N). The CAM or MAM were used to determine the $D_e$ for age calculations for samples deemed to have been well bleached and partially bleached, respectively. The u-MAM was used for samples where the $D_e$ was approaching zero Gy. The $\sigma_b$ value (0.3) was estimated by combining overdispersion from internal (see Fig. S10 for dose-recovery experiment results) and extrinsic sources in quadrature.

| Sample | Total dose-rate (Gy/ka) | g-value (%/dec.) | n/N | Overdispersion (%) | Age model chosen | $D_e$ (Gy) | Age (ka) |
|---|---|---|---|---|---|---|---|
| CHUB1918 | 3.02±0.20 | -0.6±0.9 | 194/1000 | 33 | CAM | 33.4±0.8 | 11.1±0.8 |
| CHUB1914 | 2.75±0.20 | 0.1±0.9 | 190/1500 | 37 | CAM | 32.6±1.3 | 10.4±0.8 |
| CHUB1917 | 2.77±0.20 | 0.2±1.0 | 84/900 | 39 | CAM | 26.0±1.2 | 9.4±0.8 |
| CHUB1920 | 3.14±0.20 | 1.8±0.9 | 131/1000 | 47 | CAM | 38.7±1.6 | 12.3±1.0 |
| CHUB1907 | 3.15±0.26 | 5.1±0.9 | 136/2100 | 55 | CAM | 7.1±0.4 | 2.2±0.2 |
| CHUB1921 | 2.50±0.21 | 3.2±0.9 | 68/900 | 94 | u-MAM | 1.1±0.3 | 0.5±0.1 |
| CHUB1915 | 3.34±0.20 | 0.2±0.9 | 65/1600 | 51 | CAM | 39.3±2.6 | 11.8±1.1 |
| CHUB1916 | 3.52±0.20 | -0.1±1.6 | 14/1900 | 110 | MAM | 13.8±4.5 | ~4 |

The $D_e$ values obtained for each sample are shown in Abanico plots (Fig. 5.8). The central age model (CAM) was used to determine an age for samples with symmetrical $D_e$ distributions deemed to have been well bleached prior to burial (Fig. 5.8); this included all samples except for sample CHUB1916, from the top of the alluvial fan. The minimum age model (MAM) was used for sample CHUB1907, CHUB1921 and CHUB1916 as it had an asymmetrical $D_e$ distribution. Sample CHUB1916 only yielded 14 grains out of the 1900 grains that were measured gave $D_e$ values. Because of the low yield of grains giving a $D_e$ value (Table 5.2), the age for CHBU1916 cannot be calculated to the same level of accuracy as the other samples, thus should be treated with caution. The age of CHUB1916 is still useful for contextualising the timing of alluvial fan activity in this region.

### 5.4.2 Results

The luminescence ages constrain the timing of abandonment of the braided planform (CHUB1914, CHUB1917, CHUB1918 and CHUB1920), the oldest (preserved) meandering activity (CHUB1907 and CHUB1921) and the activation of the alluvial fans (CHUB1915 and CHUB1916). The luminescence ages for the abandonment of the braided planform behaviour in the Río Chubut spans a period of ~3 ka from the end of the Younger Dryas into the Early Holocene (Marine Isotope Stage 1). The first braid plain to be abandoned was the farthest downstream site at CHUB1, dated by sample CHUB1920 at 12.3 ± 1.0 ka (Fig. 5.3). The next site to be abandoned was the sample taken farthest upstream from the widest floodplain section of the study area at site CHUB6 (sample CHUB1918 dated to 11.1 ± 0.8 ka; Fig, 5.3). Then the braid plain at site CHUB5 was abandoned at 10.4 ± 0.8 ka (CHUB1914; Fig. 5.3) and finally site CHUB4 abandoned its braided planform at 9.4 ± 0.8 ka (CHUB1917; Fig. 5.3). The oldest preserved meandering activity at site CHUB5 dated to 2.2 ± 0.2 ka from the palaeochannel sample CHUB1907. The oldest palaeochannel in a migrating meander sequence at site CHUB1 dated to 0.45 ± 0.12 ka (Sample CHUB1921; Fig. 5.3), which was more recent than the abandoned meandering surface at site CHUB5. The ages for alluvial fan activity suggest that the alluvial fan was likely active throughout the abandonment of the braided planform and continued into the mid-Holocene. Samples taken from the bottom (CHUB1915) and top (CHUB1916) of an alluvial fan (Fig. 5.3) constrains a timeframe of significant aggrading activity to between 11.8 ± 1.1 ka and ~4 ka (respectively). Note that the age of ~4 ka for the end of alluvial fan activity is an approximate age because of the low yield of grains, but nevertheless suggests that alluvial fan activity post-dates the braided planform. Therefore, the braided planform was abandoned even with the sustained activity of

the alluvial fan into the Holocene. Furthermore, the luminescence properties of the alluvial fan samples were distinctly different to the braided samples, where the alluvial fan samples had very low grain yields in comparison to the braided samples; this is likely caused by distinctly different bedrock provenances between samples, in addition to the shorter transport pathways prior to burial than the samples from the braided plains.

## 5.5 Discussion

### 5.5.1 Fluvial mechanisms of planform change

The four braided terraces are likely preserved fractions of the same braided surface as they are located the same distance above the modern channel (~3 m). The palaeofluvial landforms and sedimentological evidence preserved on the terraces indicate that the Río Chubut underwent a planform shift from a braided to meandering system between 12.3 ± 1.0 ka and 9.4 ± 0.8 ka. The palaeochannels preserved on these surfaces follow an extensive network of interconnected channels characteristic of a braided planform. The abandoned planform at site CHUB1 preserved the braided planform, including chute channels that are typical of a braided regime (Fig. 5.5). The basal gravels of these terraces (rounded gravels) also support the interpretation of past braided behavior, which differs from the modern-day sand and gravel-bedded meandering system. The chronology constraining the age of the oldest preserved meandering surfaces shows that the modern meandering regime has been active for at least 2.2 ± 0.2 ka. Given the geomorphological evidence and the mobile nature of meanders overprinting older palaeochannels, we interpret that the meandering regime did directly succeed the braided planform.

The stratigraphy of the braided terraces suggests the abandonment of the braided planform was gradual. The sand/silt unit that overlays the braided gravels indicates a loss of energy in the system where finer-grained material settled out from suspension. It is possible that the braided channel activity was waning and so depositing fine-grained sediment under a lower energy regime, or the braided channels could have been abandoned and these units of sand/silt were slack water deposits from flooding. The luminescence chronology that relates to the end of the braided activity spans a period of ~3 ka (12.3 ± 1.0 ka to 9.4 ± 0.8 ka) across the four braided terrace samples (Fig. 5.3). All four ages agree within the uncertainty of each age, however, is it more likely that this distribution of ages indicates that the loss of energy in the system during the waning channel activity across the braid plain and subsequent aggradation of finer sediments, occurred time-transgressively rather than all braid plains responding simultaneously to a change in dynamics. The fluvial sediments then transition with a

sharp boundary to a thick unit of fine-grained structureless sediment, which is identified as aeolian loess. No intrusions of fluvial sediment units were visible within the loess, which suggests these braid plains were not flooded again after the fluvial activity evident in the lower stratigraphic units.

The stratigraphy and geomorphology of the braided plain sediments indicate that the braided channels experienced a loss of discharge and aggraded finer sediments, where the braided channels then infilled with sands/silts before abandonment. In addition to many contributing factors, braided rivers are sustained by a high sediment load that forms multiple channel bars and high-energy flow, which transports a high bedload downstream. Multiple factors in a river system can drive river planform change from braiding to meandering, including: (1) decreased sediment supply driven by vegetation change (Kasse et al., 2005); (2) decreased sediment supply driven by changes in sediment availability (e.g., paraglacial adjustment and alluvial fan activity) (Ballatyne, 2002); and (3) reduced discharge (Peirce et al., 2018; Leigh, 2006). First, it is reported that glacially-fed braided rivers experience a loss of sediment supply caused by the establishment of vegetation under interglacial conditions binding the sediment on the floodplain together (Leigh et al., 2004; Mol et al., 2000), which leads to a planform shift to a single channel system (Charlton, 2007; Mol et al., 2000). However, the sparse, broadly unchanged nature of vegetation on the steppe means that the floodplain sediment is available to the river (Iglesias et al., 2014); thus, a reduction in sediment supply caused by vegetation change is regarded as unlikely to have caused the abandonment of braiding.

A reduction in sediment supply is a common cause for planform change when a valley undergoes deglaciation (Charlton, 2007) sometimes because of a reduction of discharge caused by the formation of proglacial lakes (acting as a sediment trap), which leads to a planform shift to a single channel system (Charlton, 2007; Mol et al., 2000). After glaciation, the high sediment load needed to aggrade a braid plain and form multiple channel bars is no longer available, but the high-energy flow continues to transport the bedload downstream leading to floodplain exhaustion (Ballantyne, 2002). Eventually, a single channel is incised and the braided plain is abandoned as a newly formed terrace (Charlton, 2007). This process, also termed paraglacial adjustment, can span millennial time frames depending on the rate of glacial sediment release and reworking (Ballantyne, 2002). Field observations along the Río Chubut found sediment available from riverbank collapse and channel migration throughout the system (Fig. 5.4), in alluvial fan deposits (see Section 3.2) and in the outwash plain associated with the moraines and former glacier at Epuyen, which feeds the

river as part of its glacial catchment and is eroded by the Río Chubut as part of its contemporary catchment. Therefore, we rule out the possibility that sediment exhaustion forced braided planform abandonment.

Reduced sediment supply can also be driven by gully and alluvial fan decoupling whereby sediment is no longer transported from the valley sides into the river channel (Wijdenes et al., 2000). However, differences in the luminescence properties between the braid plain and alluvial fan samples, and the lack of spatial relationship between the two geomorphological features, suggests that the braided planform was not supported by sediment supplied by local alluvial fans (see Section 4.2). The yield of grains that gave $D_e$ values were very different between braided and alluvial fan samples, which indicates that they were from different sources. The high yielding braided samples were likely sourced from an area where the bedrock is rich in K-feldspar (e.g., the Cretaceous-Tertiary volcanic, Palaeozoic intrusive and Precambrian undifferentiated bedrock in the Andes; Schenk et al., 1999) and the low yielding alluvial fan samples were likely sourced from a region more depleted in K-feldspar (e.g., the Quaternary/Tertiary sedimentary bedrock; Schenk et al., 1999). Furthermore, the ages reflecting the alluvial fan activity is dated between 11.8 ± 1.1 ka and ~4 ka, which begins during the time period of the waning braiding activity and continues after the braided regime has been abandoned until the mid-Holocene. This demonstrates that the alluvial fan sediment supply did not dictate the planform of the Río Chubut..

Another possibility is that the braided planform was sustained by sediment derived from valley erosion upstream of the braid plain areas. Formerly braided sections of the channel are located in wide segments of the valley where the large accommodation space can support a braided system and provide space for the preservation of the relict braided surface. The particular locations of the braid plains at sites CHUB5 and CHUB1 occur directly downstream of a narrowing where the valley bends sharply. This zone has the potential to erode local rock and supply sediment to the braid plains. However, the lithology and luminescence properties discussed above do not support this theory of local sediment supply and instead imply that the sediments in the braid plains are derived from nearer the headwaters. Alternatively, the waning activity, observed in the braid plain sediment stratigraphy, was likely to have been the key process that forced the transition to a single channel system, where higher discharge is required to sustain a braided river channel to entrain the high bedload. Consequently, the findings in this study show that a reduction of discharge played a key role in the planform shift.

Using the evidence outlined in this paper and modern observations of braided river systems experiencing a reduction in discharge, the processes involved in the planform shift in the Río Chubut can be interpreted. The response of a braided river when subject to decreasing discharge is a narrowing of the active width of the braid plain and subsequent confinement of the channel (Peirce et al., 2018; Tockner et al., 2006; Glova and Duncan. 2011; Ashmore et al., 2011). As the discharge was waning in the Río Chubut between 12.3 ± 1.0 ka and 9.4 ± 0.8 ka, finer-grained sand and silt was accreted in the channels on top of the gravels (Fig. 5.6). The active width would have decreased because of reduced discharge, which caused the river to narrow and concentrate its energy to fewer channels. The confined channels then had the potential to incise into the sand and silt previously deposited, perhaps from their newly concentrated stream power or through flooding where increased discharge increased the potential for channel incision. The elevation of the fluvial sediments in relation to the modern channel river level or water table (depending on sampling location) is noteworthy as the thickness of the fluvial sediments above the modern channel indicates ~90 cm of incision by the succeeding meandering regime after the braided plain had been abandoned. The relict braid plains occupy a peripheral position within the wide accommodation space of the Chubut valley, which means it is possible that confinement of the river channel, during and after the planform transition, has directed the river away from these areas leading to the accretion and preservation of overlying aeolian deposits. Alternatively, this could also infer that palaeodischarge of the newly formed meandering regime never exceeded the height of this river bank, allowing the loess to accumulate without interruption from flood sediments. The samples taken for luminescence dating were collected to constrain the age for the waning and abandonment of the braided regime (Section 3.2), and overlying fluvial sediments are interpreted as reflecting floodplain accretion during and/or after the transition in planform.

### 5.5.2 Environmental drivers of planform change (via discharge)

The chronology places the waning braided planform to the last glacial-interglacial transition after the Antarctic Cold Reversal (Fig. 5.9). This period was unstable with oceanic, climatic, and terrestrial systems responding to this deglaciation and warming into the Holocene (Kaiser et al., 2005; Cuffey et al., 2016; Iglesias et al., 2016). Palaeoenvironmental reconstructions spanning the last glacial-interglacial transition shed light on the environmental drivers that caused the braided planform to be abandoned because of reduced discharge. The last glacial terminus recorded at 40-

44°S was at 17.8 ka cal. BP in the Chilean Lake District west of the Andes (Moreno et al., 2018), where ice lobes retreated after proglacial lakes formed; this onset of deglaciation is ~6 ka out of phase with the abandonment of the braided planform and so is ruled out as the driving environmental factor. Ice sheet and lake reconstruction (Fig. 5.1; Davies et al 2020) estimate – with medium to low confidence – that the formation of Lago Epuyen occurred ~15 ka. Lake records from Laguna Huala Hué, situated west of the northern headwaters of the Río Chubut, formed after the retreat of the glacier occupying the Río Manso valley, demonstrating that the Río Chubut was likely decoupled from the ice sheet in this region before 13.5 ka cal. BP (Iglesias et al., 2012). Therefore, the Río Chubut continued to braid for ~3 ka after the modelled formation of Lago Epuyen in the Late Glacial reported in Davies et al., (2020). These extended timeframes between deglaciation and loss of braiding indicates that there was sufficient sediment in the landscape to sustain braiding in the Río Chubut and the retreat of ice margins to higher elevations during deglaciation alone was not the key driver in forcing planform change in the Río Chubut.

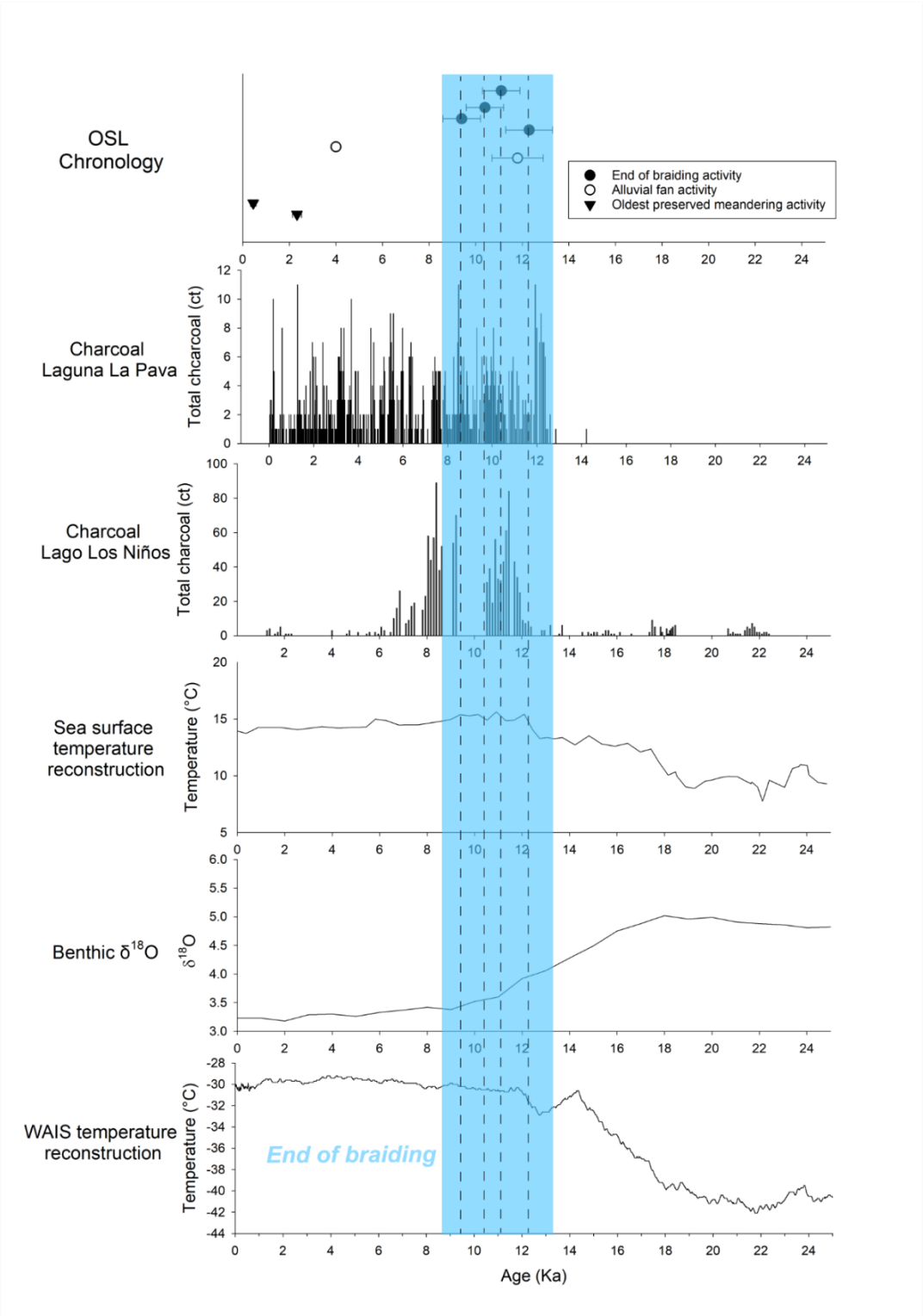


Figure 5.9. Luminescence ages for samples from the Río Chubut plotted alongside palaeoenvironmental records for the last 25 ka including charcoal records from Laguna La Pava and Lago Los Niños (Iglesias et al., 2016), sea surface temperature reconstructions from the Ocean Drilling Programme (ODP) core 1233 (Kaiser et al., 2005), global benthic $\delta^{18}O$ stack (Lisiecki and Raymo, 2005) and the West Antarctic Ice Divide ice core temperature reconstructions (Cuffey et al., 2016).

Atlantic-Pacific drainage reversals occurred across Patagonia at different times throughout the deglaciation as the ice retreated, opening up westward drainage pathways to the Pacific Ocean (Garcia et al., 2014; Garcia et al., 2019; Thorndycraft et al., 2019; Turner et al., 2005). The timing of the drainage reversals for the lakes in the Río Chubut catchment are not yet constrained, but this event would have caused a loss of water supply to the Río Chubut through either constant westward drainage over a col or episodic outburst floods (Leger et al., 2020). Palaeoenvironmental records suggest that glaciers at this latitude underwent extensive deglaciation in the 1 ka following a warm pulse at 17.1 ka cal. BP; this coincided with lake level lowering before average interglacial temperatures were reached at 16.8 ka cal. BP and peak interstadial temperatures between 16 and 15 ka cal. BP (Moreno et al., 2015, 2018). These warming conditions, subsequent lake lowering and collapse of ice lobes suggest that the drainage reversal occurred before 15 ka cal. BP between 40-44°S. On the contrary, the westward drainage routes for the lake formed in the Cisnes valley (44°S) were still blocked between 14.0 ± 0.2 and 12.9 ± 0.1 ka (Garcia et al., 2019) suggesting the drainage reversal would have occurred after this timeframe. The elevation and geometry of lakes and cols can play a role in their sensitivity to change. Therefore, the age constraints on the drainage reversal of a single lake in a different catchment is not considered a reliable analogue for proximal ice-dammed lakes in the Rio Chubut catchment. The palaeoenvironmental records produced by Moreno et al. (2015, 2018) were based on datasets from multiple lakes and moraine sequences from a range a valleys across the same latitude as the Rio Chubut catchment, and are therefore considered a more robust record from which to estimate the timing of the drainage reversal in the Chubut catchment. The braided planform of the Río Chubut persisted until 12.3 ± 1.0 ka, which suggests that drainage reversal was not a key driver of the braided planform.

The discharge of the Río Chubut would also have been controlled by past climate (principally precipitation) whereby wetter conditions (rainfall or snowmelt) increased the river discharge. Precipitation supply to the Río Chubut is influenced by multiple atmospheric systems, including the southern westerlies and easterlies, and the ENSO. ENSO was weakened or non-existent prior to ~7 ka (Moreno, 2004; Moy et al., 2002), which post-dates the change in planform documented at Río Chubut; thus, ENSO could not have controlled the delivery of precipitation to the Río Chubut catchment. Today, the easterlies atmospheric system can bring precipitation to the semi-arid plateau east of the Andes (Agosta et al., 2015; Garreaud et al., 2013) and

may have been strengthened when the westerlies were weakened in the past (Moreno et al., 2010). If the easterlies were strengthened, the alluvial fans in the catchment would likely have been activated and supplying sediment to the Río Chubut because of their location ~65-140 km east of the Andes. Luminescence properties and sediment lithology have ruled out the potential for the local alluvial fans being the dominant sediment supply to the braid plains. Additionally, the timing of activity in one alluvial fan in the Chubut valley is out of phase with the braided planform (see Section 3.2). When considering all of the evidence, it is unlikely that a strengthening of the easterlies in the past was the key driver of the braided planform; however, it is recognized that the one alluvial fan sampled in this study may not represent activity at a landscape scale.

The mid-latitude storm tracks and westerlies respond to changes in meridional temperature gradients (e.g., Lamy et al., 2010; Denton et al., 2021), and are suggested to have been weakened in intensity when the core shifted to more northerly latitudes than today during the last glaciation (Herman and Brandon, 2015). During deglaciation, the mid-latitude storm tracks and westerlies migrated southwards towards their contemporary position (McCulloch et al., 2000), but palaeoenvironmental records suggest they experienced millennial-scale variability in their intensity at different latitudes (Whitlock et al., 2007; Moreno et al., 2010; Moreno et al., 2012, 2015, 2018). Prior to ~19 ka, the westerlies were strengthened at ~44°S latitudes (Herman and Brandon, 2015). However, the westerlies weakened and shifted southwards in the Early Holocene (between 10.5 ka and 7.8 ka cal. BP) bringing drier conditions to Patagonia (Moreno et al., 2010; Whitlock et al., 2007; Iglesias et al., 2016), and specifically at ~40-44°S (i.e., the Río Chubut catchment) between 11.3 and 7.7 ka cal. BP (Moreno et al., 2018). Pollen and charcoal records along the eastern flanks of the Andes also report drier-than-present conditions in the Early Holocene, for example Laguna Huala Hué and Laguna Padre Laguna at 41°S (Iglesias et al., 2012), and Lago Los Niños and Laguna La Pava at 44°S (Fig. 5.9; Iglesias et al., 2016). Furthermore, palaeoenvironmental reconstructions from farther south in Tierra del Fuego (53°S) show that the westerlies were concentrated over this latitude by ~11 ka cal. BP (Markraf and Huber, 2010). Overall, the weakening and southward shift of the westerlies would have reduced the precipitation supply to the Río Chubut catchment and so reduced the water supply, which in turn reduced the discharge and the river's potential energy for sediment transport and erosion. These climate changes are proposed as the main driver of the planform change from a braided to meandering regime over the period between 12.3 ± 1.0 ka and 9.4 ± 0.8

ka, with precipitation reduction in Patagonia caused by variability in the mid-latitude storm tracks and westerlies leading to threshold changes in river planform. These findings highlight that modern braided rivers (e.g., the Rakaia River, New Zealand) that are experiencing a reduction in discharge could be vulnerable to similar large-scale impacts that would affect the habitats and ecosystems a braided river supports (Glova and Duncan, 1985). Furthermore, the Zealandian Switch suggests the effects of the changing southern westerlies are not confined to the southern hemisphere and can initiate climate changes across the world (Denton et al., 2021).

### 5.6 Conclusion

New geomorphological mapping of a 75 km study reach of the Río Chubut reveals the river underwent a shift in planform from a braided regime to the modern-day meandering system. Stratigraphic observations show a phase of decreasing energy in the system as the braided gravels grade towards sand/silt fluvial deposits. Luminescence dating of four widely spaced remnant terraces show that the braided regime was abandoned gradually between 12.3 ± 1.0 ka and 9.4 ± 0.8 ka. The driving factor of this planform change was the significant reductions in river discharge and associated precipitation. Palaeoenvironmental reconstructions at ~40-44°S (i.e., the Río Chubut catchment) suggest drier conditions prevailed around the timing of planform change in the Río Chubut as a result of the weakening and southward shift of the southern westerlies across Patagonia. The luminescence chronology for the shift in planform along the Río Chubut allows us to understand the environmental context of large-scale geomorphological change of a major river system in this understudied region east of the southern Andes. The findings in this study not only identify the hydroclimate as the key driver of this dramatic shift in river dynamics, but also demonstrates that the braided system withstood other large-scale changes and processes that occurred during and after deglaciation, such as decoupling from glacier and major proglacial lakes, and abrupt climate warming.

### Acknowledgments

The authors would like to thank all the landowners for granting us access to their land, including Señor Don Manuel and Señor Pascini, and Laura and Daniel at Mirador Huanache, Gualjiana for their incredible hospitality, local knowledge and for the impromptu loan of their Kayak. We are grateful to Dr. Thorndycraft and Dr. Davies for their assistance in acquiring datasets, Dr. Whitlock for her constructive discussion and Dr. Olive for her efficient ICP-MS measurements. This project was supported by a Natural Environment Research Council Doctoral Training Scholarship [NE/L002469/1].

# Chapter 6

## Timescales for channel activity in the contemporary meandering planform of the Río Chubut (~42 °S, 70°W) Argentina.

This chapter investigates the rapidity of evolution in the contemporary meandering regime in the Río Chubut (Research Question 4) by assessing the dynamics and timescales of change. Building upon the high-resolution mapping presented in Chapter 3, the dynamics and processes of the meandering regime is assessed, and luminescence dating constrains the timescales of localised channel and floodplain evolution (Objective 4.1). The autochthonous and allochthonous drivers of meander belt and floodplain evolution are discussed in the context of present and past environmental conditions of the Holocene (Objective 4.2) and the resilience of the contemporary meandering planform is assessed.

Grace. K. Skirrow, Rachel. K. Smedley, Richard. C. Chiverrell

Preparing for submission to Earth Surfaces Processes and Landforms

**Abstract**

Temporally constrained sequences of meander migration, former channel activity and floodplain evolution are determined by geomorphological analysis and luminescence dating at sites along a 75 km study reach in the Río Chubut. The results provide new insight into the former channel activity in the flood basin, timescales of sediment residence time and/or floodplain reworking, and the mobility of the actively migrating meander bends. The findings show that the extensive floodplain aids the preservation of sediments and palaeofeatures for at least 2 ka along the study reach. The geomorphological connection between the ephemeral, anastomosing channel planform and the modern meandering channel suggests that the meandering channel belt in the upper course of the study reach has been in its current position for at least 0.6 ± 0.1 ka, and older avulsion channels across the flood basin predate this age. On the shorter timescale, meander migration and cut off occur on variable timescales along the study reach, where one scrolling meander has migrated 223 m from 0.7 ± 0.5 ka to present, but another meander has undergone at least six cycles of meander scroll and cut off from 0.5 ± 0.1 ka to present. Comparing the luminescence ages with we palaeoenvironmental reconstructions suggests that the meandering planform has

withstood fluctuating water supply driven by climate variability throughout the Holocene.

### 6.1 Introduction

The Río Chubut flows ~800 km east, from the eastern flanks of the Andes mountains, through the Patagonian steppe, towards the Atlantic Ocean. The Río Chubut headwaters, and the Río Gualjaina and Río Ñorquincó tributaries are dependent on water supplied from the wetter, cooler conditions west of the forest-steppe ecotone (Peterson and Vose, 1997; Fig. 6.1). The forest-steppe ecotone is the longitudinal transect boundary (~71˚W) between the humid, densely-vegetated Andes mountains and the semi-arid, sparsely-vegetated Patagonian steppe. Palaeoenvironmental records show that the forest-steppe ecotone is sensitive to climate change and has consequently experienced fluctuations in vegetation cover, fire intensity and frequency, and lake level changes (Iglesias et al., 2014). The source of the Río Chico tributary originated from slope run off located east of the forest-steppe ecotone. The river along the 75 km study reach and its tributaries also receives ephemeral drainage from Badlands-styles gullies that fringe the valley in the badland landscape during rainfall events. Changes in precipitation and vegetation cover influence river dynamics such as discharge and sediment load (Zhang an Lu, 2009), which in turn impact river geometry and planform (Hey, 1976).

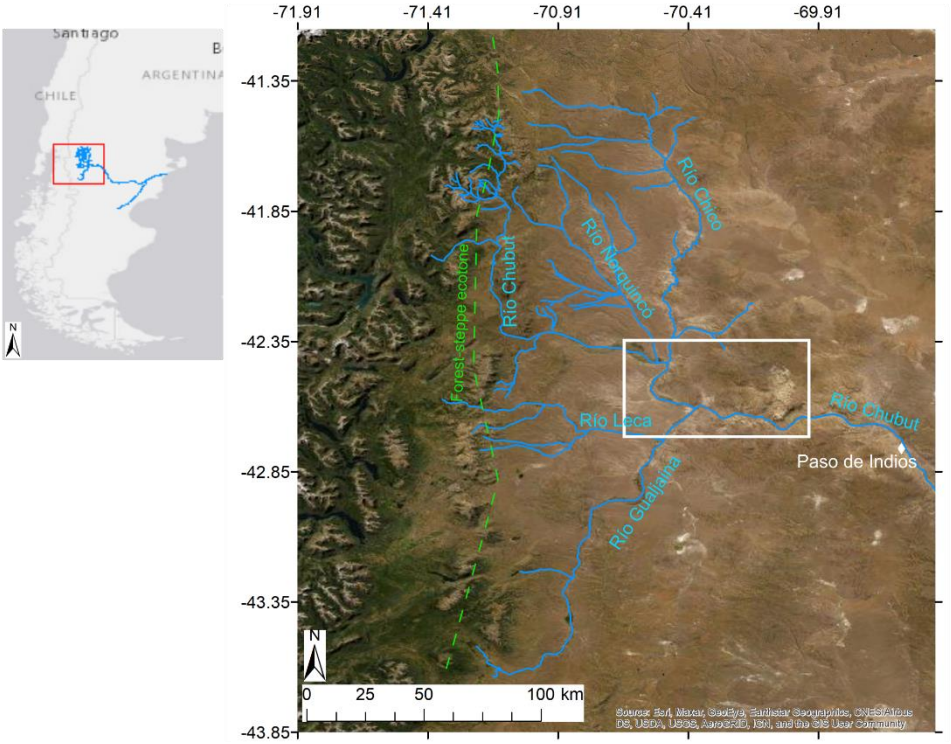


Figure 6.1. Río Chubut headwater catchment with 75 km study reach marked with a white box. The sites mentioned in this chapter are labelled with a white diamond. The approximate, modern-day forest-steppe ecotone is inferred from the colour gradient from the eastward diminishing vegetation cover.

The timing and nature of changes in the river regime show that the Río Chubut has responded to climate driven changes in water supply; this is evidenced by recent findings that attribute the abandonment of the former braided regime around the onset of the Holocene to a weakening and southward shift in the southern westerlies, after which the current meandering planform was established (Skirrow et al., 2021). The meandering planform is thought to have persisted throughout the Holocene to the present-day, sustaining a floodplain that preserves a wealth of palaeofluvial features and reflects a dynamic, meandering regime, often within a broad and low relief flood basin style setting (Skirrow et al., submitted). The preservation of palaeofluvial features and their apparent continuity to the current river gives the opportunity to understand both past processes and the evolution of this river system in the present.

This study presents mapping, geomorphology and two new luminescence ages in addition to the chronology presented in Skirrow et al (2021) to constrain the timescales of activity within an extensive flood basin. From this the implications for, sediment residence time, meander migration and channel mobility are explored in the

context of resilience of the contemporary meandering regime to environmental changes.

### 6.1.1 Study sites

Regional scale mapping of the Rio Chubut and associated tributaries identified a series of high elevation terraces (Skirrow et al., submitted). Incised below those terraces, there is an extensive lower elevation fluvial terrain of terraces and floodplain segments within 2-3 m elevation of the current river. In this low-level terrain, three study sites have been selected and they are distributed along a 75 km study reach, CHUB6, CHUB5 and CHUB1 (Fig. 6.2). They all display well preserved palaeofluvial features similar in character to the present-day meandering regime. These sites were selected because of their wide accommodation space synonymous with flood basin type behaviour (see Chapters 4 and 5) which was facilitated the excellently preserved former meandering channels (Fig. 6.2).

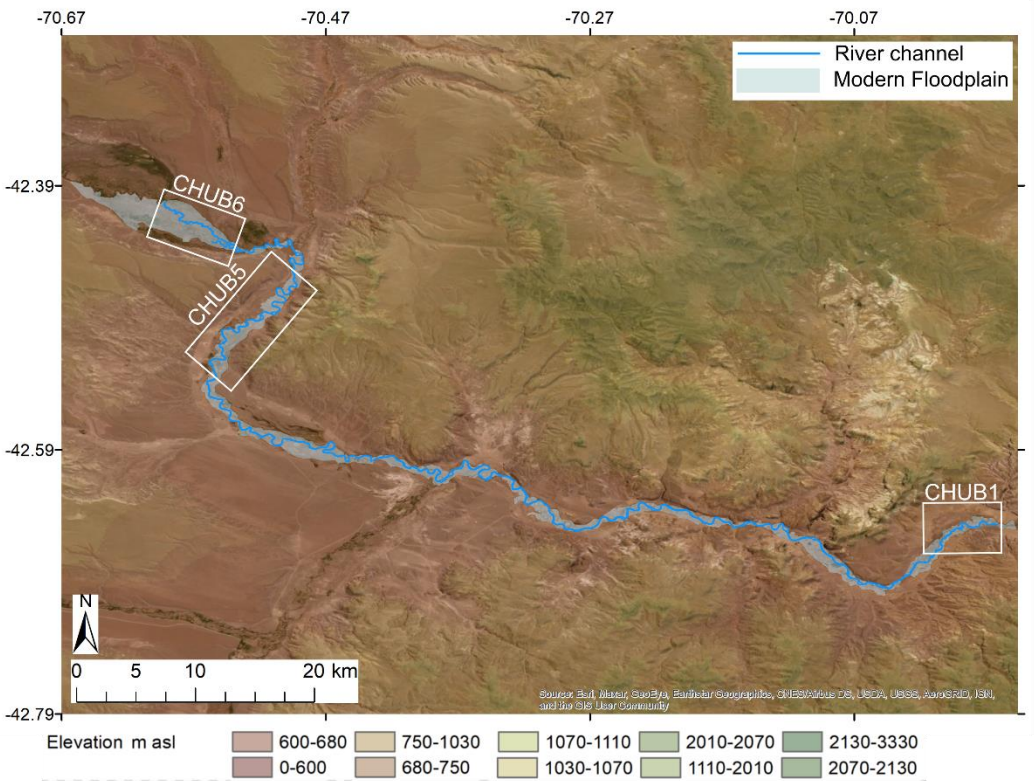


Figure 6.2. Río Chubut study reach map with white boxes indicating the study sites referenced in this chapter. Base map imagery from the World Imagery layer in ArcMap with translucent Elevation data overlay from the Shuttle Radar Topography Mission (SRTM) – 30 m resolution digital elevation model (DEM) (https://www2.jpl.nasa.gov/srtm/).

*Site CHUB6*

Situated at the upstream end of the study reach, site CHUB6 comprises a low, ~1%, gradient 13 km long wide, ~ 4km in places, expanse of floodplain. The low gradient and extent are hallmarks of a flood basin setting and sustain numerous avulsion channels and features typical of mature meandering systems. The area targeted here focusses on a downstream ~1 km reach of a ~2 km branch within an anastomosing floodplain channel located ~0.5 km north of the main river course (Fig. 6.3). The channel planform that has developed here, is initiated downstream of a knickpoint and fed by channels draining wetlands in the upstream flood basin (see Section 6.3.2). The Esri World Imagery Layer in ArcGis shows higher moisture conditions further upstream, and dry conditions in the CHUB6 reaches. The anastomosing planform ultimately connects with the modern course of the Río Chubut as a series of confluences between former channels and the active river (dry at the time of observation).

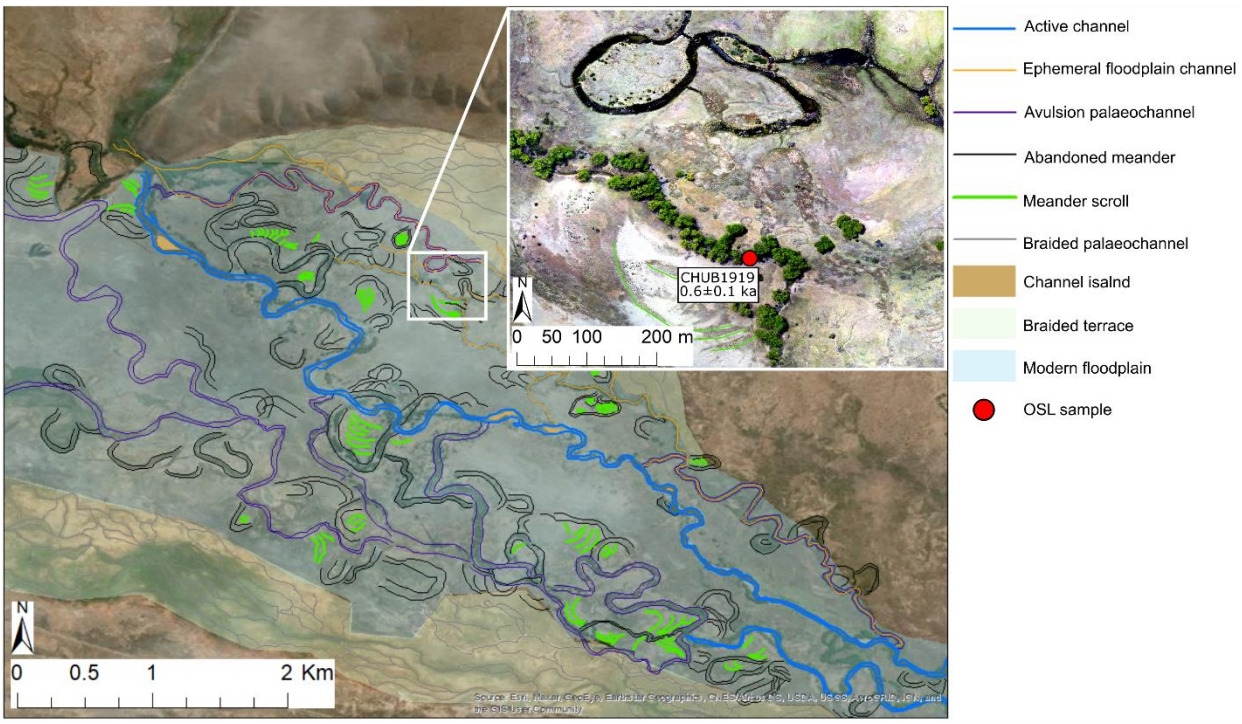


Figure 6.3. Site CHUB6 lower-level valley geomorphology with location of luminescence samples. Base map sourced from ArcMap World imagery Layer. Imagery for Inset map sourced from onsite Uncrewed Aerial Vehicle (UAV) photography.

*Site CHUB5*

Located 5-6 km downstream of site CHUB6, site CHUB5 also hosts a relatively wide (~1.5km) low gradient (~1.1%) floodplain, though slightly steeper than CHUB6. Site CHUB5 contains subdued fluvial terraces displaying relict features of both the

contemporary meandering system and of the former braided regime (see Chapter 5, Section 5.3.2). The area targeted here focusses on a 0.9 km cross-valley transect across the meandering surface extending from the edge of an older terrace to the modern channel (Fig. 6.4).

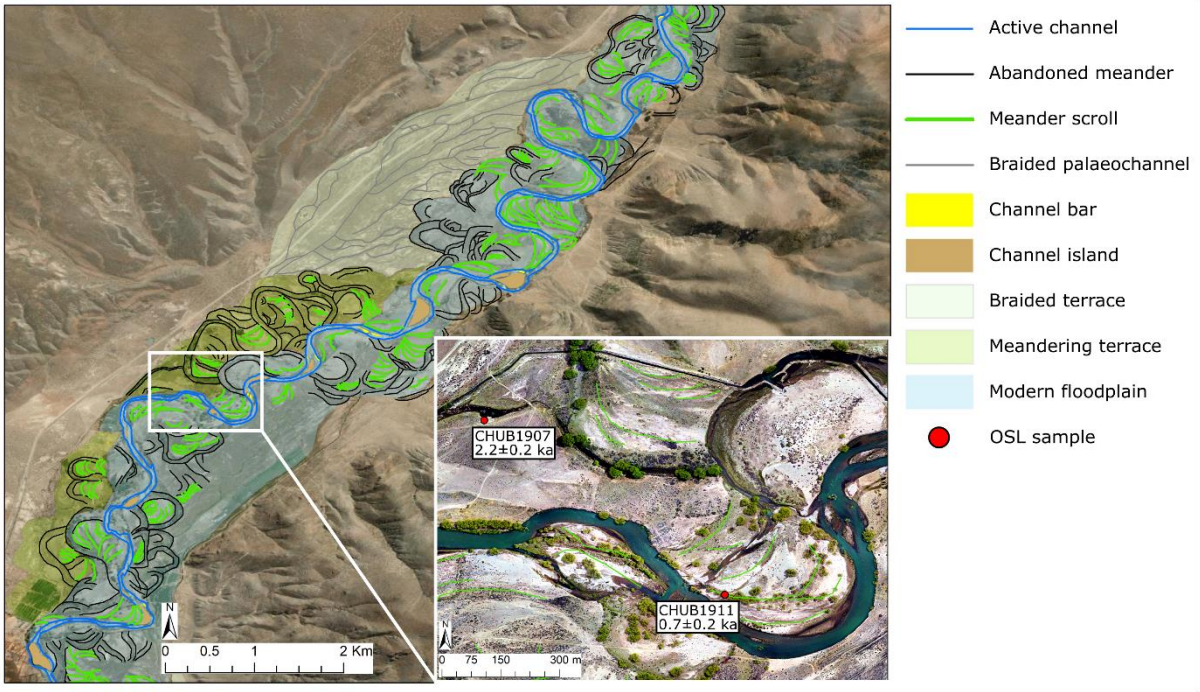


Figure 6.4. Site CHUB5 lower-level valley geomorphology with location of luminescence samples. Base map sourced from ArcMap World imagery Layer. Imagery for Inset map sourced from onsite UAV photography.

*Site CHUB1*

A further 50 km downstream, site CHUB1 is also a wide (~2.5 km) section of floodplain, with accommodation space for channels and sediments. This low gradient (1.2 %) basin displays characteristics features of the mature meandering regime of the modern river and a sector with the older and former braided planform (see Chapter 5, Section 5.5.1). The area targeted within site CHUB1 focusses on a transect extending downstream through a sequence of former meander bends (Fig. 6.5).

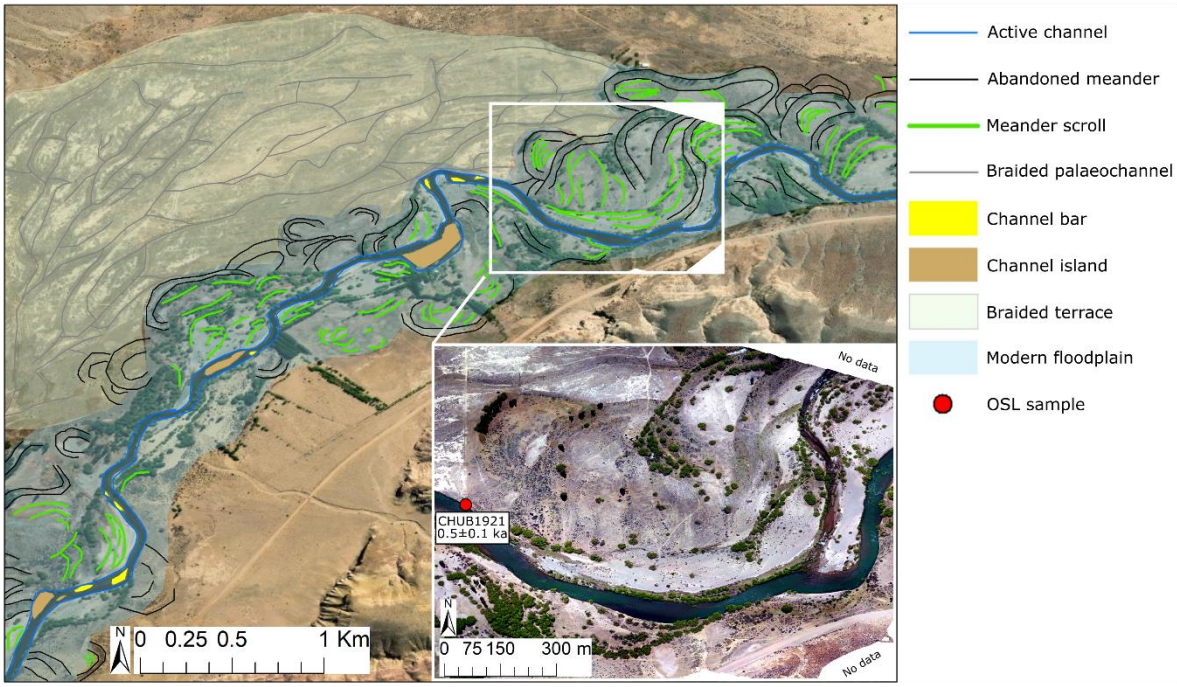


Figure 6.5. Site CHUB5 lower-level valley geomorphology with location of luminescence samples. Base map sourced from ArcMap World imagery Layer. Imagery for Inset map sourced from onsite UAV photography.

### 6.2.0 Methods

#### 6.2.1 Remote mapping

Geomorphological mapping of the lower-level valley features by Skirrow et al. (submitted) was used as the basis for identifying and contextualising smaller sites of interest along the Río Chubut study reach (see Chapter 3). High-resolution, georeferenced aerial imagery was collected using an uncrewed aerial vehicle (UAV) traversing the targeted sites and Metashape Agisoft software was used to generate high-resolution orthographic imagery (5 cm resolution) and DEMs (20 cm resolution) for in-depth geomorphological analysis (Westoby et al., 2012). More extensive lower resolution imagery was sourced from the Esri™ World Imagery Layer in ArcMap (10.8) (Maxar, Vivid (02/2021, 03/2018 ,03/2019)).

Elevation data taken along horizontal transects was extracted from the high-resolution DEMs using the 3D Analyst tool in ArcGis to generate cross-sectional profiles. Trees intersecting the transect lines obscured the visualisation of the ground surface topography and so were removed from the data set so they appear as gaps in the cross-sectional profile lines. As the channel bathymetry is unknown, the water surface of the active channels is presented as horizontal elevations using the points of intercept between water and land.

### 6.2.3 Luminescence dating

Luminescence dating measures the time that has elapsed since a body of sediment was last exposed to sunlight and then buried and shielded from light. The natural decay of K, U, Th and Rb, in addition to the contribution from cosmic rays, releases electrons which get trapped in defects in the crystalline structure of grains of quartz and K-feldspar. Over time whilst the grains remain buried and shielded from light, a dose accumulates at a constant rate (similar to charging a battery). Upon exposure to light, the trapped electrons are stimulated, evicted from their traps and emitted as photons of light. The grain releases its charge (or dose), and the luminescence signal is reset to zero (termed bleaching).

*Sample collection*

Borehole sample CHUB1919 [-42.4092, -70.56989, 518 m asl] was taken from a palaeochannel at site CHUB6. Sample CHUB1919 was taken from the basal sediments of a palaeochannel in an abandoned meandering channel belt. These sediments were highly organic and the presence of mature trees and roots surrounding the channel indicate that bioturbation may be a factor in this sample. The luminescence age represents the age at which this channel was last active.

Tube sample CHUB1911 [-42.4989, -70.53729, 498 m asl] was taken from a large migrating meander bend at site CHUB5. Sample CHUB1911 was taken from a vertical section of the meander scroll closest to the modern meander. The basal gravel deposit was sampled (10 cm-thick). The luminescence age represents the age at which the meander was last active at this site.

Samples CHUB1907 and CHUB1921, originally presented in Skirrow et al. (2021), are included here to contextualise the timing of river evolution observations. Sample CHUB1907 was taken from a fluvial surface at site CHUB5 that is characterised by relict meander bends and palaeochannels. It was identified as the oldest part of the targeted site location and as it is outside of the extents of the more recently formed features, and at the outer boundary of the fluvial surface (as was accessible) where reworking has been found to be less frequent (Van de Lageweg et al., 2016). The sample was collected next to an anthropogenically-managed drainage channel, but the sample itself was from underlying gravels and so was undisturbed by modern land management; thus, it is interpreted as meandering channel lag. The luminescence age of this sample reflects the time that has elapsed since the channel was last active at this distal location from the modern channel and provides a minimum age for the earliest meandering activity preserved at this location.

Sample CHUB1921 was collected from the oldest channel in a migrating meander sequence at site CHUB1. It was identified as the oldest preserved meander bend as it is the first of the successive meanders overriding their preceding channel. The luminescence age of this sample reflects the time that has elapsed since this channel was last active.

*Sample preparation*

Sample preparation in the laboratory followed the same procedure that was detailed in Chapter 5 (Section 5.4.1).

*Analysis and age calculation*

Dose rate ($D_r$) calculations followed the same procedure outlined in Chapter 5 (Section 4.1), and the results are detailed in Table 6.1. Equivalent doses ($D_e$) were measured using a Risø TL/OSL DA-15 automated single-grain reader equipped with a $^{90}Sr$ beta source and focussed infra-red (IR) laser (Bøtter-Jensen et al., 2003). A single aliquot regenerative dose (SAR) protocol was used (Murray and Wintle, 2000) with the post-IR IRSL protocol (Thomsen et al., 2008) on single grains of K-feldspar and the results are plotted as abanico plots (see Chapter 5, Section 5.4.1) (Fig. 6.6). Dose-recovery and residual dose experiments were performed for one sample that was representative of the sediments collected from the meandering floodplain and terraces, sample CHUB1921. The sample was subjected to an 8 hour bleach in the solar simulator prior to measurements. The results recovered the given dose within ±10 % of unity, which showed that the SAR protocol was appropriate for $D_e$ analysis, and determined an intrinsic over dispersion of 21 ± 0 %–(Fig. 6.7). $D_e$ values for individual grains were analysed using an age model to determine the overall $D_e$ for each sample. The minimum age model (MAM) was used for sample CHUB1911 and CHUB1919 because the single-grain $D_e$ distribution was asymmetrical which is typical of partially bleached samples (Table 6.2). The unlogged-MAM was used for samples as the $D_e$ values were approaching zero.

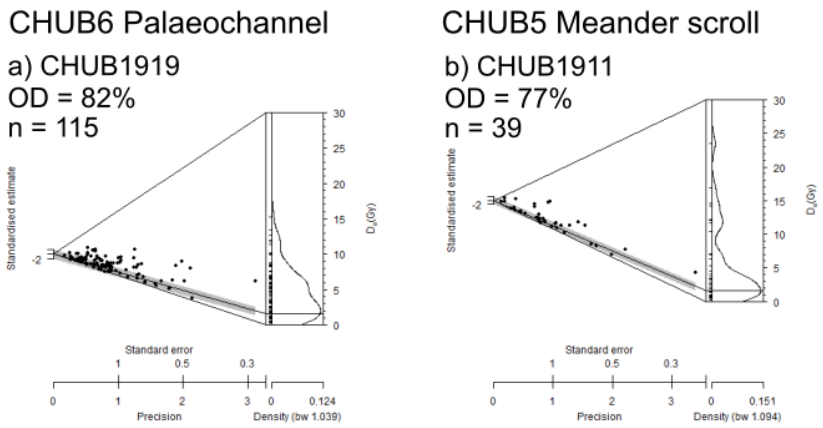


Figure 6.6. Abanico Plots showing the distribution of single-grain $D_e$ values measured for each sample. The grey line shows the unlogged MAM $D_e$ value (±1σ).

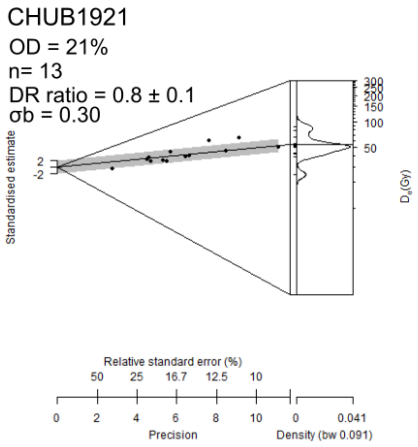


Figure 6.7. Results from dose-recovery (DR) and residual-dose recovery experiments. The grey line represents the CAM $D_e$ value. The DR ratio is the CAM $D_e$ value calculated for the residual doses subtracted from the CAM $D_e$ value calculated for the given doses, divided by the given dose (52 Gy).

Table 6.1. Environmental dose-rate results for the sedimentary samples taken from the Río Chubut, Argentina. Environmental dose-rates were determined using K, U and Th concentrations measured with ICP-MS. The dose-rates were calculated using the conversion factors of Guerin et al., (2011) and alpha (Bell, 1980) and beta (Guerin et al., 2012) dose-rate attenuation factors. Water contents were estimated following measurement in the laboratory; these values are expressed as a percentage of the mass of dry sediment, and were representative of the water contents over the burial period. An internal K-content of 10 ± 2% (Smedley et al., 2012) were used to determine the internal dose-rates. An a-value of 0.10 ± 0.02 (Balescu and Lamothe, 1993) was used to calculate the alpha dose-rates. Cosmic dose-rates were determined after Prescott and Hutton (1994). Dose-rates were calculated using the Dose Rate and Age Calculator (DRAC; Durcan et al., 2015).

| Sample | Latitude (°S) | Longitude (°W) | Depth (m) | Grainsize (µm) | Water content (%) | U (ppm) | Th (ppm) | K (%) | Internal dose-rate (Gy/ka) | External alpha dose-rate (Gy/ka) | External beta dose-rate (Gy/ka) | External gamma dose-rate (Gy/ka) | Cosmic dose-rate (Gy/ka) | Total dose-rate (Gy/ka) |
|---|---|---|---|---|---|---|---|---|---|---|---|---|---|---|
| CHUB1911 | -42.49889 | -70.53729 | 0.90 | 180-250 | 8 | 1.3±0.1 | 5.9±0.6 | 2.0±0.2 | 0.92±0.17 | 0.08±0.02 | 1.61±0.14 | 0.85±0.06 | 0.28±0.03 | 3.74±0.23 |
| CHUB1919 | -42.40920 | -70.569890 | 1.06 | 180-250 | 44 | 1.5±0.1 | 3.8±0.4 | 1.3±0.1 | 0.92±0.17 | 0.05±0.01 | 0.80±0.05 | 0.55±0.02 | 0.28±0.03 | 2.48±0.18 |

Table 6.2. Luminescence dating results for the sedimentary samples taken from the Río Chubut Argentina. The g-values (%/decade) were measured using the $pIRIR_{225}$ signal for three aliquots of K-feldspar for each sample, normalised to two days and are presented as weighted means and standard errors. The number of grains that were used to determine a $D_e$ value (n) are shown as a proportion of the total grains measured (N). The $\sigma_b$ value (0.3) was estimated by combining in quadrature the overdispersion from internal sources determined from dose-recovery experiments, and extrinsic sources.

| Sample | Total dose-rate (Gy/ka) | g-value (%/dec.) | n/N | Overdispersion (%) | Age model chosen | $\sigma_b$ | $D_e$ (Gy) | Age (ka) |
|---|---|---|---|---|---|---|---|---|
| CHUB1911 | 3.74±0.23 | 0.42±0.80 | 39/300 | 77 | u-MAM | 0.30 | 2.77±0.75 | 0.7±0.2 |
| CHUB1919 | 2.48±0.18 | 2.34±0.84 | 115/700 | 82 | u-MAM | 0.30 | 1.56±0.24 | 0.6±0.1 |

## 6.3 Results

### 6.3.1 Geomorphology

*Site CHUB6*

High-resolution aerial imagery and elevation data inform in-depth geomorphological and topographical analysis of the channel and its surroundings in the targeted area of the site CHUB6 flood basin. The inactive channel (Fig. 6.8) is heavily covered by trees which conceals most of the banks and channel bed, as a result the availability of digital elevation data for this channel is limited. Nonetheless, cross-sectional profiles of the channel from the breaks in vegetation shows the channel to be ~1.5 m deep and ~9.6 m wide, between 3-4 times smaller than the present day more single thread channel system. This channel is sinuous and characterised by incision, which is identified in the aerial imagery where no evidence of rapid lateral migration (point bars, and/or meander scroll forms) is observed for this channel. Cross-sectional profiles support this due to the steep-sided and relatively symmetrical bank geometry (Fig. 6.8a; Transects 1-4).

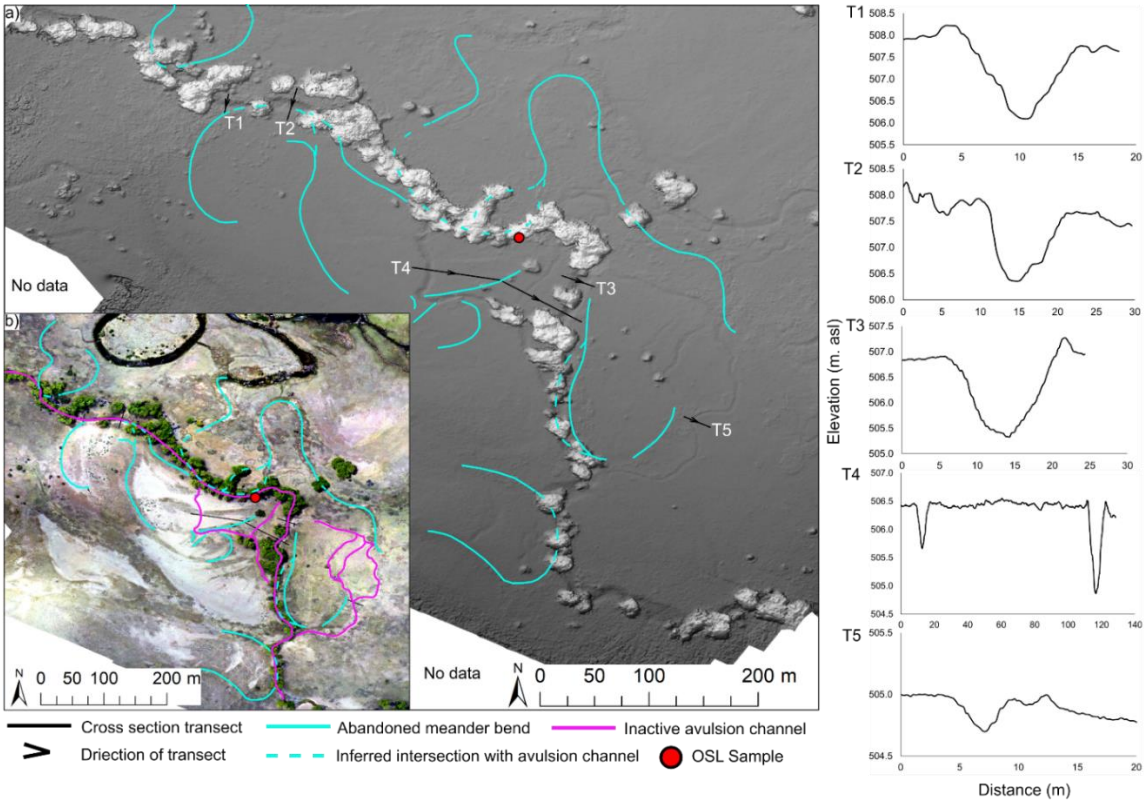


Figure 6.8. Topographical and geomorphological analysis of the targeted channel and surrounding areas at site CHUB6. T is an abbreviation for Transect; T1 is Transect 1 for example. High-resolution DEM and aerial imagery sourced from onsite UAV photography. Cross section data collected from the DEM.

The inactive channel in Fig. 6.8 occupies fragments of older channels, irrespective of chronological age, especially meander apexes (Fig. 6.8). It forms a more direct route to the next channel that bypasses meander necks and more distal portions of older channels. The surrounding geomorphology is subdued and not resolved in the lower resolution DEM but the high-resolution imagery displays an array of large abandoned meander bends with well-developed point bars and meander scroll formations (Fig. 6.8b). More minor channels deviate from the main channel and show the same characteristics on a smaller scale (Fig. 6.8; Transect 4 and 5). The minor channel intersected by Transect 4 (~10 m along the transect) is situated upon a large meander scroll formation (Fig. 6.8b), at first cutting south across the crescent shaped scroll bars and then turning east in conjunction with the path of relict scroll bars and meander apexes before re-joining the main channel.

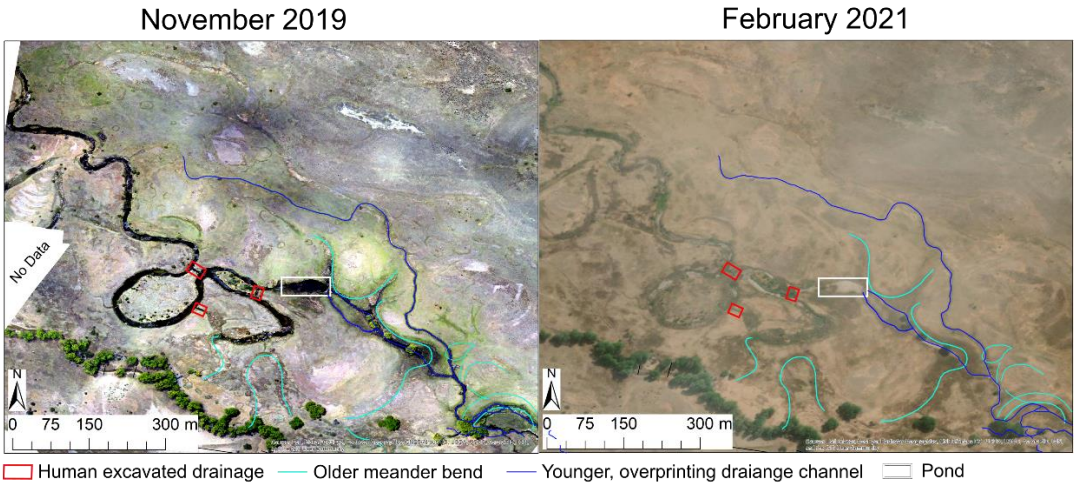


Figure 6.9. Comparison of channel activity on site CHUB6 taken in the austral spring and the end of the austral summer. Left image: imagery taken from a UAV in the field (09/11/2019), georeferenced image tiles mosaiced using Agisoft Metashape stoftware. Right image: imagery from the World Imagery Layer in ArcMap 10.8 sourced from Maxar (Vivid, 28/02/2021).

The channel located north of that described in Fig. 6.8 is active in the UAV imagery and it appears to pond in a meander bend. Overflow from the pond occupies channels of differing chrono-morphological age that have been connected by more recently formed channels (as described above). Human intervention is evident in the northern channel where two channels have been excavated to concentrate flow towards the pond area and one to direct drainage from the large meander loop to a south-easterly channel (Fig. 6.9) (inactive at the time imagery was collected).

Imagery from two different time stamps evidences the modern ephemeral regime of the northern channel (Fig. 6.9). UAV aerial imagery, taken in November 2019, shows water occupying the channel but the Maxar, Vivid imagery from February 2021 (Esri™ Global Imagery Layer) shows the channel to be dry (Fig. 6.9). The channel described above and in Fig. 6.9 is not occupied by the river in November 2019 but field observations from 09/11/2019 report saturated ground within the channel.

*Site CHUB5*

The floodplain cross-sectional profile at site CHUB5 shows that the floodplain is of low relief with a subdued terrace (Fig. 6.10). The transect extends across a relatively tight meander loop to the northwest of the current river, and former channels immediately upstream suggest persistence and presence of a tighter loop in the past. There is an elevation difference of only 80 cm over the 858 m transect (0.1 % slope). The cross-section records areas of uncharacteristic, higher elevation than the furthest

point from the modern river. The start of the transect intersects two - possibly three - anthropogenic irrigation channels, potentially modified from an existing back channel. These anthropogenic channels direct water across the floodplain, and supply water to the two former meander bends located directly upstream of the transect. In places, anthropogenic floodplain irrigation utilises the lower-lying ground in existing abandoned channels (Fig. 6.10 i and ii). Next, the transect intersects an abandoned meander bend that was progressing in a northeast direction (Fig. 6.10 iii) before it was cut off, and that section of channel was incorporated into a meander with a larger wavelength (Fig 6.10a). The transect then crosses the subdued terrace edge, where the morphology reflects a multi-channel chute formation (Fig. 6.10a iv and b). A back channel is located immediately down transect and reflects a more confined channel structure of two channels that are separated by a bar (Fig. 6.10a v). One of the channels was active at a reduced flow at the time the imagery was collected, and the exposed geometry of the channel bed reflects a point bar in the cross-sectional profile (Fig. 6.10c). A clear boundary separates the channel in the transect section vi and the south easterly scrolling forms from the progression of the modern meander (Fig 6.10a). The chute channels and back channel are the most recently incised channels on the floodplain which is indicated by the lower elevation than the rest of the floodplain transect and the current occupation of subsidiary drainage (Fig. 6.10d iv and v). There are no obvious abandoned meander channels after that of section vi (Fig. 6.10a v) and only scroll bars mark the migration of the modern meander over 223 m to its contemporary position. The profile of the modern point bar demonstrates progressive scrolling activity with the lower gradient banks of scroll bars sloping towards the channel to meet steep cut banks (Fig 6.10d vi).

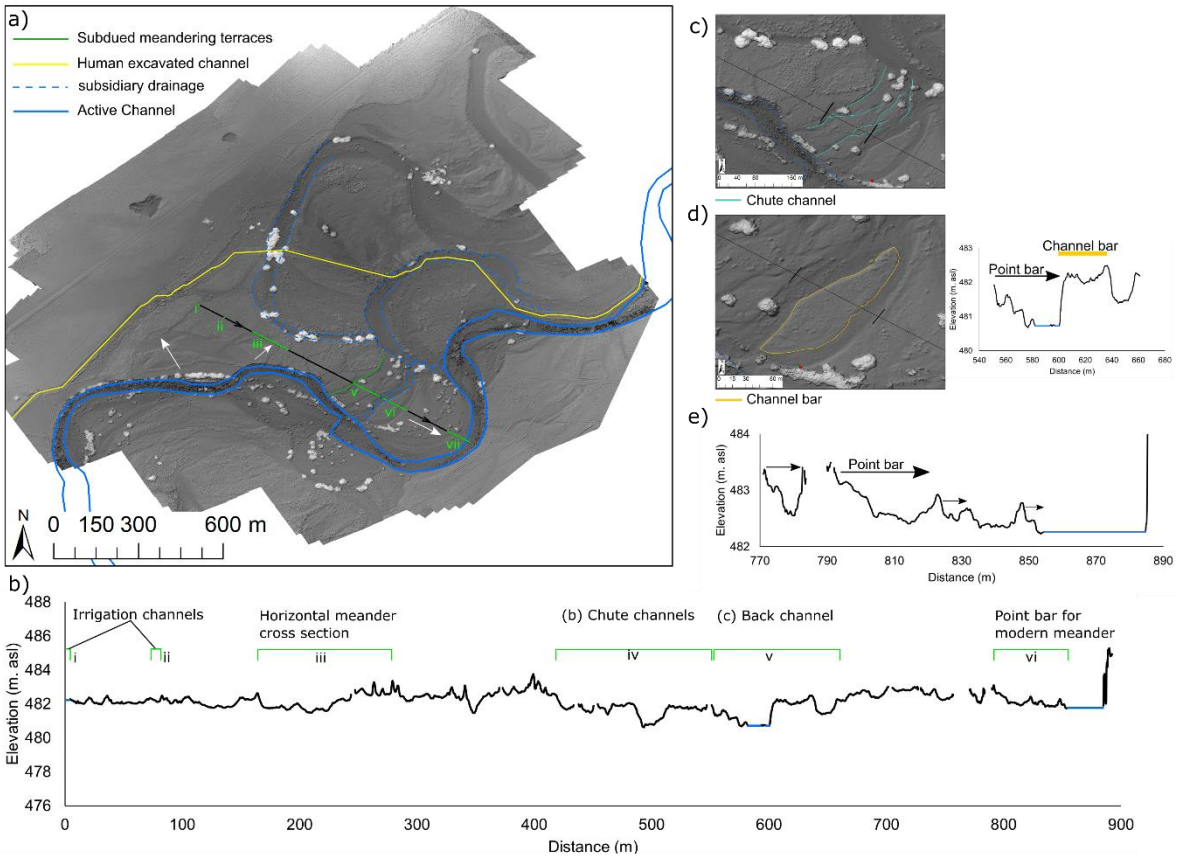


Figure 6.10. Topographical and geomorphological analysis of the floodplain cross-section at site CHUB5. White arrows indicate the direction of meander expansion. High-resolution DEM and aerial imagery sourced from onsite UAV photography. Cross-section data collected from the DEM.

The meander bend pointing northwest and positioned directly upstream of the transect is connected in a temporal morphological sequence to two adjacent former meander bends, both displaying evidence of lateral migration and abandonment via chute cut off. These meanders have been connected to an artificial water supply by human excavated drainage channels (Fig 6.10a).

*Site CHUB1*

The floodplain topography at site CHUB1 is steeper than the floodplain and terrace at site CHUB5 with a 1.0% slope along Transect 1 (861 m) towards the modern channel. The geomorphology and topography show a series of six well preserved, mature, abandoned meander bends overriding each other in sequence to its current position. The relative age of meanders in this sequence is extrapolated from the order in which they cross-cut each other; the oldest of the meanders is positioned to the west while younger meanders formed successively eastward (Fig. 6.11a). Channel migration patterns in the meander sequence shows a general westward and

northward scrolling within the abandoned meander bends. The direction of scrolling is indicated by the geomorphological progression of the meander apex and crescent shaped scroll bars, and the topographical direction of the cross-sectional profiles where a lower gradient bank of the point bar slopes towards the channel to meet a steep cut bank (Fig. 6.5c).

The aerial imagery shows a more subtle pattern of abandoned channels to the south of the meanders that show a preferential eastward gradient and scrolling direction (Transect 2; Fig. 6.11d). The channel fragment that is overridden by the meander sequence is identified as the oldest channel on this section of floodplain (sampled for luminescence dating); cross-sectional profile of Transect 2 (25 – 50 m) indicates a westward scrolling direction (Fig. 6.11d).

South of Transect 2 is the modern southward scrolling point bar, the eastern extent has been abandoned where the penultimate meander in the sequence has been succeeded by the modern channel and a new point bar is aggrading on the inside of the newly forming meander. Sediment infill is occurring at the upstream end of the penultimate meander neck and is considered to be no longer supporting the thalweg but is not yet part of the floodplain and still contains water (at the time imagery was captured).

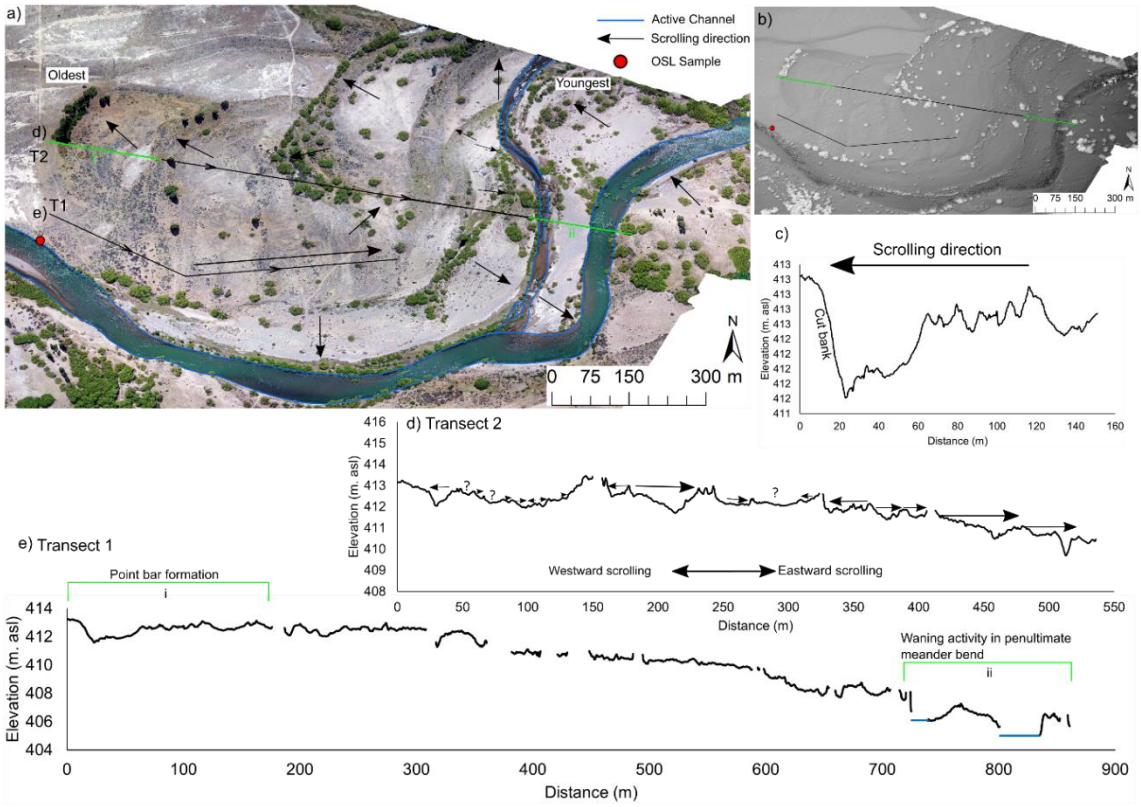


Figure 6.11. Topographical and geomorphological analysis of the floodplain cross section at site CHUB5. T is an abbreviation for Transect; T1 is Transect 1 for example. High-resolution DEM and aerial imagery sourced from onsite UAV photography. Cross section data collected from the DEM.

### 6.3.2 Luminescence dating

The luminescence age at site CHUB6 (Sample CHUB1919) represents the time that has elapsed since the last deposition of channel lag sediments (i.e. since the channel was last active). This age is constrained to 0.6 ± 0.1 ka where this channel was last active.

The luminescence age at site CHUB5 represents the time that has elapsed since the channel was last active in that position (i.e. since the last deposition of channel lag sediments). The river was last active in the channel represented by sample CHUB1911 at 0.7 ± 0.2 ka where is then migrated 223 m to its modern position through the scrolling of the point bar in the direction of the meander apex.

The age of luminescence samples CHUB1907 (2.2 ± 0.2 ka) (Fig. 6.4) and CHUB1921 (0.5 ± 0.1 ka) (Fig. 6.5), initially presented in Skirrow et al. (2012), constrain the oldest meandering activity at the targeted floodplain sections at sites CHUB5 and CHUB1, respectively. Sample CHUB1907 represents a minimum age for the earliest channel activity preserved on the meandering terrace at site CHUB5. The

results show that this fluvial surface preserves abandoned channels at least 2.2 ± 0.2 ka in age.

The luminescence age at site CHUB1 represents the minimum time that has elapsed since the river was last active in the channel represented by sample CHUB1921 (i.e. since the last deposition of channel lag sediments) and estimates the maximum time taken for the channel to migrate to its modern position. The river was last active in this channel by 0.5 ± 0.1 ka. The sequence of six well preserved meanders that override this channel formed after 0.5 ± 0.1 ka and before the present day.

## 6.4 Discussion

### 6.4.1 Channel processes

The zone on site CHUB6 which hosts the anastomosing floodplain channel preserves features from two phases of fluvial activity; older meandering activity synonymous with the main channel of the Río Chubut has been succeeded by an anastomosing planform that is active ephemerally in the present (Skirrow et al., submitted; Chapter 3 Section 3.3.2). The comparable geometry of the underlying meander bends to the modern channel and former meander belts suggests they are artifacts of the contemporary meandering regime when it occupied this zone of the floodplain and, like the other meander belts, was likely abandoned through avulsion. Whilst the anastomosing planform occupies the older meander bends, it likely receives all of its drainage from a wetland upstream of a knickpoint in the valley rather than diverting water from the main channel Río Chubut. Therefore, it is not considered to be residual activity of the former meander belt, but later re-occupied these channels as a floodplain channel supplied separately to the main channel Río Chubut. The anastomosing floodplain channel supplies drainage to the modern Río Chubut through a series of confluences which demonstrates the contemporaneous activity with the active channel belt.

Discharge, sediment load, sediment types and slope can all influence the width, depth, velocity, and planform of a channel (Hey, 1976). The planform and geometry of the anastomosing floodplain channel at site CHUB6 (Fig. 6.8) demonstrates the prevalence of incisional processes in the anastomosing planform in contrast to the preferential lateral erosion of the modern meandering river. Anastomosing planforms are initiated by the incision of multiple channels on an unconfined surface during periods of high flow or flood conditions, commonly linked with avulsion, initiated from crevasse splay channels (Makaske, 2001; Smith et al., 1989 (see Chapter 5, Section 5.3.2) The commencement of the anastomosing planform here, occurs immediately

downstream of a knickpoint where the accommodation space between the modern meander belt and the valley slopes is confined. The sudden expansion of accommodation space downstream of the knickpoint could facilitate the splay-like conditions that is linked with the establishment of anastomosing channels (Bridge and Leeder, 1979). Under normal conditions, anastomosing channels are characterised by low energy flow and along a low gradient (Makaske, 2001) which is reflected by the finer grain sediments in the top 0.9 m of the sampled channel (sample CHUB1919). The high-resolution aerial imagery shows that anastomosing channels targeted here incised the older, subdued meander bends to form its path (Fig. 6.8). Channels preferentially occupy floodplain areas with frequent relict channels because they comprise a more erodible channel substrate that facilitates more efficient channel incision, as evidenced in the Mississippi and Red River (Aslan et al., 2005). This process and the low gradient of the floodplain likely also explains the uncharacteristic, large meander loop in the northern channel (Fig. 6.9). Channel incision and further anabrancing in anastomosing planforms usually occurs during high flow or flood conditions (Harwood and Brown, 1993).

Comparison of aerial imagery taken from November 2019 (when the northern channel was active) and February 2021 (when the northern channel was inactive) shows the northern channel has an ephemeral regime. Imagery collected from the UAV demonstrates that although this channel does not support the main thalweg of the Río Chubut, it is still occupied at times of higher flow. The timing of the photography places the dry channel conditions at the end of the austral summer (February) and the waterlain conditions in the austral spring (November), so it is possible that the ephemeral activity in this channel is driven by seasonal changes in water supply. Weather and climate data from Paso de Indios (-42.90˚N, -71.20˚W, 785 m) shows a 51% seasonal difference in precipitation, from an average total of 118.4 mm in the austral autumn/winter months to only 58.0 mm in the austral spring/summer months (over 22 years) (Peterson and Vose, 1997). Greater water availability in the autumn/winter months likely drives seasonal activity in ephemeral channels.

The geomorphology at site CHBU5 demonstrates the natural dynamics of the mature meandering system in the Río Chubut, including meander expansion, meander scrolling, meander cut off, point bar development and chute channels (Hickin and Nanson, 1975; Stølum, 1998; van de Lageweg et al., 2014). The two former meander loops show that the river is laterally eroding the breadth of the floodplain along this reach, and meander expansion and scrolling processes form large complex meander loops (Brice, 1974). These large meanders were abandoned through chute cut off

which occurs when the flow exceeds the transport capacity of the channel, causing a more direct chute channel to incise and bypasses the meander bend (Viero et al., 2018). Anthropogenic drainage channels facilitate drainage to the two former meander loops and the back channel on the floodplain (Fig. 6.10) at an artificially low flow, but peak flow and flood conditions would occupy this and the chute channels naturally. The Río Chubut has experienced intense floods over the last 30 years, with 137 flood events exceeding 200 $m^3 s^{-1}$ at Gualjaina (Estacion-2301) where the annual daily maximum discharge is just 29.9 $m^3 s^{-1}$ (Secretería de Infraestructura y política Hídricia, 2018). The chute channels and back channel on the CHUB5 floodplain allow river flow to bypass the active meander bend during peak flow or flood conditions (Zinger et al., 2013) which over time, can lead to the progressive incision of the channel and eventual cut off of the meander loop in favour of the more direct chute channel (Hooke, 1995; Constantine et al., 2010).

The abandoned meander bends preserved at site CHUB1 show features consistent with mature meander bends that have expanded and increased in sinuosity through scrolling and lateral erosion (Brice, 1974; Hickin and Nanson, 1975). The series of six meander bends formed successively in a downstream direction through cycles of meander scroll and cut off where each meander was cut off by the river in place of a more direct path, which then developed into a meander itself (Yan et al., 2021). The penultimate meander bend is still active but no longer supports the thalweg; bedload channel fill has begun due to the decreased energy in the channel which typically continues until the up- and downstream ends of the meander are completely cut off from inflow from the river, after that the channel is infilled by sediment supplied by over bank flow (Allen, 1965).

Modern land management practices are evident at site CHUB6 and site CHUB5, which is artificially modifying the supply of water to former meander bends and channels. At site CHUB6, the ephemeral occupation of the channel is likely natural, however, drainage channels are used to increase drainage to targeted parts of the channel or to direct water into other channels nearby to distribute water to other parts of the floodplain. Drainage ditches have been excavated to direct water into two former meander bends at site CHUB5. Former channels such as the back/floodplain channel on the meandering terrace have been utilised in artificial drainage for their existing gradient and channel geometry.

### 6.4.2 Floodplain evolution

The current floodplain and meandering terraces targeted in this study preserve palaeofluvial features up to 2.2 ± 0.2 ka. However, the meandering planform was likely initiated after the abandonment of the braided regime which occurred time-transgressively between 12.3 ± 1.0 ka and 9.4 ± 0.8 ka (Skirrow et al., 2021). At the targeted section of site CHUB5, the age of the oldest preserved meandering channel deposit (2.2 ± 0.2 ka) suggests the meandering regime is reworking the floodplain and subdued terraces here, on a time scale of at least ~2 ka.

The anastomosing channel represented by sample CHUB1919 at site CHUB6 (0.6 ± 0.1 ka) puts broad temporal constraints on the modern meandering channel belt and older avulsion channels across the flood basin. Satellite imagery shows that the downstream extent of the channel flows into the modern channel, indicating that the modern meander belt was established when the anastomosing channel was last active (Fig. 6.8). Therefore, it is inferred that the older channel belts spread across the CHUB6 flood basin (described in Skirrow et al, submitted, Chapter 3) were active prior to 0.6 ± 0.1 ka.

The luminescence ages corresponding to the meander migration observed on site CHUB5 (Fig. 6.10) and CHUB1 (Fig. 6.11) shed light on the mobility of the modern channel. The channel represented by CHUB1907 was last active by 0.7 ± 0.2 ka when it then migrated, via scrolling action, 223 m to its current position. The luminescence age for the oldest channel at site CHUB1 suggests that the channel mobility is greater here than the meander at site CHUB5. Over the period between 0.5 ± 0.1 and the present day, this section of the channel has migrated 754 m through at least six cycles of meander development and cut off in a successive easterly direction. The difference in age between the outer boundary of the fluvial surface (samples CHUB1907) and those proximal to the channel (samples CHUB1911 and CHUB1921) could be reflecting different residence times for sediments deposited across the floodplain. Numerical modelling, simulating a highly sinuous meandering river found that the greatest potential for channel preservation is at the outer boundary of the meander belts whereas reworking of the inner surface is more frequent (Van de Lageweg et al., 2016).

### 6.4.3 Holocene headwater environment

Past and present environmental change in Patagonia is influenced by key climate systems such as the ENSO (Moreno, 2004), and the mid-latitude storm tracks and westerlies, which vary in latitudinal extent and intensity in response to changing

meridional temperature gradients (e.g., Lamy et al., 2010). According to the geomorphological findings of Skirrow et al., 2021 (see Chapter 5), the meandering planform in the Río Chubut directly follows the braided planform and so, although the timing of the onset is not constrained, it is likely that the meandering planform has persisted throughout the Holocene. The strong, eastward orographic rainfall gradient and the western source of the major tributaries means that the Río Chubut is fed predominantly from precipitation and run off from the eastern flanks of the Andes mountains, with ephemeral contributions from the gullies that drain the badlands landscape during rainfall events in the steppe (Skirrow et al, submitted; Chapter 2, Section 2.1.2). The strong vegetation gradient from forest in the west, to steppe in the east demonstrates the spatial difference in water availability between the catchment headwaters and the Steppe dominated middle course (Fig. 6.1; Iglesias et al., 2014). The Chubut headwaters are also vulnerable to temporal shifts in water supply due to its interaction with climatically sensitive forest-steppe ecotone (Iglesias et al., 2014).

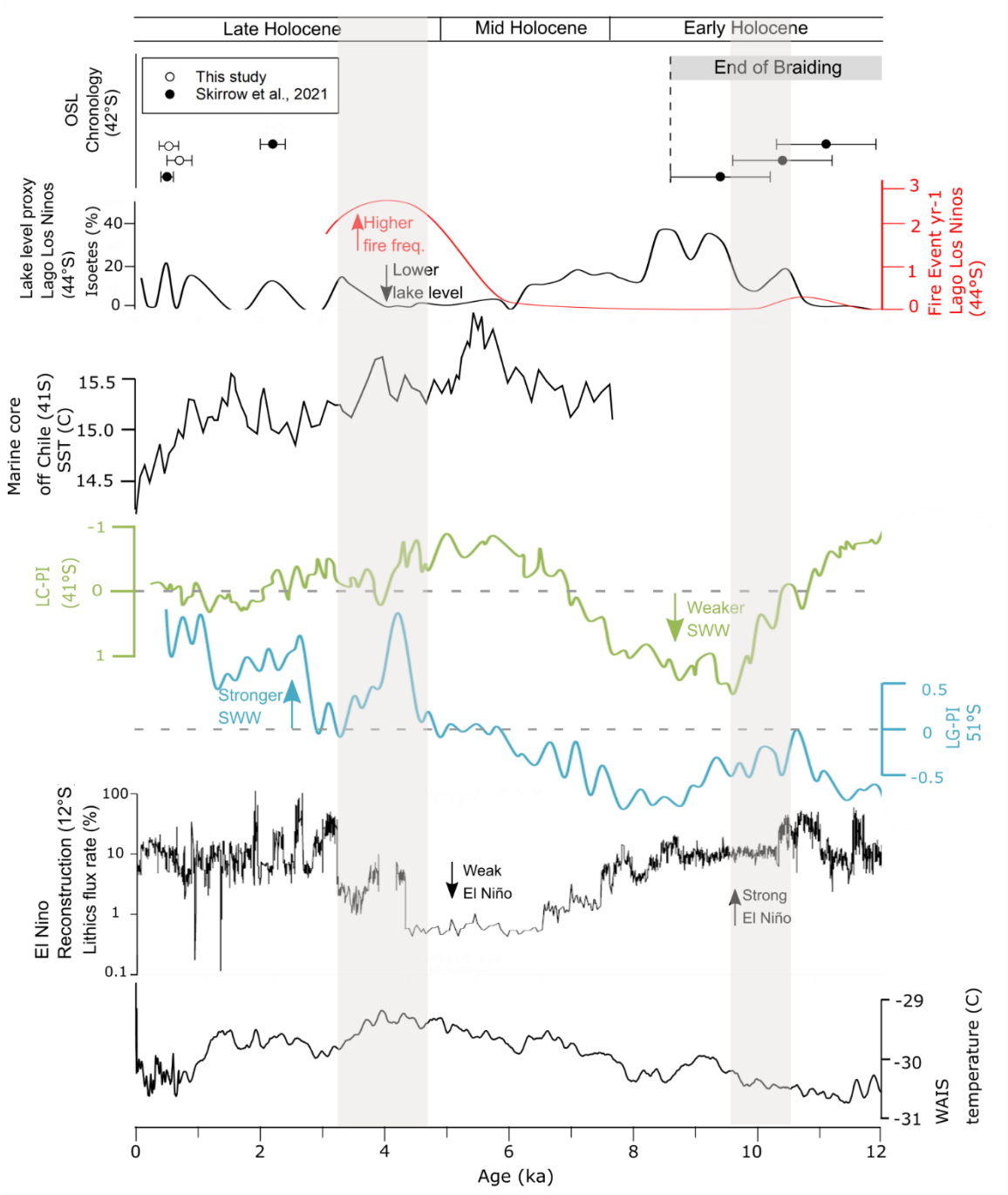


Figure 6.12. Luminescence ages for samples from the Río Chubut plotted alongside palaeoenvironmental records for the last 12 ka including fire frequency and lake level proxy records from Lago Los Niños (Iglesias et al., 2016), Sea surface temperature (SST) record from the GeoB 3313-1 marine core (Lamy et al., 2002), palaeovegetation index for Lago Condorito (LC-PI) and Lago Guanaco (LG-PI) representing the relative strength of southern westerly (SWW) influence (Fletcher and Moreno, 2011), El Niño reconstruction from the SO147-106KL marine core (Rein et al 2005) and the surface temperature reconstruction for the West Antarctic Ice Divide ice core (WAIS) (Cuffey et al., 2016).

Palaeoenvironmental reconstructions from the latitudinal reaches of the Río Chubut headwaters show climate, vegetation and water supply have been variable throughout the Holocene (Iglesias et al., 2012, 2014, 2016, 2018), and the forest steppe ecotone has shifted eastward and westward on millennial timescales in response to changes in climate and fire regime (Iglesias et al., 2014). The continued presence of the southern westerlies at ~41˚S after deglaciation provided enough moisture for *Northofagus* forest to establish in the headwaters of the Rio Chubut during the post-glacial (14.2 cal. ka BP) (Iglesias et al., 2016). The southern westerlies gradually shifted poleward to further south than their contemporary position, which brought drier conditions across Patagonia in the early Holocene (~10 cal. ka BP) (Fig. 6.12; Fletcher and Moreno, 2011), and led to a planform shift from a braided to a meandering planform in the Río Chubut (see Chapter 5; Skirrow et al., 2021). The reconstruction of ENSO Strength and frequency at 12˚S shows strong ENSO conditions throughout the early Holocene which would have brought greater rainfall to South America (Fig. 6.12; Rein et al 2005); more locally. However, records from the Chilian Lake District (41-44˚S) only detect an El Niño signal in northwest Patagonia after ~7 cal. ka BP (Moreno, 2004), brought wetter conditions and greater variability to the region when they strengthened. The influence of the southern westerlies at 41˚S is variable on millennial-centennial time scales, but it gradually increased into the mid-Holocene bringing greater moisture availability (Fig. 6.12; Fletcher and Moreno, 2011). East of the Andes at 44˚S, lake levels at Lago Los Niños increase and show variability through the early Holocene which stabilised into the mid-Holocene (Fig. 6.12; Iglesias et al., 2016). Between ~3.5 and 4.5 ka, high fire frequency and low lake levels at Lago Los Niños indicate drier conditions toward the southern extent of the Río Chubut catchment (44˚S) (Fig. 6.12; Iglesias et al., 2016). This is synchronous with elevated surface temperatures in Antarctica (Fig. 6.12; Cuffey et al 2016), and a weakening of the southern westerlies at 41˚S and a strengthening at 51˚S (Fig. 6.12; Fletcher and Moreno, 2011), suggesting that the southern westerlies moved to a more southerly position in the early stages of the late Holocene and reduced the water supply to the Río Chubut. Sea surface temperatures and Antarctic surface temperatures decline after ~ 4 ka, whilst the influence of the southern westerlies broadly stabilises at 41˚S. El Niño is strong at 12˚S and lake level are the most variable after ~3.5 ka which could have caused instability in water supply to the Río Chubut headwaters on millennial time scales.

The Río Chubut has likely sustained its meandering planform throughout the Holocene despite the variability in water supply demonstrated by

palaeoenvironmental records (Fig. 6.12). The planform thresholds in meandering systems include stream power, and sediment availability and transport. Increased stream power beyond the threshold for a channel can cause instability and force a river to braid or incise (Schumm, 1977 as cited in Bledsoe and Watson, 2001), sediment availability beyond a threshold can also induce braiding if there is sufficient stream power to mobilise it (Friend and Sinha, 1993). An increase in sediment transport can lead to a widening of the channel which, beyond a threshold, will destabilise the sinuous channel and it will begin to braid (Métilier et al., 2017). Despite this, meandering planforms are highly adaptable as seen from their persistence in an array of environments (Li et al., 2017); for example, channel width, sinuosity and meander stability adapt to changes in flow regime, sediment supply and vegetation cover (Ahmed et al., 2019; Hooke, 2022, Zhu et al., 2022). Factors effecting the sediment availability includes riparian bank vegetation and the ~3 m thick accumulation of fine-grained loess that is overlying much of the lower valley floodplain and subdued terraces; thus, restricting the accessibility to sediments in the study reach. Palaeoenvironmental reconstructions show that the meandering regime did not surpass any planform thresholds despite experiencing millennial-to-centennial scale fluctuations in water supply throughout the Holocene. Comparison to the former braided planform is limited because the magnitude of these shifts has not been characterised and so the key factors of planform resilience between the meandering and braided regime cannot be concluded.

### 6.5 Conclusion

The relative temporal evolution of geomorphological sequences of meander migration, floodplain evolution channel activity along the 75 km study reach in the Río Chubut are temporally constrained here by luminescence dating. Firstly, the new data shows that floodplain and terrace sediments accumulated by the contemporary meandering regime have a residence time of at least ~2.2 ± 0.2 ka. Secondly, the data shows that sediment mobility is greater in the immediate proximity of the modern channel. The targeted channel section at site CHUB5 migrated 233 m over 0.7 ± 0.2 ka by the process of meander scrolling. The sequence of abandoned meander studied at site CHUB1 migrated 754 m over 0.5 ± 0.1 ka to its modern position through at least six cycles of meander development and cut off; Finally, the data shows that the anastomosing floodplain channel was last active at 0.6 ± 0.1 ka and drained to the modern meander belt. The geomorphological connection to the modern meander belt implies that it has been active for at least 0.6 ± 0.1 ka and older channel belts across the CHUB6 flood basin predate this. Palaeoenvironmental reconstruction and

assessment of recorded river discharge shows that the meandering planform is resilient to intense flooding and withstood the climate driven, water supply variability throughout the Holocene.

# Chapter 7

# Synthesis

This synthesis draws together the key finding of this research and relates them to the four research questions outlined in Chapter 1. Here, an extended discussion on the long-term dynamics of glacially-fed river systems demonstrates that the impacts of deglaciation and climate change on river regime is global. Paraglacial processes can act as a "buffer" between the extreme environmental shifts between glacial and interglacial conditions which many rivers are still experiencing today. However, the sensitivity to changes in water supply in the Río Chubut demonstrated that the paraglacial "buffer" is vulnerable to the allogenic drivers of warmer climatic conditions. Examples of rivers from around the world show that drivers and thresholds of change are unique to the geographic position and internal dynamics of every river system, and future climate change scenarios pose a threat to contemporary glacially-fed and paraglacial river regimes. Limitations and further work are also discussed and cover a broad range of future research directions that would build upon the findings of this thesis and enhance the new datasets presented here.

## 7.1 Synthesis of findings

### Research Question 1: Are different fluvial regimes recorded in the geomorphology of the Río Chubut?

Geomorphological analyses presented in Chapter 3 showed that the Río Chubut has undergone historic large-scale shifts in behaviour, including deep valley incision, planform change and channel migration. The contemporary Rio Chubut today is characterised as a mature meandering system, with reaches that display locally flood basin characteristics (Bridge, 2003; Lewin et al., 2005; Ashworth and Lewin, 2012). Previously mapped glacial features in the Río Chubut headwaters show that the feeders to the system have changed on the timescales of glacial-interglacial cycles (Caldenius, 1932; Glasser et al., 2008; Davies et al., 2020; Leger et al., 2020), where the river was fed by glacial drainage and/or drainage from proglacial lakes under glacial conditions, and precipitation and snowmelt under interglacial conditions. A series of higher-level terraces that broadly correspond in elevation across the Río Chubut and associated tributary valleys and are comprised of poorly-sorted, rounded

gravels indicate at least three stages of valley incision: (1) the floodplain aggraded at ~60-70 m above the modern river profile; (2) after which the river incised by ~20 m to then aggrade fluvial surfaces at ~40-50 m; and (3) this was followed by ~30 m of incision to the lowest and youngest of these higher-level terraces at ~10-20 m.

Geomorphological analyses of the features at lower-level elevations within the valley show that the Río Chubut in the past shifted from a braided planform to its contemporary meandering regime. Excellent preservation of subtle fluvial features is a product of the wide floodplain accommodation space, leading to preservation extensive palaeofluvial features of the modern meandering system and displays locally evidence of flood basin characteristics, including channel avulsion and an evaporitic floodplain lake.

Findings from the higher-level terrace framework correspond to a portion of the extensive La Pampas Formations, which have been attributed to glaciofluvial outwash from past glaciations (Martínez and Coronato, 2008). The three stages of valley incision described in Chapter 3 pertain to numerous shifts between aggradational and incisional river regimes. The abandonment of braided planform preserved in the lower-level valley demonstrates another large-scale shift in river regime and is discussed in Chapter 5. The flood basin and meandering planform floodplain features characterise the contemporary river regime.

The findings from the mapping performed to address Research Question 1 provided a geomorphological framework to test Research Questions 2, 3 and 4 when combined with analysis of the stratigraphy to determine the depositional conditions that prevailed when these landforms were created, in addition to luminescence dating to determine the timing of these shifts in river behaviour.

**Research Question 2: What were the driving environmental conditions that forced the aggradation of the higher-level terraces in the Río Chubut?**

The formation of the large gravel deposits, identified in Chapter 3, was driven by the sediment supplied to the system when glaciers occupied the Río Chubut headwaters. The upper sediment units for terrace levels T1 (~59 m) and T4 (4 m) were analysed and identified as glaciofluvial outwash according to the sedimentology and former glacial connection to the headwaters. These terraces are part of a series of geological formations named La Pampas, and, prior to this study, they were correlated tentatively to MIS 4-2 (Cabana and Confluencía Formations) (Martínez and Coronato, 2008). However, the luminescence chronology presented here showed that terrace

level T1 and T4 were in their later stages of aggradation at 85.4 ± 7.8 ka (MIS 5) and 17.8 ± 1.4 ka (MIS 2), respectively.

The lack of glacial and palaeoenvironmental records for MIS 5 mean that precise paleoclimate and ice sheet activity for the Patagonian region is unknown. However, globally the climate was cooler than present but warmer than glacial conditions, global ice volumes, sea surface temperatures and Antarctica temperature reconstructions show that ice volumes were high, and temperatures lower compared to the peak of the MIS 5 interglacial (MIS 5e) but were still warmer than the MIS 6 and MIS 4-2 glaciations (Lisiecki and Raymo, 2005; Ho et al., 2012; Jouzel et al., 2007). Aggradation of glaciofluvial outwash requires direct glacial drainage to the Río Chubut which, during the interglacial of MIS 5, is a challenging concept. The paraglacial legacy renders catchments enriched with materials, and later adjustment can mobilise glaciofluvial sediments for tens of thousands of years after decoupling from ice lobes (Ballantyne, 2002), which could explain the aggradation of glacially derived sediments during MIS 5. The luminescence chronology, when applied to the higher-level terrace framework (Chapter 3), suggests that the sediment that form terraces between ~60-70 m and ~4 m aggraded between 85.4 ± 7.8 ka and 17.8 ± 1.4 ka. The deposits within the higher-level terraces in this sequence likely aggraded prior to 85.4 ± 7.8 ka and were then abandoned by incision. The sedimentary analyses and luminescence chronology showed that the Cabaña and Confluencia Formations in the Río Chubut and tributaries were products of glacially derived sediments and their phases of aggradation spanned multiple glacial-interglacial cycles.

**Research Question 3: What were the driving environmental conditions that forced the Río Chubut to change its planform?**

After the higher-level terrace T4 at (~4 m) was aggraded (Cabaña Formation; see Chapter 4) the river incised and aggraded to the level of the most recent braided planform which is preserved in the lower-level valley (see Chapter 5). This would have occurred after 17.8 ± 1.4 ka (after the aggradation of terrace level T4) and before 12.3 ± 1.0 (before the abandonment of the braided planform). This transition occurred during a time of deglaciation where the Patagonian Ice Sheet retreated from the plateau into the higher altitudes of the Andes Mountains (Davies et al., 2020). During this time, the region experienced shifts in climate regimes, where the southern westerlies were migrating latitudinally in response to changing temperature gradients (e.g. Killian and Lamy, 2012 and Moreno et al., 2018). The braided planform persisted

for ~3 ka after the modelled deglaciation of the headwaters and the system experienced paraglacial adjustment (see Chapter 5).

Chapter 5 expands upon the identification of a planform shift from a braided to meandering regime in the lower-level valley in Chapter 3. Graded fluvial sediments overlying the braided gravels indicated that a reduction in water supply (i.e. energy) led to the abandonment of the braided planform (Charlton, 2007; Mol et al., 2000). Luminescence dating constrained the timing of the abandonment of braiding as a time-transgressive shift between 12.3 ± 1.0 ka and 9.4 ± 0.8 ka, and this coincided with a weakening and southward shift of the southern westerlies that brought drier conditions across the headwaters of the Río Chubut (Whitlock et al., 2007; Markraf and Huber, 2010; Moreno et al., 2010; Iglesias et al., 2016). After the shift in planform, the river system assumed a meandering planform that has persisted to the present.

**Research Question 4: On what time scale is the modern meandering Río Chubut evolving?**

Geomorphological features identified in Chapter 3 indicated that evolutionary processes characterised the Río Chubut river system, such as floodplain sediment storage, meander migration and cut-off, and the vacating of channels (Van de Lageweg et al., 2016; Brice, 1974; Hickin and Nanson, 1975; Stølum, 1998; Bridge and Leeder, 1979). Chapter 6 demonstrated that the contemporary Río Chubut meandering system has evolved variably over millennial to seasonal timescales. Luminescence dating showed that the floodplain system has preserved sediments and palaeofeatures dating to the last 2.2 ± 0.2 ka. As such, it is difficult to interpret what the river system was doing during the period of time between 9.4 ± 0.8 ka (when the last braided plain was preserved) and 2.2 ± 0.2 ka (when the older evidence of meandering is recorded by this study) because of the lack of geomorphological evidence and chronology for meandering features older than 2.2 ± 0.2 ka. It is possible that different river regimes were active in this timeframe and the remnants have been cannibalised or buried by subsequent fluvial activity, but the geomorphological connection between the braided terraces and meandering planform to suggests that the meandering planform evolved after the abandonment of braided regime and persisted throughout the Holocene. Channel migration timescales were variable, one meander scrolled 223 m over the course of 0.7 ± 0.2 ka, whereas another section of channel has undergone six cycles of meander development and cut-off within the last 0.5 ± 0.1 ka. The shortest timescale of change observed from aerial and satellite imagery is the seasonal occupation of an

ephemeral floodplain channel in the flood basin, where increased precipitation in the the austral winter months bring water supply to the channel. Gauge station data shows that the modern river experiences relatively frequent extreme flooding which facilitates morphological changes observed on the Río Chubut floodplain including avulsion and meander cut off (Zinger et al., 2013; Secretería de Infraestructura y política Hídricia, 2018; Wong et al., 2015).

### 7.2 Extended discussion

Globally, glacially-fed rivers display large-scale shifts in behaviour in response to decoupling from glacial feeders similar to the Río Chubut since MIS5 to the present-day as recorded in this study. Greater seasonal sensitivity has been observed in deglaciated rivers as the loss of ice meltwater contributions in summer dry seasons means that discharge cannot be sustained year-round (Anderson and Radić, 2020). A switch from aggradation to incision was observed in the Po River, Italy, in response to glacial drainage switching to lake drainage feeders as glacial sediment was trapped in the lakes whilst water supply to the river was maintained (Bruno et al., 2018). Secondary impacts of deglaciation include glacio-isostatic uplift which drove incision in the previously glaciated valley of the Yorkshire River Ouse, England, and abandoned gravel deposited during the last glaciation ~30 m above the modern floodplain (Bridgland et al., 2010). Rates of uplift are poorly constrained for the Río Chubut headwaters, but it likely impacts the headwaters and upper course of the river due to the proximity to the former Patagonian Ice Sheet. The rate of uplift north of 46.5°S is <8 mm a−1, which suggests the Río Chubut catchment was not subject to rapid crustal uplift during after the last glaciation (Dietrich et al., 2010). Conversely, more recent uplift estimates suggest there was ~130 m of uplift at 43˚S, 71˚W (Palena) which could have similarly occurred in the Río Chubut headwaters and impacted the study site.

Deglaciation is driven by climatic warming, which impacts the river corridor in conjunction with glacial retreat. The establishment of vegetation is a common response to warmer temperatures in a post-glacial environment, which binds floodplain sediments and increases the resilience to reworking leading to greater bank and floodplain stability, as seen in the Stanley River, Tasmania (Nanson et al., 1995). A model of bio-morphological succession is presented by Corenblit et al. (2011) which suggests vegetation plays a key role in the transition from a braided to meandering planform by stabilising lower activity floodplain areas and promoting the narrowing and subsequent incision of the channel. Vegetation also impacts the water supply to

the system by intercepting slope run off and slowing the regulating the flow to the channel (Tabacchi et al., 2000). In the context of the Río Chubut, the sparsely vegetated steppe environment means that vegetation has not impacted the sediment supply to the river. However, dense forest established in the headwaters by ~10-15 cal. ka BP (Iglesias et al., 2014) likely impacted the water supply regime by slowing the flow to the river and buffering variable run off.

Base level change can also impact upon river systems as a result of deglaciation. For example, the upper Mississippi River incised twice during the last glaciation by ~15 m and ~40 m. This incision lowered the base level of its tributaries, including the lower Chippewa River, which experienced minimal floodplain development and channel instability that still persists today (Falkner et al., 2016). As for marine draining river systems such as the Rio Chubut, the rise in global sea level associated with global deglaciation raises river base level and lowers gradient (Marra et al., 2008). Impact of base level elevation includes a reduction in channel competency and valley aggradation (Blum and Törnqvist, 2000; Marra et al., 2008). Sea-level change is evident along the coastline of the Chubut province including the mouth of the Río Chubut with inactive coastal features such as raised beaches, lagoons and palaeocliffs (Schillizi et al., 2014). Therefore, sea level rise associated with global deglaciation likely this impacted the Río Chubut.

Paraglacial adjustment is an important process in rivers responding to deglaciation. This is a suite of processes that can provide somewhat of a buffer to glacially-fed river systems during the high magnitude environmental shift from glacial to interglacial conditions. For example, a glacially-fed braided river can continue to braid post-glaciation on millennial timescales due to the extensive residual glacial sediments left in the valley. However, this thesis has demonstrated that the braided planform of the Río Chubut under the influence of paraglacial adjustment was reliant upon sustained water supply (Chapter 5). Contemporary braided river systems under the influence of paraglacial adjustment include the Waiau River, New Zealand (Clayton, 1968) and the Tagliamento River, Italy (Monegato et al., 2007). Despite the "buffer" paraglacial adjustment provides, paraglacial braided rivers are still vulnerable to climate and environmental change.

Global retreat of glaciers and ice sheets mean that more river systems will become decoupled from their glacial feeders in the near future. Future climate scenarios predict a loss in global ice volume by up to 41% by 2100, the more vulnerable, smaller ice masses such as the southern South American, central European, north Asian

glaciers are predicted to have reduced in volume by up to 80% by 2100 (Radić et al., 2014). Whilst autogenic processes of paraglacial adjustment have the potential to buffer large-scale geomorphological impacts, key factors such as water supply, vegetation or base-level change could prompt substantial changes in river regime.

Future climate change scenarios predict a southward shift in the core of the southern westerlies (Deng et al., 2022), although there is large uncertainty in these projections as identified within the IPCC AR6. As observed in northern Patagonia, this could bring drier conditions to present day braided river systems in southern Patagonia and New Zealand, which are situated in under their current position of the southern westerlies. Given the observations on the Río Chubut made in this thesis, a reduction in water supply brought by drier climatic conditions could compromise the braided planform of these paraglacial systems (Shulmeister et al., 2019). Braided rivers are important ecosystems that support unique compositions of flora and fauna including a substantial population of endangered species (Tockner et al., 2006). Braided planforms also provide a range of conditions across the width of the braid plain including the gravel bed used by fish, including salmon and trout species, for feeding, resting and spawning (Mosley, 1982). Braided rivers also hold recreational value (Grove et al., 2015), and are of great cultural and spiritual importance to indigenous peoples, such as the Rakaia River, New Zealand which is part of the history and identity of the Ngāi Tahu iwi (Māori tribe) (Mahaanui Kurataiao, 2013).

Increased seasonality, and the magnitude and frequency of weather extreme events is also predicted and has the potential to push rivers past critical discharge thresholds and induce changes in regime (Schneider et al., 2013). This thesis demonstrates the high dependency of the Río Chubut on Andean water supply which, is predicted to experience a “critical” decrease in water yield by up to 40% under the 1.5˚C warming scenario (Natalia et al., 2020). In 2016, Chile experienced widespread drought when precipitation decreased by 50 % (Garreaud, 2018), which shows the potential for future drought conditions with climate change. The projected decrease in water supply will impact the whole ~800 km river; from putting strain on the water supply for more than 250,000 people (Natalia et al., 2020) and farming practices dependent on floodplain irrigation (Gallardo, 2016). The study reach section of Río Chubut is also prone to relatively frequent extreme floods driven by snowmelt in the Andes (Kaless et al., 2014; Secretería de Infraestructura y política Hídricia, 2018), intensification of weather extremes could cause an increase in frequency and/or magnitude of flood risk which drive geomorphological changes including channel widening, decrease in sinuosity and avulsion (Hooke, 2007, Dean and Schmidt, 2013; Wong et al., 15).

### 7.3 Limitations and Further work

There were limitations that restricted the overall outcomes of this project, particularly fieldwork restrictions, limited site access and time constraints meant that the array of avulsion channels at site CHUB6 and much of the floodplain sediments north of the riverbank were not able to be sampled for luminescence dating, which resulted in a lack of chronology for these large-scale avulsions and limited ages representing the oldest sediments retained in the floodplain substrate and meander migration sequences. Furthermore, time restrictions meant that sampling the whole of the higher-level terrace framework for luminescence dating, beyond the exploratory pilot research presented here, fell outside the scope of this project. In that as an alternative, luminescence samples were collected from the oldest and youngest of the higher-level terraces in the Chubut valley and provides new age constraint for the formation of the La Pampas formations in the Rio Chubut study reach and associated tributaries. The work provides proof-of-concept for future research using luminescence dating to constrain further the timescales of fluvial dynamics in the Rio Chubut and La Pampas formations.

Overall, the luminescence samples that were collected provide new chronologies for previously undated features in Río Chubut and offer new insights into the timescales and drivers of change.

The characterisation of the past river response to glaciation and climate shifts expands the understanding of the land system response to long-term environmental change in this climatically important region of Patagonia. This research establishes new pathways for further research such as:

- Applying luminescence dating more widespread and systematically to derive a formal chronology for the higher-level terrace framework and wider La Pampas Formations to better understand the extent of glacial sediment supply to the catchment through the Late Quaternary.
- Constraining latitudinal variations in the response of the eastward draining major river systems in Patagonia (e.g. Río Negro, Río Deseado, Río Santa Cruz and Río Gallegos). Each of these systems have and continue to respond to deglaciation, and a new extended dataset would provide timescales of paraglacial adjustment on a regional scale and facilitate an assessment of the synchrony of changes between these differing rivers to infer environmental drivers. For example, rivers at different latitudes may respond at different times to changes in water supply related to shifts in the southern westerlies.

- Understanding the amount of freshwater that could was injected into the south Atlantic Ocean by the eastward draining river systems, and the subsequent impacts on thermohaline circulation,
- Understanding the extent palaeofluvial features in the river corridor outside of the maximum ice limits could shed light on past environmental conditions, where evidence is not preserved in the Andes because of more extensive glaciations.
- Understanding the competency and sediment connectivity of former regimes and flooding extremes in mobilising glacial fluvial outwash sediments downstream in the Río Chubut.

There are also further avenues of research that indirectly relate to the finding of this study but would provide greater environmental context for the fluvial changes observed here for the Río Chubut. Groundwater is a key influence on water supply to the lower Río Chubut, but the study of which was outside the scope of this project. However, further work investigating the contribution, influence, and sensitivity of the groundwater exchange with the Río Chubut would generate a more accurate and higher resolution assessment of its sensitivity to changes in water supply for the whole river. Research from the lower course of the river reports spatially variable discharge contributions ranging from groundwater between 6 and 24% (Torres et al., 2021). The exchange of water between channel and groundwater is also bi-directional where the Río Chubut can both receive and lose discharge to the ground water aquifers (Torres et al., 2021). An aquifer in the central Chubut Province has been investigated and those results suggest there is also an exchange in water between the aquifer and the river channel in the middle course river (Gallardo, 2016). Groundwater extraction is being explored as an alternative water supply to the rivers in the Río Chubut valley because of increasing desertification and growing water shortage concerns (Gallardo, 2016)

The ~3 m accumulation of windblown loess on the Río Chubut floodplain along the study reach was observed in the field and, whilst also outside the scope of this project, presents the opportunity for further work on the drivers and impacts of aeolian sedimentation. Loess is a valuable sediment deposit that can shed light on sediment provenance, prevailing wind direction, dust flux and accumulation rate (Shao et al., 2011; Gao et al., 2021). The interaction between the aeolian deposits and the rivers also has the potential highlight areas of contemporary and historic floodplain inactivity (White et al., 2013).

Whilst glaciofluvial outwash has been used to constrain the timing of ice advance and still stands of the ice margins of the Patagonian ice sheet, the distal sandur deposits mapped and dated in the Río Chubut are not appropriate for this application as they are not linked directly to specific moraine limits and the sediments could have been remobilised under paraglacial adjustment processes. Therefore, the timing of deglaciation for the Río Chubut headwater remains poorly constrained. Further work in characterising and constraining the timing of glacial retreat, establishment and decline of proglacial lakes, and the presence westward drainage in the feeder valleys of the Río Chubut headwaters would determine the timing of influential shifts between the glacial and post-glacial catchment and could potentially distinguish between sandur or paraglacial origins within the distal La Pampas gravels.

Further work across Patagonia could turn its focus to the impacts on river regime in response to the shift from direct glacial- to lacustrine-feeders and the sensitivity of the fluvial system to climate and environmental drivers. The switch from glacial to lacustrine drainage is well evidenced and age constrained in glacial geomorphology of the eastern Andes including Lago Buenos Aires (Rio Deseado) and Lago Pueyrredón (Río Pinturas) which have age constrained records of ice margins and former lake shorelines (Davies et al., 2020) and records of rapid glacial lake drainage (Glasser et., 2016). The long-term impacts on river regime are yet to be characterised for these systems, as well as the freshwater input to the southern Atlantic Ocean during phases of glacial melt.

Ultimately, the response to climate change in glacially-fed rivers is unique for each valley given the diversity of internal dynamics and allogenic environmental drivers (determined by geographic position). Whilst this thesis characterises the key drivers and constrains the timing of long-term change in a glacially-fed river system, it cannot be applied as a true analogue for other systems because of the vast global diversity of drivers and dynamics to glacially-fed rivers. The understanding of drivers and impacts in glacially-fed rivers, particularly those at risk of decoupling from their glacial feeders, is advanced by the further study of these types of rivers under different allogenic and autogenic conditions. A global representation of these issues is forming in the published literature (see Section 2.0) and is required to characterise the unique interactions with different climate systems, ecosystems and internal dynamics that will dictate the impacts of deglaciation and climate change on glacially-fed rivers.

### 7.4 Concluding remarks

Changes in water and sediment supply are key drivers of river regime. The headwaters of the major eastward draining river systems in Patagonia have been subject to transient occupation by the Patagonian ice sheet in conjunction with several glacial-interglacial cycles. The research questions and objectives of this thesis address the overarching aim to understand the long-term dynamics of the glacially-fed river systems in Patagonia, using the Río Chubut, Argentina, as a case study. A combination of high-resolution geomorphological mapping and sedimentological and stratigraphic analysis of the Río Chubut highlights the processes of past and present fluvial regimes, and the mechanisms of change. A total of ten luminescence ages anchor key phases of activity in time and shed light on the different timescales of change. In the context of published palaeoenvironmental reconstructions, it was revealed that the Río Chubut under its braided regime was more sensitive to drier conditions brought by the weakening and southward shift of the southern westerlies than it was to the deglaciation of its headwaters at the end of the last glaciation. However, the contemporary meandering regime has persisted through and is probably sustained by the climatic variability of the Holocene.

Whilst every braided, glacially-fed river system is unique in its environmental drivers and internal dynamics. The case of the Río Chubut suggests that increased aridity and reduced water supply can be a greater threat to a paraglacial braided planform than decoupling from glacial feeders. With the paraglacial legacy of sediment and continued adjustment there is sufficient sediment, but the loss of water was more telling in driving changing river planform. This has implications for other river systems in light of future climate change. The projected southward shift in the southern westerlies could reduce the water supply to areas of the mid-latitudes in the Southern Hemisphere (e.g. southern South America, New Zealand) and induce a change in planform, furthermore the reduction in water supply would incur social, economic, and ecological impacts. Future climate scenarios predict a reduction in water supply to the Andes mountains and Patagonian steppe. Therefore, understanding the key drivers, dynamics and reliance of glacially-fed and paraglacial rivers is important for future water resource and ecosystem management.

## References


Agosta, E.A., Hurtado, S.I. and Martin, P.B., 2020. “Easterlies”-induced precipitation in eastern Patagonia: Seasonal influences of ENSO'S FLAVOURS and SAM. *International Journal of Climatology*, 40(13), 5464-5484.

Aguayo, R., León-Muñoz, J., Vargas-Baecheler, J., Montecinos, A., Garreaud, R., Urbina, M., Soto, D. and Iriarte, J.L., 2019. The glass half-empty: climate change drives lower freshwater input in the coastal system of the Chilean Northern Patagonia. *Climatic Change*, 155(3), 417-435.

Ahmed, J., Constantine, J.A. and Dunne, T., 2019. The role of sediment supply in the adjustment of channel sinuosity across the Amazon Basin*. Geology,* 47(9), 807-810.

Allen, J.R., 1965. A review of the origin and characteristics of recent alluvial sediments. *Sedimentology*, 5(2), 89-191.

Anderson, S. and Radić, V., 2020. Identification of local water resource vulnerability to rapid deglaciation in Alberta. *Nature Climate Change*, 10(10), 933-938.

Ashworth, P.J. and Lewin, J., 2012. How do big rivers come to be different?. *Earth-Science Reviews*, 114(1-2), 84-107.

Aslan, A., Autin, W.J. and Blum, M.D., 2005. Causes of river avulsion: insights from the late Holocene avulsion history of the Mississippi River, USA*. Journal of Sedimentary Research,* 75(4), 650-664.

Balescu, S. and Lamothe, M., 1993. Thermoluminescence dating of the Holsteinian marine formation of Herzeele, northern France. *Journal of Quaternary Science*, 8(2), 117-124.

Ballantyne, C.K., 2002. A general model of paraglacial landscape response. *The Holocene*, 12(3), 371-376.

Bell, W.T., 1980. Alpha dose attenuation in quartz grains for thermoluminescence dating. *Ancient Tl*, 12(8), 4-8

Bendle, J.M., Palmer, A.P., Thorndycraft, V.R. and Matthews, I.P., 2017. High-resolution chronology for deglaciation of the Patagonian Ice Sheet at Lago Buenos Aires (46.5 S) revealed through varve chronology and Bayesian age modelling. *Quaternary Science Reviews*, 177, 314-339.

Bertrand, S., Hughen, K., Sepúlveda, J. and Pantoja, S., 2014. Late Holocene covariability of the southern westerlies and sea surface temperature in northern Chilean Patagonia. *Quaternary Science Reviews*, 105,195-208.

Blombin, R., Murray, A., Thomsen, K.J., Buylaert, J-P., Sobhati, R., Jansson, K.N. and Alexanderson, H., 2012. Timing of the deglaciation in southern Patagonia: Testing the applicability of K-feldspar IRSL. *Quaternary Geochronology*, 10, 264 – 272.

Blum, M.D. and Törnqvist, T.E., 2000. Fluvial responses to climate and sea-level change: a review and look forward. *Sedimentology*, 47, 2-48.

Bøtter-Jensen, L., Andersen, C.E., Duller, G.A.T., and Murray, A.S., 2003. Developments in Radiation, Stimulation and Observation Facilities in Luminescence Measurements. *Radiation Measurements*, 37, 535-541.

Brice, J.C., 1974. Evolution of meander loops. *Geological Society of America Bulletin*, 85(4), 581-586.

Bridge, J.S. and Leeder, M.R., 1979. A simulation model of alluvial stratigraphy. *Sedimentology*, 26(5), 617-644.

Bridge, J.S., 2003. *'Floodplains' Rivers and floodplains: forms, processes, and sedimentary record*. John Wiley & Sons.

Bridgland, D.R. and Westaway, R., 2014. Quaternary fluvial archives and landscape evolution: a global synthesis. *Proceedings of the Geologists' Association*, 125(5-6), 600-629.

Bridgland, D.R., Westaway, R., Howard, A.J., Innes, J.B., Long, A.J., Mitchell, W.A., White, M.J. and White, T.S., 2010. The role of glacio-isostasy in the formation of post-glacial river terraces in relation to the MIS 2 ice limit: evidence from northern England. *Proceedings of the Geologists' Association*, 121(2), 113-127.

Broecker, W.S. and Denton, G.H., 1990. The role of ocean-atmosphere reorganizations in glacial cycles. *Quaternary science reviews*, 9(4), 305-341.

Bruno, L., Piccin, A., Sammartino, I. and Amorosi, A., 2018. Decoupled geomorphic and sedimentary response of Po River and its Alpine tributaries during the last glacial/post-glacial episode*. Geomorphology,* 317,184-198.

Buffington, J.M. and Montgomery, D.R., 2013. Geomorphic classification of rivers. 'In' Shroder, J.; Wohl, E., ed. *Treatise on Geomorphology; Fluvial Geomorphology*, San Diego, CA: Academic Press. (Vol. 9) 730-767.

Bull, W.B., 1991. *Geomorphic responses to climatic change*. Oxford University Press. New York

Caldenius. 1932. Las Glaciaciones Cuaternarias en la Patagonia y Tierra del Fuego. *Geografiska Annaler*, 14(1-2), 1-164.

Charlton, R., 2008. *Fundamentals of fluvial geomorphology*. Routledge.

Chavaillaz, Y., Codron, F. and Kageyama, M., 2013. Southern westerlies in LGM and future (RCP4. 5) climates. *Climate of the Past*, 9(2), 517-524.

Church, M., 1983. Pattern of instability in a wandering gravel bed channel. 'In' *Modern and ancient fluvial systems*. International Association of Sedimentologists Special Publication, Oxford, UK. (Vol. 6) 169-180

Clayton, L., 1968. Late Pleistocene glaciations of the Waiau valleys, north Canterbury*. New Zealand journal of geology and geophysics,* 11(3), 753-767.

Constantine, J.A., McLean, S.R. and Dunne, T., 2010. A mechanism of chute cutoff along large meandering rivers with uniform floodplain topography*. Bulletin,* 122(5-6), 855-869.

Corenblit, D., Baas, A.C., Bornette, G., Darrozes, J., Delmotte, S., Francis, R.A., Gurnell, A.M., Julien, F., Naiman, R.J. and Steiger, J., 2011. Feedbacks between geomorphology and biota controlling Earth surface processes and landforms: a review of foundation concepts and current understandings. *Earth-Science Reviews*, 106(3-4), 307-331.

Coronato, A., Martínez, O. and Rabassa, J., 2004. Glaciations in Argentine Patagonia, southern South America. *Developments in Quaternary sciences*, 2, 49-67.

Cuffey, K.M., Clow, G.D., Steig, E.J., Buizert, C., Fudge, T.J., Koutnik, M., Waddington, E.D., Alley, R.B. and Severinghaus, J.P., 2016. Deglacial temperature history of West Antarctica. *Proceedings of the National Academy of Sciences*, 113(50), 14249-14254.

Davies, B.J., Darvill, C.M., Lovell, H., Bendle, J.M., Dowdeswell, J.A., Fabel, D., Garcia, J-L., Geiger, A., Glasser, N.F., Gheorghiu, D.M., Harrison, S., Hein, A.S.,

Kaplan, M.R., Martin, J.R. V., Mendelova, M., Palmer, A., Pelto, M., Rodes, A., Sagredo, E.A., Smedley, R.K., Smellie, J.L., Thorndycraft, V.R., 2020. The evolution of the Patagonian Ice Sheet from 35 ka to the Present Day (PATICE). *Earth-Science Reviews,* 204, 103-152.

DB City. Chubut Information [online] updates: 2022. accessed: 18/02/2022. Province Chubut, Argentina - City, Town and Village of the world (db-city.com)

Deng, K., Azorin-Molina, C., Yang, S., Hu, C., Zhang, G., Minola, L. and Chen, D., 2022. Changes of Southern Hemisphere westerlies in the future warming climate. *Atmospheric Research,* 106040.

Denton, G.H., Heusser, C.J., Lowel, T.V., Moreno, P.I., Andersen, B.G., Heusser, L.E., Schlühter, C. and Marchant, D.R., 1999. Interhemispheric linkage of paleoclimate during the last glaciation. *Geografiska Annaler: Series A, Physical Geography*, *81*(2), 107-153.

Doughty, A.M., Schaefer, J.M., Putnam, A.E., Denton, G.H., Kaplan, M.R., Barrell, D.J., Andersen, B.G., Kelley, S.E., Finkel, R.C. and Schwartz, R., 2015. Mismatch of glacier extent and summer insolation in Southern Hemisphere mid-latitudes. *Geology*, 43(5), pp.407-410.

Duan, J.G. and Julien, P.Y., 2005. Numerical simulation of the inception of channel meandering. Earth Surface Processes and Landforms: *The Journal of the British Geomorphological Research Group*, 30(9), 1093-1110.

Duller, G.A.T., 1992. Luminescence chronology of raised marine terraces south-west North Island New Zealand. *Unpublished PhD thesis*, University of Wales, Aberystwyth.

Durcan, J.A., King, G.E. and Duller, G.A., 2015. DRAC: Dose Rate and Age Calculator for trapped charge dating. *Quaternary Geochronology,* 28, 54-61.

Faulkner, D.J., Larson, P.H., Jol, H.M., Running, G.L., Loope, H.M. and Goble, R.J., 2016. Autogenic incision and terrace formation resulting from abrupt late-glacial base-level fall, lower Chippewa River, Wisconsin, USA. *Geomorphology,* 266, 75-95.

Ferguson, R.I. and Werritty, A., 1983. Bar development and channel changes in the gravelly River Feshie, Scotland. 'In' *Modern and ancient fluvial systems*. International Association of Sedimentologists Special Publication, Oxford, UK. (Vol. 6) 181-193.

Fletcher, M.S. and Moreno, P.I., 2011. Zonally symmetric changes in the strength and position of the Southern Westerlies drove atmospheric CO2 variations over the past 14 ky. *Geology,* 39(5), 419-422.

Flint, R.F. and Fidalgo, F., 1964. Glacial geology of the East flank of the Argentine Andes between Latitude 39 10′ S. and Latitude 41 20′ S. *Geological Society of America Bulletin,* 75(4), 335-352.

Fraser, C.I., Nikula, R., Ruzzante, D.E. and Waters, J.M., 2012. Poleward bound: biological impacts of Southern Hemisphere glaciation. *Trends in ecology & evolution*, 27(8), 462-471.

Friedkin, J.F., 1945. *A laboratory study of the meandering of alluvial rivers*. United States Waterways Experiment Station.

Friend, P.F. and Sinha, R., 1993. Braiding and meandering parameters. *Geological Society, London, Special Publications*, 75(1), 105-111.

Gallardo, A.H., 2016. Groundwater exploration for rural water supply in an arid region of southern Argentina. *Geosciences*, 6(2), 28.

Gao, X., Hao, Q., Ge, J., Han, L., Fu, Y., Wu, X., Deng, C., Marković, S.B. and Guo, Z., 2021. Paleowind directions from the magnetic fabric of loess deposits in the western Chinese Loess Plateau and implications for dust provenance. *Quaternary Research*, 103, 74-87.

García, J.L., Maldonado, A., de Porras, M.E., Delaunay, A.N., Reyes, O., Ebensperger, C.A., Binnie, S.A., Luethgens, C. and Méndez, C., 2019. Early deglaciation and paleolake history of Río Cisnes glacier, Patagonian ice sheet (44 S). *Quaternary Research*, 91(1), 194-217.

Garreaud, R.D. 2018. Record-breaking climate anomalies lead to severe drought and environmental disruption in western Patagonia in 2016. *Climate Research*, 74, 217-229.

Garreaud, R.D., Boisier, J.P., Rondanelli, R., Montecinos, A., Sepúlveda, H.H. and Veloso-Aguila, D., 2020. The central Chile mega drought (2010–2018): a climate dynamics perspective. *International Journal of Climatology*, 40(1), 421-439.

Gilbert, G.K., 1877. *Report on the Geology of the Henry Mountains*. US Government Printing Office.

Glasser, N. and Jansson, K., 2008. The glacial map of southern South America. *Journal of Maps*, 4(1), 175-196.

Glasser, N. F., Jansson, K. N., Harrison, S., & Kleman, J. 2008. The glacial geomorphology and Pleistocene history of South America between 38°S and 56°S. *Quaternary Science Reviews*, 27(3-4), 365-390.

González Díaz, E. F. 1993a. Mapa Geomorphológico del Sector de Cushman (NO de Chubut): reinterpretación genética y secuencial de sus principals geoformas. *XII Congreso Geológico Argentino*, Actas 6, 56-65. Menoza

González Díaz, E. F. 1993b. Propuesta evolutive geomórfica para el sector de Cushamen (NO de Chubut) durante ell apso TerciarioSuperior-Cuaterario. *XII Congreso Geológico Argentino*, Actas 6, 66-72. Mendoza.

González Díaz, E.F. and Andrada de Palomera, R.P. 1996. Nueva propuesta genética y evolutiva geomórfica de la "Pampa" de Gualjaina, NO del Chubut extrandino. *XIII Congreso Geológico Argentino and III Congreso de Exploración de Hidrocarburos*, Actas 4,221-230. Buenos Aires.

Grove, P., Parker, M., Gray, D.P. and Behrens, F.M.L., 2015. Land use change on the margins of lowland Canterbury braided rivers, 1990-2012. Christchurch, New Zealand: Environment Canterbury Regional Council.

Guerin, G., Mercier, N. and Adamiec, G., 2011. Dose-rate conversion factors: update. *Ancient TL,* 29, 5 – 8.

Guerin, G., Mercier, N., Nathan, R., Adamiec, G. and Lefrais, Y., 2012. On the use of the infinite matrix assumption and associated concepts: A critical review. *Radiation Measurements,* 47, 778 – 785.

Harwood, K. and Brown, A.G., 1993. Fluvial processes in a forested anastomosing river: flood partitioning and changing flow patterns. *Earth Surface Processes and Landforms*, 18(8), 741-748.

Hein, A. S., Hulton, N. R., Dunai, T. J., Sugden, D. E., & Kaplan, M. R. 2010. The chronology of the Last Glacial Maximum and deglacial events in central Argentine Patagonia. *Quaternary Science Reviews*, 29(9-10), 1212-1227.

Hein, A.S., Hulton, N.R., Dunai, T.J., Schnabel, C., Kaplan, M.R., Naylor, M. and Xu, S., 2009. Middle Pleistocene glaciation in Patagonia dated by cosmogenic-nuclide

measurements on outwash gravels. *Earth and Planetary Science Letters*, 286(1-2), 184-197.

Hein, A.S., Hulton, N.R., Dunai, T.J., Sugden, D.E., Kaplan, M.R. and Xu, S., 2010. The chronology of the Last Glacial Maximum and deglacial events in central Argentine Patagonia. *Quaternary Science Reviews*, 29(9-10), 1212-1227.

Hein, A.S., Dunai, T.J., Hulton, N.R. and Xu, S., 2011. Exposure dating outwash gravels to determine the age of the greatest Patagonian glaciations. *Geology,* 39(2), 103-106.

Hein, A.S., Cogez, A., Darvill, C.M., Mendelova, M., Kaplan, M.R., Herman, F., Dunai, T.J., Norton, K., Xu, S., Christl, M. and Rodés, Á., 2017. Regional mid-Pleistocene glaciation in central Patagonia. *Quaternary Science Reviews*, 164, 77-94.

Herman, F., Brandon, M. 2016. Mid-latitude glacial erosion hotspot related to equatorial shifts in southern Westerlies. *Geology,* 43, 987-990.

Hey, R.D., 1976. Geometry of river meanders. *Nature*, 262(5568), 482-484.

Hickin, E.J. and Nanson, G.C., 1975. The character of channel migration on the Beatton River, northeast British Columbia, Canada. *Geological Society of America Bulletin,* 86(4), pp.487-494.

Ho, S.L., Mollenhauer, G., Lamy, F., Martínez-Garcia, A., Mohtadi, M., Gersonde, R., Hebbeln, D., Nunez-Ricardo, S., Rosell-Melé, A. and Tiedemann, R., 2012. Sea surface temperature variability in the Pacific sector of the Southern Ocean over the past 700 kyr. *Paleoceanography*, 27(4).

Hooke, J. M. 1984. Changes in river meanders: a review of techniques and results of analyses. *Progress in Physical Geography: Earth and Environment*, 8(4), 473–508.

Hooke, J.M., 1995. River channel adjustment to meander cutoffs on the River Bollin and River Dane, northwest England. *Geomorphology,* 14(3), 235-253.

Hooke, J., 2003. Coarse sediment connectivity in river channel systems: a conceptual framework and methodology. *Geomorphology,* 56(1-2), 79-94.

Hooke, J.M., 2004. Cutoffs galore!: occurrence and causes of multiple cutoffs on a meandering river. *Geomorphology,* 61(3-4), 225-238.

Hooke, J.M., 2022. Morphodynamics of a meandering channel over decadal timescales in response to hydrological variations. *Earth Surface Processes and Landforms*.

Hughes, P.D., Gibbard, P.L. and Ehlers, J., 2013. Timing of glaciation during the last glacial cycle: evaluating the concept of a global 'Last Glacial Maximum'(LGM). *Earth-Science Reviews,* 125,171-198.

Hulton, N.R.J., Sugden, D.E., Payne, A.J., Clapperton, C.M., 1994. Glacier modelling and the climate of Patagonia during the last glacial maximum*, Quaternary Research.* 42, 1e19.

Huntley, D.J. and Lamothe, M., 2001. Ubiquity of anomalous fading in K-feldspars and the measurement and correction for it in optical dating. *Canadian Journal of Earth Sciences*, 38(7), 1093-1106.

Iglesias, V., Whitlock, C., Bianchi, M.M., Villarosa, G. and Outes, V., 2012. Climate and local controls of long-term vegetation dynamics in northern Patagonia (Lat 41 S). *Quaternary Research*, 78(3), 502-512.

Iglesias, V., Whitlock, C., Markraf, V., & Bianchi, M. M. 2014. Postglacial history of the Patagonian forest/steppe ecotone (41–43°S). *Quaternary Science Reviews*, 94, 120-135.

Iglesias, V., Markgraf, V., & Whitlock, C. 2016. 17,000 years of vegetation, fire and climate change in the eastern foothills of the Andes (lat. 44°S). *Palaeogeography, Palaeoclimatology, Palaeoecology*, 457, 195-208.

Iglesias, V., Haberle, S.G., Holz, A. and Whitlock, C., 2018. Holocene dynamics of temperate rainforests in West-Central Patagonia. *Frontiers in Ecology and Evolution*, 5, 177.

IPCC, 2021: Summary for Policymakers. In: Climate Change 2021: The Physical Science Basis. Contribution of Working Group I to the Sixth Assessment Report of the Intergovernmental Panel on Climate Change [Masson-Delmotte, V., P. Zhai, A. Pirani, S. L. Connors, C. Péan, S. Berger, N. Caud, Y. Chen, L. Goldfarb, M. I. Gomis, M. Huang, K. Leitzell, E. Lonnoy, J.B.R. Matthews, T. K. Maycock, T. Waterfield, O. Yelekçi, R. Yu and B. Zhou (eds.)]. Cambridge University Press. In Press. Mehran, A., A. AghaKouchak, and T. J.Phillips (2014), Evaluation of CMIP5 continental precipitation simulations relativeto satellite-based gauge-adjusted

obser-vations, J. *Geophysical Research*. Atmosphere, 119,1695–1707, doi:10.1002/2013JD021152.

Jara, I.A. and Moreno, P.I., 2012. Temperate rainforest response to climate change and disturbance agents in northwestern Patagonia (41 S) over the last 2600 years. *Quaternary Research*, 77(2), 235-244.

Jouzel, J., Masson-Delmotte, V., Cattani, O., Dreyfus, G., Falourd, S., Hoffmann, G., Minster, B., Nouet, J., Barnola, J.M., Chappellaz, J. and Fischer, H., 2007. Orbital and millennial Antarctic climate variability over the past 800,000 years. *Science*, 317(5839), 793-796.

Kamp, U., and Owen, L.A., 2012, Polygenetic landscapes, in Owen, L.A*., Treatise of Geomorphology*: Amsterdam, Netherlands, Elsevier. (5) 370-393

Kelley, S.E., Kaplan, M.R., Schaefer, J.M., Andersen, B.G., Barrell, D.J., Putnam, A.E., Denton, G.H., Schwartz, R., Finkel, R.C. and Doughty, A.M., 2014. High-precision 10Be chronology of moraines in the Southern Alps indicates synchronous cooling in Antarctica and New Zealand 42,000 years ago. Earth and Planetary Science Letters, 405, 194-206.

Kiden, P. and Tornqvist, T.E., 1998. CORRESPONDENCE-Can river terrace flights be used to quantify Quaternary tectonic uplift rates?. *Journal of Quarternary Science*, 13(6), 573.

Kilian, R. and Lamy, F., 2012. A review of Glacial and Holocene paleoclimate records from southernmost Patagonia (49–55 S). *Quaternary Science Reviews*, 53, 1-23.

Knighton, D. A. and Nanson, G.C., 1993. Anastomosis and the continuum of channel pattern. *Earth Surface Processes and Landforms*, 18(7), pp.613-625.

Lambert, F., Delmonte, B., Petit, J.R., Bigler, M., Kaufmann, P.R., Hutterli, M.A., Stocker, T.F., Ruth, U., Steffensen, J.P. and Maggi, V., 2008. Dust-climate couplings over the past 800,000 years from the EPICA Dome C ice core. *Nature*, 452(7187), 616-619.

Lamy, F., Kilian, R., Arz, H. W., Francois, J.-P., Kaiser, J., Prange, M., & Steinke, T. 2010. Holocene changes in the position and intensity of the southern westerly wind belt. *Nature Geoscience*, 3, 695-699.

Lamy, F., Rühlemann, C., Hebbeln, D. and Wefer, G., 2002. High-and low-latitude climate control on the position of the southern Peru-Chile Current during the Holocene. *Paleoceanography*, 17(2), 16-1.

Lawrimore, J.H., Menne, M.J., Gleason, B.E., Williams, C.N., Wuertz, D.B., Vose, R.S. and Rennie, J., 2011. An overview of the Global Historical Climatology Network monthly mean temperature data set, version 3. Journal of Geophysical Research: *Atmospheres*, 116, D19121.

Leger, T. P., Hein, A. S., Bingham, R. G., Martini, M. A., Soteres, R. L., Sagredo, E. A., & Martínez, O. A. 2020. The glacial geomorphology of the Río Corcovado, Río Huemul and Lago Palena/General Vintter valleys, northeastern Patagonia (43°S, 71°W)*. Geomorphology,* 16(2), 651-668.

Leger, T.P., Hein, A.S., Bingham, R.G., Rodés, Á., Fabel, D. and Smedley, R.K., 2021a. Geomorphology and 10Be chronology of the Last Glacial Maximum and deglaciation in northeastern Patagonia, 43° S-71° W. *Quaternary Science Reviews*, 272, 107194.

Leger, T.P., Hein, A.S., Goldberg, D., Schimmelpfennig, I., Van Wyk de Vries, M.S., Bingham, R.G., Aumaitre, G. and ASTER Team, 2021b. Northeastern Patagonian glacier advances (43° S) reflect northward migration of the Southern Westerlies towards the end of the last glaciation. *Frontiers in Earth Science*, 910.

Leopold, L.B. and Miller, J.P., 1954. *A postglacial chronology for some alluvial valleys in Wyoming*. Washington, DC: US Government Printing Office, 90.

Leopold, L.B. and Wolman, M.G., 1957. *River channel patterns: braided, meandering, and straight*. US Government Printing Office.

Lewin, J., Macklin, M.G. and Johnstone, E., 2005. Interpreting alluvial archives: sedimentological factors in the British Holocene fluvial record. *Quaternary Science Reviews*, 24(16-17), 1873-1889.

Lisiecki, L.E. and Raymo, M.E., 2005. A Pliocene-Pleistocene stack of 57 globally distributed benthic δ18O records. *Paleoceanography*, 20(1).

Lopez, P., Chevallier, P., Favier, V., Pouyaud, B., Ordenes, F. and Oerlemans, J., 2010. A regional view of fluctuations in glacier length in southern South America. *Global and Planetary Change*, 71(1-2), 85-108.

Maddy, D., 1997. Uplift-driven valley incision and river terrace formation in southern England. Journal of Quaternary Science: *Published for the Quaternary Research Association*, 12(6), 539-545.

Mahaanui Kurataiao Ltd. 2013. 'Rakaia Ki Hakatere', in Mahaanui Iwi Management Plan. Mahaanui Kurataiao Ltd, Christchurch. 314-355

Makaske, B., 2001. Anastomosing rivers: a review of their classification, origin and sedimentary products*. Earth-Science Reviews,* 53(3-4), 149-196.

Marengo, J.A., Pabón, J.D., Díaz, A., Rosas, G., Ávalos, G., Montealegre, E., Villacis, M., Solman, S. and Rojas, M., 2011. Climate change: evidence and future scenarios for the Andean region. *Climate change and biodiversity in the tropical Andes*. IAI-SCOPE-UNESCO, Paris, France, 110-127.

Marín, V.H., Tironi, A., Paredes, M.A. and Contreras, M., 2013. Modeling suspended solids in a Northern Chilean Patagonia glacier-fed fjord: GLOF scenarios under climate change conditions. *Ecological modelling*, 264, 7-16.

Markgraf, V., Dodson, J.R., Kershaw, A.P., McGlone, M.S. and Nicholls, N., 1992. Evolution of late Pleistocene and Holocene climates in the circum-South Pacific land areas. *Climate Dynamics*, 6(3), 193-211.

Markgraf, V., Webb, R.S., Anderson, K.H. and Anderson, L., 2002. Modern pollen/climate calibration for southern South America. *Palaeogeography, Palaeoclimatology, Palaeoecology*, 181(4), 375-397.

Markgraf, V. and Huber, U.M., 2010. Late and postglacial vegetation and fire history in Southern Patagonia and Tierra del Fuego. *Palaeogeography, Palaeoclimatology, Palaeoecology*, 297(2), 351-366.

Marra, F., Florindo, F. and Boschi, E., 2008. History of glacial terminations from the Tiber River, Rome: Insights into glacial forcing mechanisms. *Paleoceanography*, 23(2).

Martínez, O. 2002. Geomorfologia y geología de los depósitos glaciarios y periglaciarios de la región comprendida entre los 43˚ y 44˚ lat. Sur y 70˚30' y 72˚ long. Oeste, Chubut, República Argentina. Unpublished Ph.D. as cited in Martínez, O.A. and Coronato, A.M., 2008. The late Cenozoic fluvial deposits of Argentine Patagonia*. Developments in Quaternary Sciences,* 11, 205-226.

Martínez, O. 2005: Incisión fluvial y glaciaciones durante el Pleistoceno a los 43º l.s., noroeste de la Provincia de Chubut. En: *XVI Congreso Geológico Argentino*, Actas, 135-140.

Martínez, O.A. and Coronato, A.M., 2008. The late Cenozoic fluvial deposits of Argentine Patagonia*. Developments in Quaternary Sciences,* 11, 205-226.

Martínez, O., González, M., Toppazzini, M. and Kutschker, A., 2014. Mantos de grava y evolución del paisaje en el suroeste de la provincia del Chubut (Argentina), desde el Mioceno hasta el presente. *Revista de la Sociedad Geológica de España*, 27(2), 39-50.

McCulloch, R.D., Fogwill, C.J., Sugden, D.E., Bentley, M.J. and Kubik, P.W., 2005. Chronology of the last glaciation in central Strait of Magellan and Bahía Inútil, southernmost South America. Geografiska Annaler: Series A, *Physical Geography*, 87(2), 289-312.

Mendelova, M., Hein, A.S., Rodes, A., Smedley, R.K. and Xu, S., 2020a. Glacier expansion in central Patagonia during the Antarctic Cold Reversal followed by retreat and stabilisation during the Younger Dryas. *Quaternary Science Reviews*, 227, 106047.

Mendelová, M., Hein, A.S., Rodés, Á. and Xu, S., 2020b. Extensive mountain glaciation in central Patagonia during Marine Isotope Stage 5. *Quaternary Science Reviews*, 227, 105996.

Mercer, J.H., 1976. Glacial history of Southernmost South America 1. *Quaternary research*, 6(2), 125-166.

Mercer, J.H., 1984. Simultaneous climatic change in both hemispheres and similar bipolar interglacial warming: Evidence and implications. *Climate processes and climate sensitivity*, 29, 307-313.

Métivier, F., Lajeunesse, E. and Devauchelle, O., 2017. Laboratory rivers: Lacey's law, threshold theory, and channel stability. *Earth Surface Dynamics*, 5(1), 187-198.

Miall, A.D., 1996. The Geology of Fluvial Deposits: Sedimentary Facies, Basin Analysis and Petroleum Geology. Springer, *Berlin*, 582

Middleton, B.A. and Kleinebecker, T., 2012. *The effects of climate-change-induced drought and freshwater wetlands. In Global Change and the Function and Distribution of Wetlands*. Springer, Dordrecht. 117-147

Milankovitch, M.K., 1941. Kanon der Erdbestrahlung und seine Anwendung auf das Eiszeitenproblem. *Royal Serbian Academy Special Publication*, 133, 1-633.

Miró, R., 1967. Geología glaciaria y preglaciaria del Valle de Epuyén. *Revista de la Asociación Geológica Argentina*, 22(2).

Monegato, G., Ravazzi, C., Donegana, M., Pini, R., Calderoni, G. and Wick, L., 2007. Evidence of a two-fold glacial advance during the last glacial maximum in the Tagliamento end moraine system (eastern Alps). *Quaternary Research*, 68(2), 284-302.

Moreno, P. 2004. Millennial-scale climate variability in northwest Patagonia over the last 15 000 yr*. Journal of Quaternary Science,* 19(1), 35-47.

Moreno, P.I., François, J.P., Villa-Martínez, R.P. and Moy, C.M., 2009. Millennial-scale variability in Southern Hemisphere westerly wind activity over the last 5000 years in SW Patagonia. *Quaternary Science Reviews*, 28(1-2), 25-38.

Moreno, P. I., Videla, J., Valero-Garcés, B., Alloway, B. V., Heusser, L. E. 2018. A continuous record of vegetation, fire-regime and climatic changes in northwestern Patagonia spanning the last 25,000 years. *Quaternary Science Reviews*, 198, 15-36.

Moreno, P.I., Francois, J.P., Moy, C.M. and Villa-Martínez, R., 2010. Covariability of the Southern Westerlies and atmospheric CO2 during the Holocene*. Geology,* 38(8), 727-730.

Moreno, P.I., Denton, G.H., Moreno, H., Lowell, T.V., Putnam, A.E. and Kaplan, M.R., 2015. Radiocarbon chronology of the last glacial maximum and its termination in northwestern Patagonia. *Quaternary Science Reviews*, 122, 233-249.

Moreno, P.I., Videla, J., Valero-Garcés, B., Alloway, B.V. and Heusser, L.E., 2018. A continuous record of vegetation, fire-regime and climatic changes in northwestern Patagonia spanning the last 25,000 years. *Quaternary Science Reviews*, 198, 15-36.

Moreno, P.I., 2020. Timing and structure of vegetation, fire, and climate changes on the Pacific slope of northwestern Patagonia since the last glacial termination. *Quaternary Science Reviews*, 238, 106328.

Mosley, M.P., 1982. Analysis of the effect of changing discharge on channel morphology and instream uses in a braided river, Ohau River, New Zealand. *Water resources research*, 18(4), 800-812.

Moy, C. M., Seltzer, G. O., Rodbell, D. T., Anderson, D. M. 2002. Variability of El Niño/Southern Oscillation activity at millennial timescales during the Holocene epoch. *Nature*, 420, 162-165.

Mundo, I.A., Masiokas, M.H., Villalba, R., Morales, M.S., Neukom, R., Le Quesne, C., Urrutia, R.B. and Lara, A., 2012. Multi-century tree-ring based reconstruction of the Neuquén River streamflow, northern Patagonia, Argentina*. Climate of the Past,* 8(2), 815-829.

Murphy, J.J., 1869. On the nature and cause of the glacial climate. *Quarterly Journal of the Geological Society*, 25(1-2), 350-356.

Nanson, G.C., Rust, B.R. and Taylor, G., 1986. Coexistent mud braids and anastomosing channels in an arid-zone river: Cooper Creek, central Australia. *Geology*, 14(2), 175-178.

Nanson, G.C., Young, R.W., Price, D.M. and Rust, B.R., 1988. Stratigraphy, sedimentology and late-Quaternary chronology of the Channel Country of western Queensland. In *Fluvial geomorphology of Australia,* 151-175.

Nanson, G.C., Barbetti, M. and Taylor, G., 1995. River stabilisation due to changing climate and vegetation during the late Quaternary in western Tasmania, Australia*. Geomorphology,* 13(1-4), 145-158.

Nanson, G.C. and Knighton, A.D., 1996. Anabranching rivers: their cause, character and classification. *Earth surface processes and landforms*, 21(3), 217-239.

Natalia, P., Silvia, F., Silvina, S. and Miguel, P., 2020. Climate change in northern Patagonia: critical decrease in water resources. *Theoretical and Applied Climatology*, 140(3), 807-822.

Panza, J. L. 2002: La cubierta detrítica del Cenozoico superior. En: Geología y Recursos Naturales de Santa Cruz. *XV Congreso Geológico Argentino*. 1 (17). (M. J. Haller, Ed). 259– 284.

Pasquini, A.I., Lecomte, K.L. and Depetris, P.J., 2008. Climate change and recent water level variability in Patagonian proglacial lakes, Argentina. *Global and Planetary Change*, 63(4), 290-298.

Pazzaglia, F., 2013. 'Fluvial Terraces' in Shroder, J. Treatise on Geomorphology, *Academic Press*. 9, 379-412.

Peterson, T.C., and Vose, R.S., 1997: An overview of the Global Historical Climatology Network temperature database. *Bulletin of the American Meteorological Society*, 78 (12), 2837-2849.

Prescott, J.R. and Hutton, J.T., 1994. Cosmic ray contributions to dose rates for luminescence and ESR dating: large depths and long-term time variations. *Radiation measurements,* 23(2-3), 497-500.

Quattrocchio, M.E., Borromei, A.M., Deschamps, C.M., Grill, S.C. and Zavala, C.A., 2008. Landscape evolution and climate changes in the Late Pleistocene–Holocene, southern Pampa (Argentina): evidence from palynology, mammals and sedimentology. *Quaternary International*, 181(1), 123-138.

Rabassa, J., Coronato, A.M. and Salemme, M., 2005. Chronology of the Late Cenozoic Patagonian glaciations and their correlation with biostratigraphic units of the Pampean region (Argentina). *Journal of South American Earth Sciences*, 20(1-2), 81-103.

Radić, V., Bliss, A., Beedlow, A.C., Hock, R., Miles, E. and Cogley, J.G., 2014. Regional and global projections of twenty-first century glacier mass changes in response to climate scenarios from global climate models. *Climate Dynamics*, 42(1), 37-58.

Ramos, V.A. and Ghiglione, M.C., 2008. Tectonic evolution of the Patagonian Andes. *Developments in quaternary sciences,* 11, 57-71.

Recasens, C., Ariztegui, D., Gebhardt, C., Gogorza, C., Haberzettl, T., Hahn, A., Kliem, P., Lisé-Pronovost, A., Lücke, A., Maidana, N. and Mayr, C., 2012. New insights into paleoenvironmental changes in Laguna Potrok Aike, southern Patagonia, since the Late Pleistocene: the PASADO multiproxy record. *The Holocene,* 22(11), 1323-1335.

Rein, B., Lückge, A., Reinhardt, L., Sirocko, F., Wolf, A. and Dullo, W.C., 2005. El Niño variability off Peru during the last 20,000 years. *Paleoceanography*, 20(4).

Rust, B.R., 1981. Sedimentation in an arid-zone anastomosing fluvial system; Cooper's Creek, central Australia. *Journal of Sedimentary Research*, 51(3), 745-755

Sagredo, E.A. and Lowell, T.V., 2012. Climatology of Andean glaciers: A framework to understand glacier response to climate change. *Global and Planetary Change*, 86, 101-109.

Schenk, C.J, Viger, R.J., and Anderson, C.P., 1999. Maps showing geology, oil and gas fields and geologic provinces of the South America region: U.S. *Geological Survey Open-File Report.* 97-470-D, 12

Schillizi, R.A., Spanguolo, J.O. and Luna, L., 2014. Morfología de la costa atlántica entre Punta Ninfas y Cabo Dos Bahías, Chubut, Argentina. *Revista del Museo de la Plata*, 14(117), 1-15.

Schneider, C., Laizé, C.L.R., Acreman, M.C. and Flörke, M., 2013. How will climate change modify river flow regimes in Europe?. *Hydrology and Earth System Sciences*, 17(1), 325-339.

Schumm, S.A., 1965. Quaternary paleohydrology. *In The Quaternary of the US*. Princeton University Press, 783-794.

Schumm, S. A. 1977. The Fluvial System, Wiley-Interscience, New York, 338. As cited in Bledsoe, B.P. and Watson, C.C., 2001. Logistic analysis of channel pattern thresholds: meandering, braiding, and incising. *Geomorphology,* 38(3-4), 281-300.

Schumm, S.A., 1977. *The fluvial system*. Wiley. New York

Schumm, S.A., 1985. Patterns of alluvial rivers. Annual Review of Earth and Planetary Sciences, 13, 5.

Secretaría de Energía Presidencia de la Nación. 2020. Portencia Instalada Energía Electrica. [accessed 20/06/2022] [available from: https://www.argentina.gob.ar/economia/energia/planeamiento-energetico/panel-de-indicadores/potencia-instalada]

Secretería de Infraestructura y política Hídricia 2018. 'Historico-Estacion 2318' Available at: https://snih.hidricosargentina.gob.ar/Filtros.aspx# (Accessed: 12/05/2022)

Shao, Y., Wyrwoll, K.H., Chappell, A., Huang, J., Lin, Z., McTainsh, G.H., Mikami, M., Tanaka, T.Y., Wang, X. and Yoon, S., 2011. Dust cycle: An emerging core theme in Earth system science. *Aeolian Research*, 2(4), 181-204.

Shulmeister, J., Thackray, G.D., Rittenour, T.M., Fink, D. and Patton, N.R., 2019. The timing and nature of the last glacial cycle in New Zealand. *Quaternary Science Reviews*, 206, 1-20.

Singer, B.S., Ackert Jr, R.P. and Guillou, H., 2004. 40Ar/39Ar and K-Ar chronology of Pleistocene glaciations in Patagonia*. Geological Society of America Bulletin,* 116(3-4), 434-450.

Skirrow, G.K., Smedley, R.K., Chiverrell, R.C. and Hooke, J.M., 2021. Planform change of the Río Chubut (~ 42° S, ~ 70° W, Argentina) in response to climate drivers in the southern Andes*. Geomorphology,* 393, 107924.

Skirrow, G.K., Smedley, R.K., Chiverrell, R.C. submitted. The fluvial geomorphology of the Río Chubut valley and tributaries, *Journal of Maps* (~42°S, ~70°W, Argentina).

Slaymaker, O., 2009. *Proglacial, periglacial or paraglacial?. Geological Society,* London, Special Publications, 320(1), 71-84.

Smedley, R. K., Glasser, N. F., Duller, G. A. 2016. Luminescence dating of glacial advances at Lago Buenos Aires (~46 °S), Patagonia. *Quaternary Science Reviews*, 134, 59-73.

Smedley, R.K, Duller, G.A.T., Pearce, N.J.G. and Roberts, H.M., 2012. Determining the K-content of single-grains of feldspar for luminescence dating*. Radiation Measurements,* 47, 790-796.

Smedley, R.K. and Duller, G.A.T., 2013. Optimising the reproducibility of measurements of the post-IR IRSL signal from single-grains of feldspar for dating*. Ancient TL,* 31 (2), 49 – 58.

Smedley, R.K., Duller, G.A.T. and Roberts, H.M., 2015. Bleaching of the post-IR IRSL signal from individual grains of K-feldspar: Implications for single-grain dating*. Radiation Measurements,* 79, 33-42.

Smedley, R.K. and Pearce, N.J.G., 2016. Internal U, Th and Rb concentrations of alkali-feldspar grains: Implications for luminescence dating*. Quaternary Geochronology,* 35, 16-25.

Smedley, R.K., Glasser, N.F. and Duller, G.A.T., 2016. Luminescence dating of glacial advances at Lago Buenos Aires (~ 46 S), Patagonia. *Quaternary Science Reviews*, 134, 59-73.

Smedley, R.K. 2018. Dust, sand and rocks as windows into the past. *Elements*, 14 (1), 9-14

Smedley, R.K. and Skirrow, G.K., 2020. Luminescence dating in fluvial settings: overcoming the challenge of partial bleaching. *In Palaeohydrology*, 155-168. Springer, Cham.

Smith, D.G. and Smith, N.D., 1980. Sedimentation in anastomosed river systems; examples from alluvial valleys near Banff, Alberta. Journal of Sedimentary Research, 50(1), 157-164.

Smith, N.D., Cross, T.A., Dufficy, J.P. and Clough, S.R., 1989. Anatomy of an avulsion*. Sedimentology,* 36(1), 1-23.

Stølum, H.H., 1998. Planform geometry and dynamics of meandering rivers*. Geological Society of America Bulletin,* 110(11),1485-1498.

Stuut, J.B.W. and Lamy, F., 2004. Climate variability at the southern boundaries of the Namib (southwestern Africa) and Atacama (northern Chile) coastal deserts during the last 120,000 yr. *Quaternary Research*, 62(3), 301-309.

Tabacchi, E., Lambs, L., Guilloy, H., Planty-Tabacchi, A.M., Muller, E. and Decamps, H., 2000. Impacts of riparian vegetation on hydrological processes. *Hydrological processes*, 14(16-17), 2959-2976.

Thiel, C., Buylaert, J.P., Murray, A., Terhorst, B., Hofer, I., Tsukamoto, S. and Frechen, M., 2011. Luminescence dating of the Stratzing loess profile (Austria)–Testing the potential of an elevated temperature post-IR IRSL protocol. *Quaternary International*, 234(1-2), 23-31.

Thomsen, K.J., Murray, A.S., Jain, M. and Bøtter-Jensen, L., 2008. Laboratory fading rates of various luminescence signals from feldspar-rich sediment extracts*. Radiation measurements,* 43(9-10), 1474-1486.

Thorndycraft, V.R., Bendle, J.M., Benito, G., Davies, B.J., Sancho, C., Palmer, A.P., Fabel, D., Medialdea, A. and Martin, J.R., 2019. Glacial lake evolution and Atlantic-Pacific drainage reversals during deglaciation of the Patagonian Ice Sheet. *Quaternary Science Reviews*, 203, 102-127.

Thrasher, I.M., Mauz, B., Chiverrell, R.C. and Lang, A., 2009. Luminescence dating of glaciofluvial deposits: a review. *Earth-Science Reviews,* 97(1-4), 133-146.

Tockner, K., Paetzold, A., Karaus, U.T.E., Claret, C. and Zettel, J., 2006. Ecology of braided rivers. *Special Publication-International Association of Sedimentologists*, 36, 339.

Torres, A.I. and Campodonico, V.A., 2022. Environmental Assessment of Patagonia's Water Resources.

Torres, A.I., Niencheski, L.F., Campodonico, V.A., Pasquini, A.I., Faleschini, M. and Depetris, P.J., 2021. Hydrochemical Insight and Groundwater Supply: A Case Study of Patagonia's Chubut River. *In Anthropogenic Pollution of Aquatic Ecosystems* (205-228). Springer, Cham.

Van Daele, M., Bertrand, S., Meyer, I., Moernaut, J., Vandoorne, W., Siani, G., Tanghe, N., Ghazoui, Z., Pino, M., Urrutia, R. and De Batist, M., 2016. Late Quaternary evolution of Lago Castor (Chile, 45.6 S): Timing of the deglaciation in northern Patagonia and evolution of the southern westerlies during the last 17 kyr. *Quaternary Science Reviews*, 133, 130-146.

Van de Lageweg, W.I., Schuurman, F., Cohen, K.M., Van Dijk, W.M., Shimizu, Y. and Kleinhans, M.G., 2016. Preservation of meandering river channels in uniformly aggrading channel belts. *Sedimentology,* 63(3), 586-608.

Van de Lageweg, W.I., Van Dijk, W.M., Baar, A.W., Rutten, J. and Kleinhans, M.G., 2014. Bank pull or bar push: What drives scroll-bar formation in meandering rivers?. *Geology,* 42(4), 319-322.

Vandenberghe, J., 1995. Timescales, climate and river development. *Quaternary Science Reviews*, 14(6), 631-638.

Viero, D.P., Dubon, S.L. and Lanzoni, S., 2018. Chute cutoffs in meandering rivers: formative mechanisms and hydrodynamic forcing. *Fluvial Meanders and Their Sedimentary Products in the Rock Record*, 201-229.

Volkheimer, W., 1963. El Cuartario Pedemontano en el noroeste de Chubut (Zona Cushamen). 2º *Jornadas Geológicas Argentinas*. Actas II, 439-457.

Volkheimer, W. 1964. Estratigrafı´a de la regio´n extrandina del Departamento de Cushamen (Chubut) entre los paralelos 42 y 42300 y los meridianos 70 y 71. *Asociación Geológica Argentina*, Revista 20, 2, 85–107. Buenos Aires

Volkheimer, W. 1965. El Cuaternario pedemontano en el noroeste del Chubut (zona Cushamen). *Segundas Jornadas Geológicas Argentinas*, Actas 2, 439–451. Buenos Aires

Wenzens, G., 2005. Glacier advances east of the Southern Andes between the Last Glacial Maximum and 5,000 BP compared with lake terraces of the endorrheic Lago Cardiel (49 S, Patagonia, Argentina). *Zeitschrift für Geomorphologie*, 433-454.

Westoby, M.J., Brasington, J., Glasser, N.F., Hambrey, M.J. and Reynolds, J.M., 2012. 'Structure-from-Motion'photogrammetry: A low-cost, effective tool for geoscience applications*. Geomorphology,* 179, 300-314.

White, D., Preece, R.C., Shchetnikov, A.A. and Dlussky, K.G., 2013. Late Glacial and Holocene environmental change reconstructed from floodplain and aeolian sediments near Burdukovo, lower Selenga River Valley (Lake Baikal region), Siberia. *Quaternary International*, 290, 68-81.

Whitlock, C., Moreno, P.I. and Bartlein, P., 2007. Climatic controls of Holocene fire patterns in southern South America. *Quaternary Research*, 68(1), 28-36.

Wintle, A.G., (1973). Anomalous fading of thermo-luminescence in mineral samples. *Nature*, 245, 143-144.

Wintle, A.G. and Murray, A.S., 2006. A review of quartz optically stimulated luminescence characteristics and their relevance in single-aliquot regeneration dating protocols*. Radiation measurements,* 41(4), 369-391.

Yan, N., Colombera, L. and Mountney, N.P., 2021. Evaluation of Morphodynamic Controls on the Preservation of Fluvial Meander-Belt Deposits. *Geophysical Research Letters*, 48(16), p.e2021GL094622.

Zech, R., Zech, J., Kull, C., Kubik, P.W. and Veit, H., 2011. Early last glacial maximum in the southern Central Andes reveals northward shift of the westerlies at~ 39 ka*. Climate of the Past,* 7(1), 41-46.

Zhang, S. and Lu, X.X., 2009. Hydrological responses to precipitation variation and diverse human activities in a mountainous tributary of the lower Xijiang, China. *Catena*, 77(2), 130-142.

Zhu, L., Chen, D., Hassan, M.A. and Venditti, J.G., 2022. The influence of riparian vegetation on the sinuosity and lateral stability of meandering channels. *Geophysical Research Letters*, 49(2), 2021GL096346.

Zinger, J.A., Rhoads, B.L., Best, J.L. and Johnson, K.K., 2013. Flow structure and channel morphodynamics of meander bend chute cutoffs: A case study of the Wabash River, USA. Journal of Geophysical Research: *Earth Surface*, 118(4), pp.2468-2487. [Original source: https://studycrumb.com/alphabetizer]

# APPENDIX 1

## Supplementary Information for Chapter 3

The fluvial geomorphology of the Río Chubut valley and tributaries (~42°S, ~70°W, Argentina).

Submitted to Journal of Maps

## Map 1: The former and contemporary drainage regimes of the Río Chubut headwaters and higher-level terrace framework.

Supplement to: The fluvial geomorphology of the Río Chubut (~42°S, ~70°W, Argentina) and terrace inventory of the major tributaries.

G.K. Skirrow[1], R.C. Chiverrell[1] , R.K. Smedley[1] , J.M. Hooke[1]

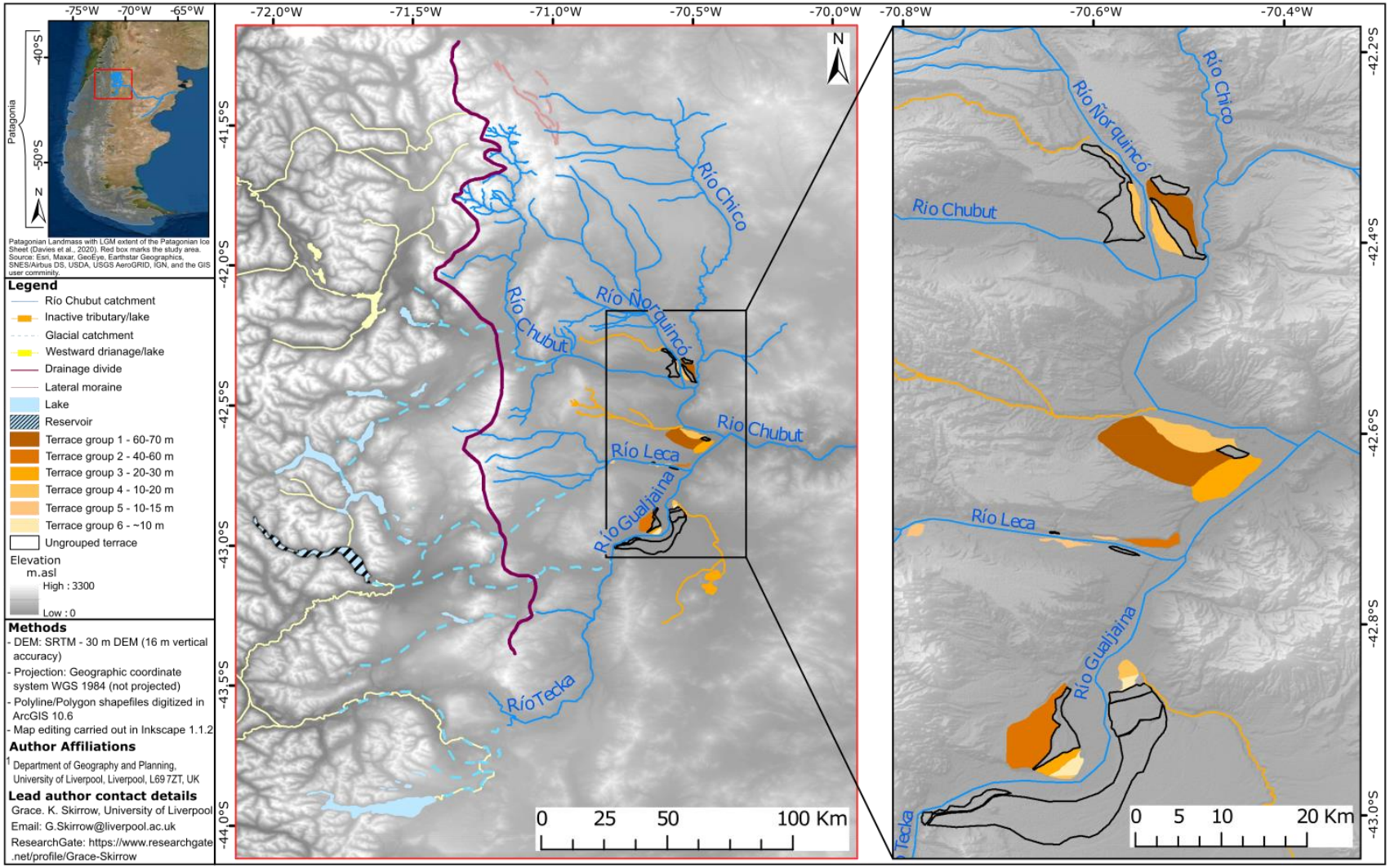

# Map 2: The fluvial geomorphology and terraces in the lower-level valley of the Río Chubut

Supplement to: The fluvial geomorphology of the Río Chubut (~42°S, ~70°W, Argentina) and terrace inventory of the major tributaries.

G.K. Skirrow[1], R.C. Chiverrell[1] , R.K. Smedley[1] , J.M. Hooke[1]

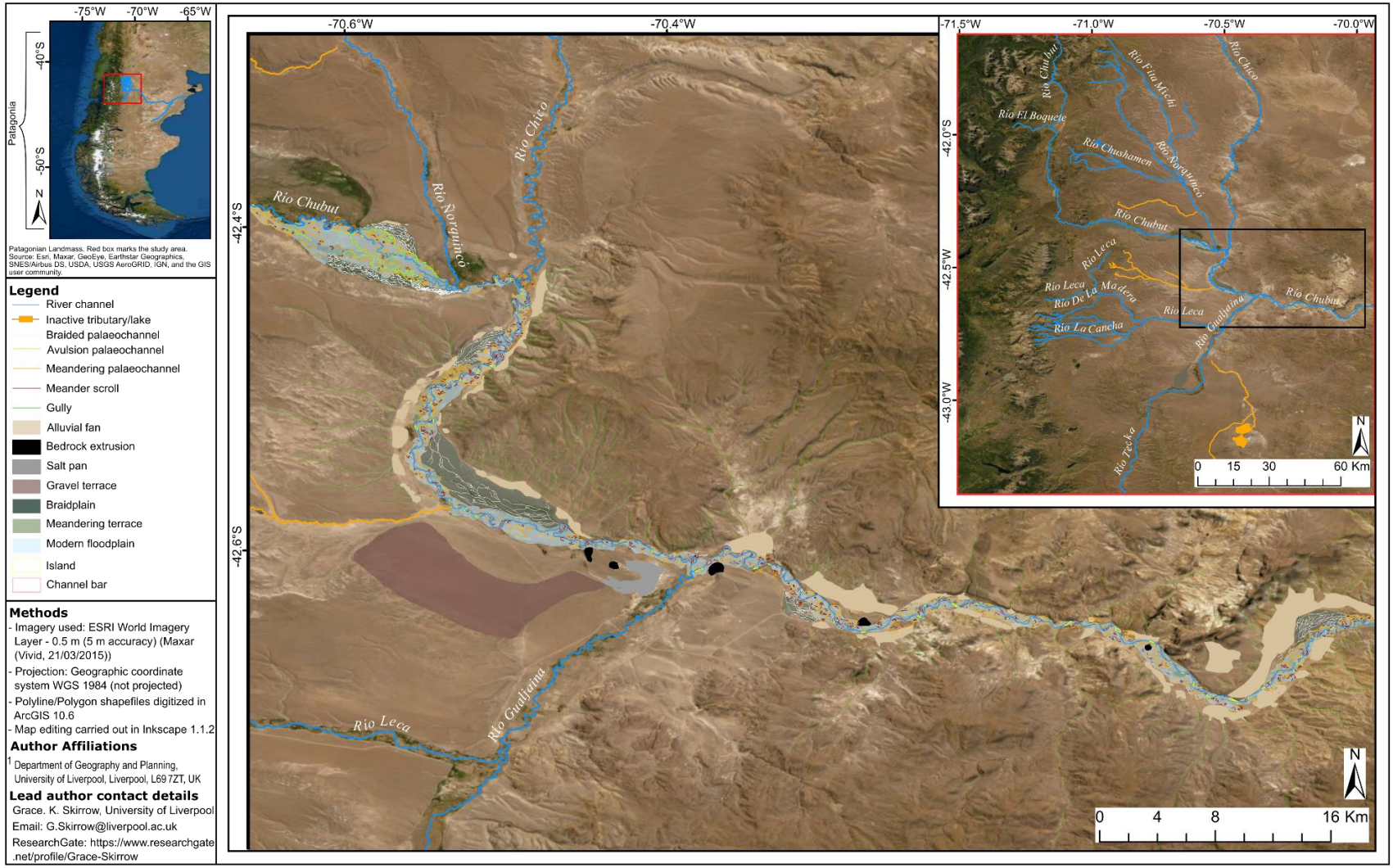

# APPENDIX 2

## Supplementary Information for Chapter 4

Andes A chronology for the La Pampas Formations: Late MIS 5 and MIS 2 sandur deposits in the Río Chubut Valley (~42˚S) Argentina

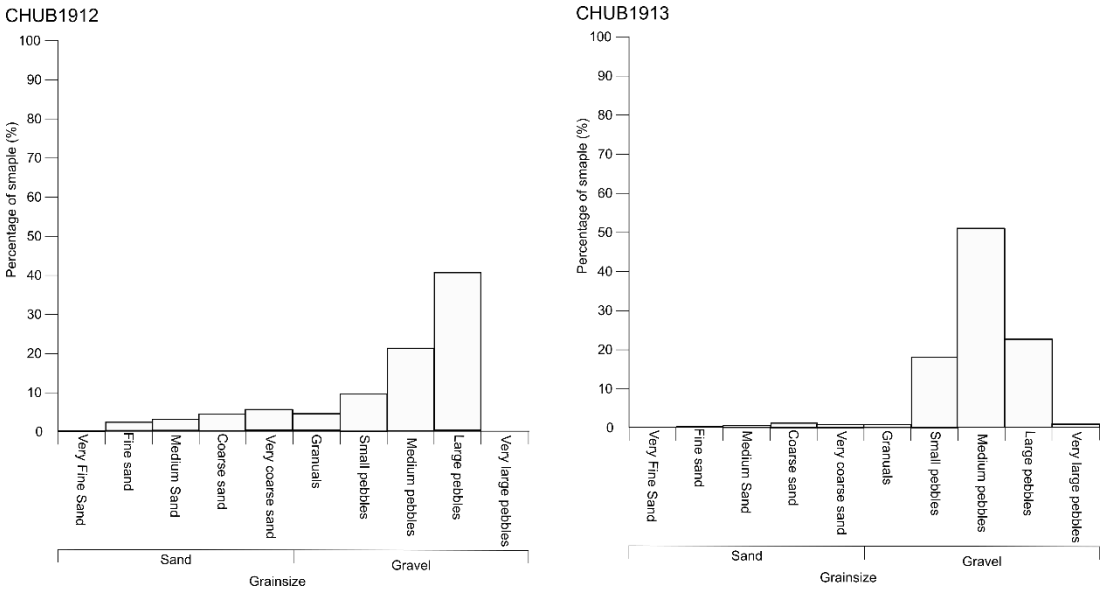


Figure S2. Comparison of grainsize composition between the lower level gravel deposit (sample CHUB1912) and the ~60 m gravel deposit (sample CHUB1913).

# APPENDIX 3

## Supplementary Information for Chapter 5

Planform change of the Rio Chubut (~42°S, ~70°W, Argentina) in response to environmental drivers in the southern Andes

Published in Geomorphology 2021

Figure S1. Sample CHUB1914, collected by standard horizontal tube procedure. Sample taken from the lowermost fluvial sediments overlying the braided gravels. Braided gravels were below the water table. Age represents the fluvial activity that immediately post-dates the braided activity on site CHUB5.

Figure S2. Sample CHUB1917, collected by the borehole sampling procedure. Sample taken from the boundary between the braided gravels and overlying floodplain sediments. Age represents the timing of the end of the braiding activity on site CHUB4.

Fig S3. Sample CHUB1918, collected by the borehole sampling procedure. Sample taken from the boundary between the braided gravels and overlying floodplain sediments. Age represents the timing of the end of the braiding activity on site CHUB6.

Fig S4. Sample CHUB1920, collected by the borehole sampling procedure. Sample taken from the boundary between the braided gravels and overlying floodplain sediments. Age represents the timing of the end of the braiding activity on site CHUB1.

Fig S5. Sample CHUB1915, collected by standard horizontal tube procedure. Sample taken from the fine grained homogenous unit at the base of the alluvial fan exposure. Age represents the oldest activity of the alluvial fan.

Fig S6. Sample CHUB1916, collected by standard horizontal tube procedure. Sample taken from the fine grained homogenous unit at the top of the alluvial fan exposure. Age represents the youngest activity of the alluvial fan.

**Luminescence sampling with an auger**

Samples were collected in the field using two techniques: (1) a light-tight tube was hammered horizontally into a vertical exposure to ensure the sample was shielded from sunlight within the tube; or (2) a borehole was extracted using an Edelman type auger with a 20 cm chamber (Fig. S7). This type of auger was used as the ground was mostly comprised of dry, compact silt/clay with underlying sands and gravels and so not compatible with russian or gouge corers. The aim for sampling using this technique was to dig the borehole with as little contamination as possible and retrieve a sample from the top of the braided palaeochannel sediments (up to 4.6m deep). Care was taken not to overfill the auger chamber or disturb the sides of the borehole when lifting and lowering the auger as this would have caused contamination of younger sediment falling to the older sediment at the bottom of the hole. Coring continued until the samplers reached the fluvial sediments, which were identified by sands and gravels. Here, the auger was cleaned to remove contamination from younger sediment; a black bag was also used as a sleeve and placed over the hole to shield the sample from sunlight. The auger was twisted to fill the chamber and pulled out of the hole into the black sleeve to keep the sample shielded from sunlight (Fig. S7.). From here, a black sample bag was placed over the sleeve so that the contents of the auger could be emptied into the sample bag without sunlight exposure. The black sample bag was then sealed. The coarse sand and gravel were often loose in the auger chamber and sometimes 2 or 3 core drives were needed to retrieve

enough sample (approx. 1 kg) for laboratory analysis. The main limitation of using the auger is that sediment facies and unit boundaries were often unclear because of the mixing caused by the auger's twisting action. Only a basic stratigraphy was able to be logged i.e. grainsize, sorting, colour, approximate moisture content for a record of stratigraphic context. Furthermore, there was potential for grain contamination from modern, surficial sediments in the sampled sediment due to wind transport; thus, single-grain analysis the finite mixture model as part of the data screening criteria was used to detect any grain contamination.

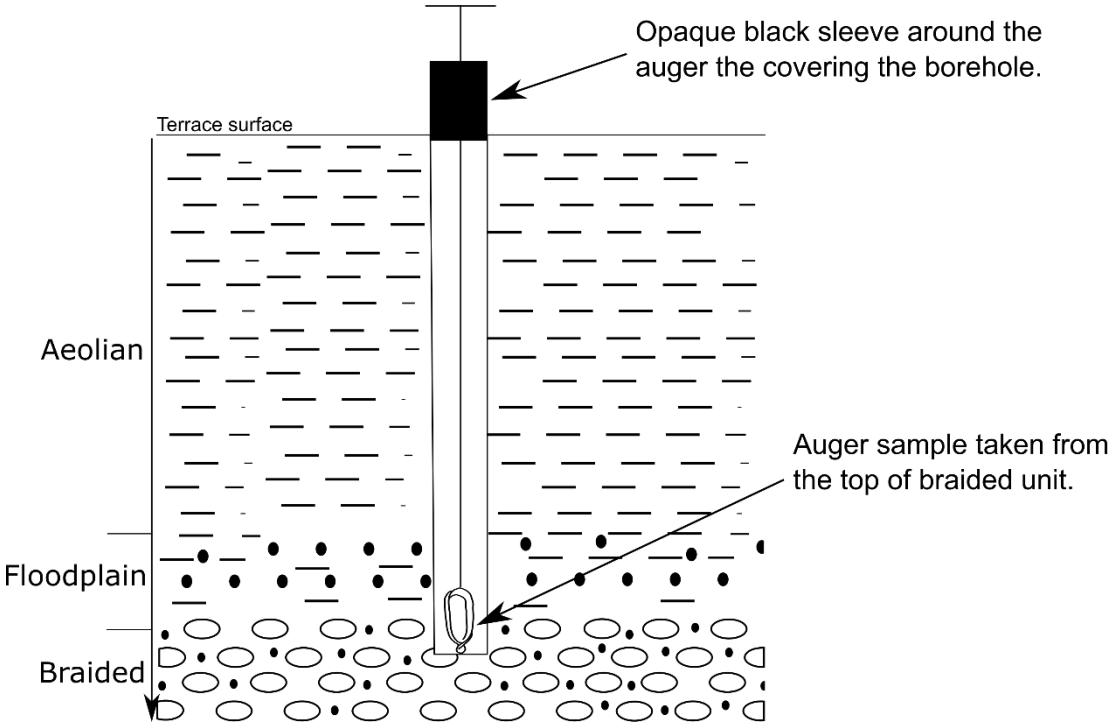


Figure S7. Schematic explaining the borehole sampling technique of braided sediments.

**Dose-recovery experiments**

Dose recovery and residual dose experiments showed that the single aliquot regenerative dose (SAR) protocol used for analysis was appropriate and determined the intrinsic overdispersion in these samples (28 ± 0.04 % for sample CHUB1917 and 21 ± 0.02 % for CHUB1921). Dose recovery and residual dose experiments that the braided terrace sediment was able to a recover a dose within the acceptance criteria (Fig S7).

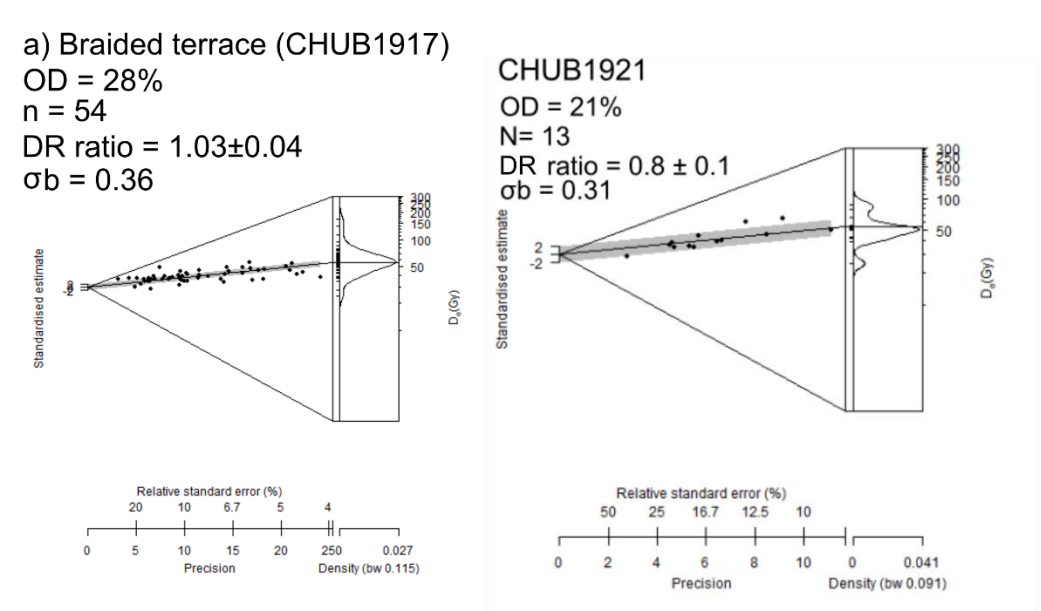


Figure S8. Results from dose recovery (DR) and residual dose experiments. The given dose used in DR was 52.5 Gy. The DR ratio is the residual subtracted from the DR, divided by the given dose. Grey line shows CAM $D_e$ Value.